NDOT Research Report

Report No. 530-13-803

Technical Memorandums (5)

Regarding project:

Streamlining Hydrologic Prediction Processes Using New and More Accurate Techniques and Methods

Memorandum 1 - March 2014
Memorandum 2 - March 2014
Memorandum 3 - October 2014
Memorandum 4 - December 2014
Memorandum 5 - June 2015

Nevada Department of Transportation

1263 South Stewart Street

Carson City, NV 89712

VIEUX, INC.

March 6, 2014

Annjanette (Annje) Dodd, PhD, PE
Kimley-Horn and Associates, Inc.
11919 Foundation Place, Suite 200, Gold River, CA 95670

RE: NDOT Project: Streamlining Hydrologic Prediction Processes Research Project

Dear Dr. Dodd:

The documents that will be reviewed for this project have been identified and listed for consideration in the attached *Reference List*. These documents represent data sources, analysis techniques and procedures that may be applicable to design storms in Nevada. Development of this list is part of the research plan: *TASK 1: Review and development of more accurate storm sizes, shapes, and durations;* and sub-task: *TASK 1.1.1 - List of documents that will be reviewed regarding previously implemented methods*. Review of these previously implemented methods will provide the basis for discussion, recommended analysis approach, and a supporting data plan submitted in subsequent technical memoranda.

If you have any questions, do not hesitate to contact us.

Sincerely,

Baxter E. Vieux, Ph.D., P.E.
Co-principal investigator
Vieux & Associates, Inc.

REFERENCE LIST

1. Allen, R. J., and A. T. DeGaetano. 2005. “Areal Reduction Factors for Two Eastern United States Regions with High Rain-Gauge Density.” *Journal of Hydrologic Engineers* 10 (4): 327–325.
2. Asquith, W., and J. S. Famiglietti. 2000. “Precipitation Areal Reduction Factor Estimation Using an Annual Maxima Centered Approach.” Journal of Hydrology 230: 55–69.
3. Asquith, W. H. 1999. “Areal-Reduction Factors for the Precipitation on the 1-Day Design Storm in Texas.” Water-Resources Investigations Report: 99–4267.
4. Asquith, W. H., and J. S. Famiglietti. 2000. “Precipitation Areal-Reduction Factor Estimation Using an Annual-Maxima Centered Approach.” Journal of Hydrology 230 (1-2): 55–69.
5. Austin, P. M., and R. A. Houze. 1972. “Analysis of the Structure of Precipitation Pattern in New England.” Journal of Applied Meteorology 11: 926–35.
6. Bacchi, B., and R. Ranzi. 1996. “On the Derivation of Areal Reduction Factors of Storms.” Atmospheric Research 42: 123–35.
7. Baeck, M. L., and J. S. Smith. 1998. “Rainfall Estimation by the WSR-88D for Heavy Rainfall Events.” Weather Forecasting 13: 416–36.
8. Battan, L. T. 1973. Radar Observations of the Atmosphere. Chicago, Illinois: University of Chicago.
9. Bedient, Philip B, Anthony Holder, Jude A Benavides, and Baxter E Vieux. 2003. “Radar-Based Flood Warning System Applied to Tropical Storm Allison.” Journal of Hydrologic Engineering 8 (6): 308–18.
10. Bell, F. C. 1976. “The Areal Reduction Factors in Rainfall Frequency Estimation.” NERC Report No. 35.
11. Bell, T. L. 1987. “A Space-Time Stochastic Model of Rainfall for Satellite Remote Sensing Studies.” Journal of Geophysical Research: 9631–44.
12. Bellin, A., and Y. Rubin. 1996. “Hydro_gen: A Spatially Distributed Random Field Generator for Correlated Properties.” Stochastic Hydrology and Hydraulics 10: 253–78.
13. Bras, R., and I. Rodriguez-Iturbe. 1976. “Rainfall Generation: A Non-Stationary Time Varying Multidimensional Model.” Water Resources Research 12 (3): 450–56.
14. Bureau, U. S. Weather. 1957. “Rainfall Intensity-Frequency Regime - Part 1: The Ohio Valley, Technical Paper No. 29 (TP-29), Washington, D.C.”
15. _____. 1958a. “Rainfall Intensity-Frequency Regime - Part 2: The Southeastern United States, Technical Paper No. 29 (TP-29), Washington, D.C.”
16. _____. 1958b. “Rainfall Intensity-Frequency Regime - Part 3: The Middle Atlantic Region, Technical Paper No. 29 (TP-29), Washington, D.C.”
17. _____. 1959. “Rainfall Intensity-Frequency Regime - Part 4: The Northeastern United States, Technical Paper No. 29 (TP-29), Washington, D.C.”
18. _____. 1960. “Rainfall Intensity-Frequency Regime - Part 5: The Great Lakes Region, Technical Paper No. 29 (TP-29), Washington, D.C.”
19. Cao, Qing, Yang Hong, Jonathan J. Gourley, Youcun Qi, Jian Zhang, Yixin Wen, and Pierre-Emmanuel Kirstetter. 2013. “Statistical and Physical Analysis of the Vertical Structure of Precipitation in the Mountainous West Region of the United States Using

11+ Years of Spaceborne Observations from TRMM Precipitation Radar." Journal of Applied Meteorology and Climatology 52 (2): 408–24. doi:10.1175/JAMC-D-12-095.1.
20. Chintalapudi, Singaiah, Hatim O. Sharif, Subash Yeggina, and Almoutaz Elhassan. 2012. "Physically Based, Hydrologic Model Results Based on Three Precipitation Products." JAWRA Journal of the American Water Resources Association 48 (6): 1191–1203. doi:10.1111/j.1752-1688.2012.00679.x.
21. Clark County Regional Flood Control District. "Hydrologic Criteria and Drainage Design Manual."
22. Collier, C. G., and P. J. Hardaker. 1996. "Estimating Probable Maximum Precipitation Using a Storm Model Approach." Journal of Hydrology: 277–306.
23. Cox, D. R., and V. Isham. 1988. "A Simple Spatial-Temporal Model of Rainfall." In Proceedings of Royal Society of London, 317–28. Series A, 415:.*Series A, 415:.
24. Crane, R. K. 1990. "Space-Time Structure of Rain Rate Fields." Journal of Geophysical Research 95: 2001–20.
25. Cudworth, Arthur G. 1989. Flood Hydrology Manual. US Dept. of the Interior, Bureau of Reclamation, Denver Office.
26. Curtis, D. C. 2001. "Storm Sizes and Shapes in the Arid Southwest." Arizona Floodplain Management Association, Fall 10 (6): 785–97.
27. Curtis, David C. 2001. "Storm Sizes and Shapes in the Arid Southwest." In Proceedings of the Arizona Floodplain Management Association Fall 2001 Meeting, Nov 8-9.
28. Curtis, David C. 2007. "Evaluation of the Spatial Structure of Storms and the Development of Design Storms." In World Environmental and Water Resources Congress 2007@ sRestoring Our Natural Habitat, 1–10. ASCE. http://ascelibrary.org/doi/abs/10.1061/40927(243)286.
29. De Michele, Carlo, Nathabandu T Kottegoda, and Renzo Rosso. 2001. "The Derivation of Areal Reduction Factor of Storm Rainfall from Its Scaling Properties." Water Resources Research 37 (12): 3247–52.
30. Dixon, Michael, and Gerry Wiener. 1993. "TITAN: Thunderstorm Identification, Tracking, Analysis, and Nowcasting-A Radar-Based Methodology." Journal of Atmospheric and Oceanic Technology 10 (6): 785–97.
31. Douglas, E. M., and A. P. Barros. 2003. "Probable Maximum Estimation Using Multifractals: Application in the Eastern United States." Journal of Hydrometeorology 4 (6): 1012–24.
32. Durrans, S. R., L. T. Julian, and M. Yekta. 2002a. "Estimation of Depth Area Relationships Using Radar Data." Journal of Hydraulic Engineering 7 (5): 356–67.
33. _____. 2002b. "Estimation of Depth-Area Relationships Using Radar-Rainfall Data." Journal of Hydrologic Engineering 70 (5): 356–67.
34. Durrans, S. Rocky, Lesley T. Julian, and Michael Yekta. 2002. "Estimation of Depth-Area Relationships Using Radar-Rainfall Data." Journal of Hydrologic Engineering 7 (5): 356–67.
35. Einfalt, T., G. Johann, and A. Pfister. 1998. "On the Spatial Validity of Heavy Point Rainfall Measurements." Water Resource Technology 37 (11).
36. Foufoula-Georgiou, E. 1989. "A Probabilistic Storm Transposition Approach for Estimating Exceedence Probabilities of Extreme Precipitation Depths." Water Resources Research 25 (5): 799–815.

37. Frederick, R. H., V. A. Myers, and E. P. Auciello. 1977. “Storm Depth Area Relations from Digitized Radar Returns.” Water Resources Research 13 (3): 675–79.
38. Geronimo, Vincent. 2004. “Regional Approach to Estimate Depth-Area Reduction Curves Using Radar-Derived Rainfall Data For Front Range?” Colorado, CE-: 5960–900.
39. Gill, T. D. 2005. “Transformation of Point Rainfall to Areal Rainfall by Estimating Areal Reduction Factors, Using Radar Data, for Texas”. Master of Science Thesis Submitted to Texas A&M University Civil Engineering.
40. Guo, James CY. 2011. “Storm Centering Approach for Flood Predictions from Large Watersheds.” Journal of Hydrologic Engineering 17 (9): 960–64.
41. Gupta, V. K., and E. C. Waymire. 1979. “A Stochastic Kinetic Study of Subsynoptic Space-Time Rainfall.” Water Resources Research 15 (3): 637–44.
42. _____. 1993. “A Statistical Analysis of Meso-Scale Rainfall as a Random Cascade.” Journal of Applied Meteorology 32: 251–67.Hansen, E. M., P. Corrigen, D. D. Fenn, and J. L. Yogel. 1994. “Probable Maximum Precipitation Estimates -Pacific Northwest States.” Hydrometeorological Report No. 57.
43. Hansen, E. M., D. D. Fenn, L. C. Schriner, R. W. Stodt, and J. F. Miller. 1988. “Probable Maximum Precipitation Estimates - United States between the Continental Divide and the 103rd Meridian.” Hydrometeorological Report No. 55A.
44. Hansen, E. M., M. J. Reidel, and F. K. Schwarz. 1977. “Probable Maximum Precipitation Estimates - Colorado River and Great Basin Drainages.” Hydrometeorological Report No. 49.
45. Hansen, E. M., L. C. Schreiner, and J. F. Miller. 1982. “Application of Probable Maximum Precipitation Estimates, United States East of the 105th Meridian.” Hydrometeorological Report No. 51.
46. Hardegree, Stuart, Steven Van Vactor, Kathleen Healy, Carlos Alonso, James Bonta, David Bosch, Dwight Fisher, Dave Goodrich, Daren Harmel, and Jean Steiner. 2003. “Multi-Watershed Evaluation of WSR-88D (NEXRAD) Radar-Precipitation Products.” In Proc. 1st Interagency Conference on Research in the Watersheds, 486–91.
47. Hershfield, D. M. 1961a. “Estimating the Probable Maximum Precipitation.” Proceedings ASCE, Journal of Hydraulics Division 87: 99–106.
48. _____. 1961b. “Rainfall Frequency Atlas of the United States for Durations from 30 Mins to 24 Hours and Return Periods from 1 Year to 100 Years.” Tech.
49. _____. 1965. “Methods of Estimating Probable Maximum Precipitation.” Journal of American Waterworks Association 57: 965–72.
50. _____. 1975. “Some Small Scale Characteristics of Extreme Storm Rainfalls in Small Basins.” Hydraulic Science Bulletin XX 1 (3): 77–85.
51. Ho, F. P., and J. T. Reidel. 1980. “Seasonal Variation of 10 Sq. Miles, Probable Maximum Precipitation Estimates - United States East of the 105th Meridian.” Hydrometeorological Report No.
52. Houghton, John G, Clarence M Sakamoto, and Richard O Gifford. 1975. Nevada’s Weather and Climate. Vol. 2. NV Bureau of Mines & Geology.
53. Jeton, Anne E., Sharon A. Watkins, Thomas J. Lopes, and Justin Huntington. 2014. “Evaluation of Precipitation Estimates from PRISM for the 1961-90 and 1971-2000 Data Sets, Nevada.” Accessed February 24. http://pubs.usgs.gov/sir/2005/5291/.
54. Koutsoyiannis, D. 1999. “A Probabilistic View of Hershfield’s Method for Estimating Probable Maximum Precipitation.” Water Resources Research 35 (4): 1313–22.

55. Lebel, Th., and J. P. Laborde. 1988. “A Geostatistical Approach for Areal Rainfall Statistics Assessment.” Stochastic Hydrology and Hydraulics 2 (4): 245–61. doi:10.1007/BF01544039.
56. Looper, Jonathan P, and Baxter E Vieux. 2012. “An Assessment of Distributed Flash Flood Forecasting Accuracy Using Radar and Rain Gauge Input for a Physics-Based Distributed Hydrologic Model.” Journal of Hydrology 412: 114–32.
57. Looper, Jonathan P, Baxter E Vieux, and Maria A Moreno. 2012. “Assessing the Impacts of Precipitation Bias on Distributed Hydrologic Model Calibration and Prediction Accuracy.” Journal of Hydrology 418: 110–22.
58. Looper, Jonathan P., and Baxter E. Vieux. 2013. “Distributed Hydrologic Forecast Reliability Using Next-Generation Radar.” Journal of Hydrologic Engineering.
59. Lopes, Thomas J., and Kip K. Allander. 2009a. Hydrologic Setting and Conceptual Hydrologic Model of the Walker River Basin, West-Central Nevada. US Geological Survey. http://pubs.usgs.gov/sir/2009/5155/.
60. _____. 2009b. Water Budgets of the Walker River Basin and Walker Lake, California and Nevada. US Geological Survey. http://pubs.usgs.gov/sir/2009/5157/.
61. Lovejoy, S., and B. Mandelbrot. 1985. “Fractal Properties of Rain, and a Fractal Model.” Tellus, Series A: 209–32.
62. Lovejoy, S., and D. Schertzer. 1985. “Generalized Scale Invariance in the Atmosphere and Fractal Models of Rain.” Water Resources Research 21 (8): 1233–50.
63. Lundquist, Jessica D., Justin R. Minder, Paul J. Neiman, and Ellen Sukovich. 2010. “Relationships between Barrier Jet Heights, Orographic Precipitation Gradients, and Streamflow in the Northern Sierra Nevada.” Journal of Hydrometeorology 11 (5): 1141–56. doi:10.1175/2010JHM1264.1.
64. Marshall, R. J. 1980. “The Estimation and Distribution of Storm Movement and Storm Structure, Using a Correlation Analysis Technique and Rain-Gauge Data.” Journal of Hydrology 48: 19–39.
65. _____. 1983. “A Spatial Temporal Model of Storm Rainfall.” Journal of Hydrology 62: 53–62.
66. Mays, L. W. 1996. Water Resources Handbook. New York: McGraw-Hill.
67. Michele, C. D., T. K. Nathabandu, and R. Rosso. 2001. “The Derivation of Areal Reduction Factor from Its Scaling Properties.” Water Resource Research 37 (12): 3247–52.
68. Miller, JF, RH Frederick, and RJ Tracey. 1973. “NOAA Atlas 2, Precipitation-Frequency Atlas of the Western United States” 3.
69. Moore, James N., and Ray C. Riley. 2014. “Comparison of Temporal Rainfall Distributions for Near Probable Maximum Precipitation Storm Events for Dam Design.” In Proceedings of the 1993 Annual Conference of the Association of State Dam Safety Officials, Minneapolis, MN. Accessed February 24. https://www.nrcs.usda.gov/Internet/FSE_DOCUMENTS/16/nrcs143_014796.pdf.
70. Myers, V. A., and R. M. Zehr. 1980. “A Methodology for Point to Area Rainfall Frequency Ratios”. NOAA Technical Report, National Weather Service, Silver Springs, Maryland, U.S. Department of Commerce, National Oceanic and Atmospheric Administration, NWS 24.
71. Niemczynowicz, J. 1991. “On Storm Movement and Its Applications.” Atmospheric Research: 109–27.

72. O'Hara, Brian F, Gary E Barbato, John W James, Heather A Angeloff, Tom Cylke, Brian O'Hara, Gary Barbato, John James, and Heather Angeloff. 2007. Weather and Climate of the Reno-Carson City-Lake Tahoe Region: Nevada Bureau of Mines and Geology Special Publication 34. NV Bureau of Mines & Geology.
73. Oceanic, National, and Atmospheric Administration (NOAA). 2013. "Http://hdsc.nws.noaa.gov." NOAA Atlas 14 – Precipitation Frequency Atlas of the United States. Viewed November 10.
74. Olivera, Francisco, Janghwoan Choi, Dongkyun Kim, and Ming-Han Li. 2008. "Estimation of Average Rainfall Areal Reduction Factors in Texas Using NEXRAD Data." Journal of Hydrologic Engineering 13 (6): 438–48.
75. Omolayo, AS. 1993. "On the Transposition of Areal Reduction Factors for Rainfall Frequency Estimation." Journal of Hydrology 145 (1): 191–205.
76. Organization, World Meteorological. 1986. "Manual for Estimation of Probable Maximum Precipitation." Operational Hydrologic Rep.
77. Over, T., and V. Gupta. 1996. "A Space-Time Theory of Mesoscale Rainfall Using Random Cascades." Journal of Geophysical Research 101 (26).
78. Rakhecha, P. R., and C. Clark. 2002. "Areal PMP Distribution for One-Day to Three-Day Duration over India." Applied Meteorology 9: 399–406.
79. Riley, Ray C., and James N. Moore. 2014. "Storm Distribution Developed from World Curve Data and It's Potential Areal Application." Accessed February 24. https://www.nrcs.usda.gov/Internet/FSE_DOCUMENTS/16/nrcs143_014770.pdf.
80. Rodriguez-Iturbe, I., D. R. Cox, and P. S. Eagleson. 1986. "Spatial Modeling of Total Storm Rainfall." In Proceedings of Royal Society of London, 27–50. Series A, 403:.Series A, 403:.
81. Rodriguez-Iturbe, I., D. R. Cox, and V. Isham. 1987. "Some Models for Rainfall Based on Stochastic Point Processes." In Proceedings of Royal Society of London, 269–88. Series A, 410:.Series A, 410:.
82. Rodriguez-Iturbe, I., and H. M. Mejia. 1974. "On the Transformation of Point Rainfall to Areal Rainfall." Water Resources Research 10 (4): 729–35.
83. Sherman, R. J. 1977. "The Speed and Direction of the Movement of Storm Rainfall Patterns." Meteorological Office, Bracknel, Berkshire, U 551 (515).
84. Siriwardena, L., and P. E. Weinmann. 1996. "Development and Testing of Methodology to Derive Areal Reduction Factors for Long Duration Rainfalls." =
85. Sivapalan, M., and G. Bloschl. 1998. "Transformation of Point Rainfall to Areal Rainfall: Intensity-Duration Frequency Curves." Journal of Hydrology 204 (91): 150–67.
86. Smith, J. A., and A. A. Bradley. 1994. "Space Time Structures of Extreme Storm Rainfall in the Southern Plains." Journal of Applied Meteorology 33: 1402–17.
87. Smith, J. A., and W. F. Krajewski. 1987. "Statistical Modeling of Space-Time Rainfall Using Radar and Rain Gauge Observations." Water Resources Research 23 (10): 1893–1900.
88. Srikanthan, R. 1995. "A Review of the Methods for Estimating Areal Reduction Factors for Design Rainfalls." Cooperative Research Center for Catchment Hydrology 3 (3): 1–15.
89. Stedinger, Jery R. 1983. "Design Events with Specified Flood Risk." Water Resources Research 19 (2): 511–22.

90. Stewart, E. J. 1989. “Areal Reduction Factors for Design Storm Construction: Joint Use of Rain Gauge and Radar Data.” International Association of Hydrological Sciences Publication 181: 31–49.
91. Svensson, C., and P. R. Rakhecha. 1998. “Estimation of Probable Maximum Precipitation for Dams in the Hongru River Catchment, China.” Theoretical and Applied Climatology 59: 79–91.
92. Swain, Robert E, John F England, Kenneth L Bullard, and David A Raff. 2006. Guidelines for Evaluating Hydrologic Hazards. US Department of the Interior, Bureau of Reclamation.
93. Syed, K. H. 2003. “Spatial Characteristics of Thunderstorm Rainfall Fields and Their Relation to Runoff.” Journal of Hydrology 271: 1–21.
94. Teegavarapu, Ramesh S.V., Tadesse Meskele, and Chandra S. Pathak. 2012. “Geo-Spatial Grid-Based Transformations of Precipitation Estimates Using Spatial Interpolation Methods.” Computers & Geosciences 40: 28–39. doi:10.1016/j.cageo.2011.07.004.
95. Veneziano, D., and A. Langousis. 2004. “Areal Reduction Factors for Multifractal Rainfall.” Geophysical Research Abstracts 6.
96. Venugopal, V., E. Foulfoula-Georgiou, and V. Sapozhnikov. 1999a. “A Space Time Downscaling Model of Rainfall.” Journal of Geophysical Research: 705–21.
97. _____. 1999b. “Evidence of Dynamic Scaling in Space Time Rainfall.” Journal of Geophysical Research: 599–610.
98. Vieux, B. E., and P. B. Bedient. 1998. “Estimation of Rainfall for Flood Prediction from WSR-88D Reflectivity: A Case Study 17-18 October 1994.” Weather Forecasting 13: 407–15.
99. Vieux, Baxter E, and Philip B Bedient. 2004. “Assessing Urban Hydrologic Prediction Accuracy through Event Reconstruction.” Journal of Hydrology 299 (3): 217–36.
100. Vieux, BE, and JE Vieux. 2005. “Statistical Evaluation of a Radar Rainfall System for Sewer System Management.” Atmospheric Research 77 (1): 322–36.
101. Vogel, John L, and Lesley T Julian. 1996. “Semiarid Precipitation Frequency Project Contrasted with Previously Published Rainfall Atlases.” Transportation Research Record: Journal of the Transportation Research Board 1523 (1): 130–40.
102. Warner, Thomas T., Edward A. Brandes, Juanzhen Sun, David N. Yates, and Cynthia K. Mueller. 2000. “Prediction of a Flash Flood in Complex Terrain. Part I: A Comparison of Rainfall Estimates from Radar, and Very Short Range Rainfall Simulations from a Dynamic Model and an Automated Algorithmic System.” Journal of Applied Meteorology 39 (6): 797–814.
103. Waymire, E., and V. K. Gupta. 1981a. “The Mathematical Structure of Rainfall Representations 2, a Review of the Theory of Point Processes.” Water Resources Research 17 (1273-1285): 1453–65.
104. _____. 1981b. “The Mathematical Structure of Rainfall Representations, 1, A Review of the Stochastic Rainfall Models.” Water Resources Research 17: 1261–72.
105. Yilmaz, Koray K., Terri S. Hogue, Kuo-lin Hsu, Soroosh Sorooshian, Hoshin V. Gupta, and Thorsten Wagener. 2005. “Intercomparison of Rain Gauge, Radar, and Satellite-Based Precipitation Estimates with Emphasis on Hydrologic Forecasting.” Journal of Hydrometeorology 6 (4).

106. Young, CB. 2002. “Comparing NEXRAD Operational Precipitation Estimates and Raingage Observations of Intense Precipitation in the Missouri River Basin.” In AGU Spring Meeting Abstracts, 1:17.
107. Zawadzki, I. 1973. “Statistical Properties of Precipitation Patterns.” Journal of Applied Meteorology 12: 459–72.
108. Zehr, R. M., and V. A. Myers. 1984. Depth-Area Ratios in the Semi-Arid Southwest United States. NOAA Technical Memorandum NWS HYDRO-40.
109. Zurndorter, E. A., F. K. Schwarz, E. M. Hansen, D. D. Fenn, and J. F. Miller. 1986. “Probable Maximum and TVA Precipitation Estimates with Areal Distribution for Tennessee River.” Hydrometeorological Report No. 45.

DRAFT TECHNICAL MEMORANDUM

To: Dr. Annjanette Dodd, Ph.D., P.E.
Kimley-Horn and Associates

From: Dr. Baxter Vieux, Ph.D., P.E.
Vieux & Associates, Inc.

Date: March 14, 2014

Re: Nevada Department of Transportation, Research Project No. P530-13-803
Streamlining Hydrologic Prediction Processes Using New and More Accurate Techniques and Methods.

---

1. Introduction

This technical memorandum reviews past methods for characterizing rainfall distribution for design purposes in Nevada. From this review, an approach is recommended for developing spatial and temporal distributions of storm structure. The development of representative design storms is anticipated to result in a streamlined method for more accurate hydrologic prediction by the Nevada Department of Transportation (NDOT). The motivation of the proposed research is to improve the accuracy of design storms used as input to hydrologic models for hydraulic structure design. Climatologically based design storm characteristics will be derived that accurately represent the types of storms that occur in Nevada.

2. Review of Previous Methods

Review of previous methods is divided into two main parts: 1) storm event analysis and 2) depth area reduction factors. Storm event analysis will determine the characteristics of storms prevalent in Nevada such as storm size, shape, and duration. Depth area reduction factors (DARFs) transform point precipitation estimates into distributed rainfall estimates that can be applied to a drainage area. Currently, the NDOT drainage manual (NDOT, 2006) specifies that acceptable hydrologic methods are the rational method, regression equations, statistical analysis, and synthetic modeling. Due to the lack of streamflow gage data in Nevada, both regression equation and statistical analysis can be inadequate to estimate peak discharge and design hydrographs for portions of the state. Therefore, the rational method and synthetic modeling are used to estimate peak discharge and hydrographs for design purposes. The NDOT drainage manual specifies that for synthetic modeling the Soil Conservation Service (SCS) unit hydrograph method shall be used to develop a design hydrograph. The SCS unit hydrograph method requires the use of a dimensionless hyetograph. As with most synthetic modeling approaches, the time sequence of rainfall depth is needed for transformation of precipitation into direct runoff (Bedient et al., 2013).

For temporal distributions, the NDOT drainage manual specifies NOAA Atlas 14 Volume 1

(Bonnin et al., 2004) as the dimensionless hyetograph. Also, synthetic modeling for large drainage areas requires the use of DARFs to transform point precipitation estimates to average depths over a drainage area. Hershfield (1961b) developed maps of rainfall depths corresponding to specific return periods for the entire United States using sparsely distributed rain gauges, but without taking into account the complex topography of the West. NOAA Atlas 2 Volume VII was then developed by Miller et al. (1973), which covers the State of Nevada in an attempt to better analyze the influences of terrain on rainfall. As of 2004, however, the National Weather Service (NWS) had adopted NOAA Atlas 14 Volume 1 for frequency estimates across Nevada. NOAA Atlas 14 (Bonnin et al., 2004) recommends the use of Technical Paper (TP) 40 (Hershfield, 1961b) DARFs as being applicable rather NOAA Atlas 2 Volume VII.

2.1. Precipitation and Flooding in Nevada

Much of Nevada lies within the Great Basin where "the topography is characterized by rugged mountains, flat valleys with occasional buttes and mesas, and sandy desert regions". (Zorn, 2013). There are more than 200 separate north-south oriented mountain ranges across the state of Nevada, which can reach elevations in excess of 10,000 ft., while the southern area of the state is part of the Mojave Desert with elevations below 500 ft.

Most of the precipitation that falls across Nevada is due, in large part, to Pacific fronts or Great Basin lows (Houghton, 1969; Houghton et al., 1975). While both are associated with moisture from the Pacific Ocean, the former tends to bring more precipitation to the western part of the state from December to February, with totals diminishing rapidly towards the east and away from the Sierra Nevada. Great Basin lows, however, are more likely to cause precipitation over the entire state since low pressure is located directly over the region. These lows are the main source of precipitation over central and eastern sections of Nevada, usually from April - June. Overall, there is an inverse relationship between temperature and precipitation because of the dependency of precipitation on both elevation and latitude.

As noted above, precipitation in Nevada is greatly impacted by the topography of the state, namely the presence of the Sierra Nevada Mountains. As prevailing westerly winds from the Pacific Ocean push air up over the mountains, the process of condensation removes much of the moisture from the atmosphere (Lundquist et al., 2010). This drying is further enhanced on the easterly side of the range where the air sinks and is then warmed through compression. As a result, the largest annual precipitation totals in Nevada are generally confined to the extreme western portions of the state while much of the lower elevations receive little rainfall due to a rain shadowing effect (Houghton et al., 1975; NOAA, 1985).

Moist air from the Gulf of Mexico and Gulf of California is occasionally transported into the state, and when combined with strong surface heating, generates showers and thunderstorms particularly across the south and east. Maddox et al. (1980) found that significant flash flood events were often associated with a westward-moving, inverted trough tracking across the southwestern United States. Under these conditions, torrential downpours and resultant flash flooding have been documented in the Las Vegas area, for example (Randerson, 1976; Li et al., 2003).

Houghton et al. (1975) found that despite the arid to semi-arid nature of much of the state, both flooding and flash flooding can occur in Nevada. The river and stream system generally originates in the mountains and is largely dependent on melting snow and precipitation occurring during the spring. Warm, spring rains on top of a large snowpack have been known to produce regional flooding across the state as rivers encroach on their floodplains (Peck and Richardson, 1962). For example, the Truckee River that passes through the City of Reno has experienced several moderate to major floods over the past several decades (Underwood et al., 2009; Kaplan et al., 2009). As part of the Great Basin, most rivers and streams in Nevada have no outside drainage into the ocean and simply flow into lakes with no outlets or into shallow sinks.

Flash flooding is a significant threat during the warmer months as convection, especially during the monsoon season. The North American Monsoon (NAM) generally reaches its peak across the Southwestern United States from July through early September (Hales, 1972; Brenner, 1974; Douglas et al., 1993; Higgins et al., 1997; Adams and Comrie, 1997; Higgins et al., 1998; Adams and Stensrud, 2007) and can produce short-duration, high-intensity rainfall (Lopes and Allander, 2009a,b) as atmospheric moisture, usually from moisture surges originating in the Gulf of California, is introduced into normally arid regions. Areas that have a very low annual average precipitation can still experience cloudburst storms when conditions are favorable. This can result in considerable runoff due to poorly-absorbent soil as well as a lack of vegetation, potentially producing flooding in a location several miles away from where the rain actually fell as water is transported down dry creek beds or washes. Alluvial-fan flooding occurs when rain falls over fan-shaped landforms that are fairly common at the base of mountain ranges in arid and semi-arid regions. These fans develop as a result of water-transported sediment being deposited when it reaches flatter land, resulting in high-velocity flows that can be unpredictable in nature. In some cases, the floodwaters can pick up enough sediment that a slurry can form, resulting in debris and mud flows that are capable of carrying large objects such as boulders with them (Welborn, 2013). According to National Climatic Data Center Storm Reports (2014), flash flooding can occur across Nevada at any time of year, though it appears to be most common from July – September, coinciding with the peak of the NAM.

2.2. Characterizing Rainfall Distribution

2.2.1. Rainfall Frequency

Rainfall data, used for design storm purposes, has typically been provided by the National Weather Service for various parts of the country including Nevada. The NWS usually has divided the continental United States based on the 105th meridian. One of the early studies for areas east of the 105th meridian was performed in the NWS Technical Paper 40 (TP-40) by Hershfield (1961a,b). The DARF curves presented in TP-40 were developed in NWS Technical Paper 29 (TP-29) (U.S. Weather Bureau, 1957) from dense rain gauge networks located in the Midwest and Northeast. Even though these DARFs were developed from data from the Midwest and Northeast, they have been used throughout the United States. No geographical or seasonal variation in DARF is presented in TP-29 making it less applicable. It should be noted that NOAA Atlas 14 did not update the DARFs from the original TP-29. Also, due to the lack of dense rain gauge networks west of the 105th meridian, these same DARFs were recommended for use in Nevada, California, and Utah. Precipitation frequency atlases have been updated for

the United States in NOAA Atlas 14 (Bonnin et al., 2004). Similar techniques have been used in the estimation of probable maximum precipitation in Hydrometeorological Reports (HMR) 49, 51, and 55A (Hansen et al., 1982, 1984, 1988), Hydrometeorological Report 53 (Ho and Reidel, 1980), and Koutsoyiannis (1999). Adjustments to PMP values described in HMR 49 (Hansen et al., 1984) account for areal reduction factors, elevation and duration. Complex terrain and wind and moisture patterns make the assignment of orographic enhancement difficult especially in PMP magnitude rainfall. Hansen et al. (1984) suggest that it is more practical to base the estimation of orographic effects primarily on observed variations in precipitation and terrain. Thus, actual storm areal distributions in relation to terrain are important to identifying orographic enhancement and its effects on spatial distribution or rainfall.

More recent studies regarding the spatial distribution of rainfall have attempted to mitigate some of the shortcomings related to sparse rain gauge networks present in HMR 49. For example, the effects of orography are accounted for using Parameter-elevation Regressions on Independent Slopes Model (PRISM) reported by Jeton et al. (2014). This model uses a hybrid statistical-geographic approach by employing regression equations to account for voids in surface observing stations by analyzing elevation on a cell by cell basis, and also considering parameters such as "slope orientation". Recognizing whether a mountain is a windward or leeward facing slope, for example, allows the model to take into account any orographic enhancement or rain shadowing that may occur (Daly and Bryant, 2013; Jeton et al., 2014). Orographic enhancement of precipitation is modeled in Mountain Mapper (Schaake et al., 2004), and is used by the California Nevada River Forecast Center (CNRFC) to create a gridded precipitation map between gauges for hydrologic modeling purposes. Parzybok and Tomlinson (2006) report the use of the Storm Precipitation Analysis System (SPAS) for mapping rainfall in areas dominated by orographic enhancement of rainfall. PRISM, SPAS and Mountain Mapper are all methods for distributing rainfall in areas that lack detailed observations from rain gauge or radar due to terrain blockages.

2.2.2. Temporal distributions

Design storms generally are composed of a point depth based on a return frequency, a temporal distribution, and a DARF based on the drainage area. The NDOT drainage manual specifies that point depth frequency estimates be obtained from NOAA Atlas 14. NOAA Atlas 14 contains general temporal distributions that divide Nevada into only two main regions. The NOAA Atlas 14 applies the same temporal distribution or shape throughout the project area without local specificity (Bonnin et al., 2004). Further, hyetographs in NOAA Atlas 14 were not separated by season, but rather, includes all events regardless of the month in which they occur. A threshold was applied such that any accumulation had to exceed the 2-yr return interval for a particular duration. The NWS computed precipitation accumulations for continuous time intervals of 6-, 12-, 24- and 96-hr, as opposed to single events or storms. As a result, the NWS hyetographs may contain parts of one, or more than one precipitation event. The resulting hyetographs were smoothed by a moving window weighted average smoothing technique on each curve. With the approach taken, i.e. not segmenting the rainfall into specific events, there was little difference among states in the Great Basin, as presented in NOAA Atlas 14.

2.2.3. Hydrometeorological Homogeneous Areas

Hydrometeorological homogeneous areas (HHAs) represent areas that have similar statistical characteristics regarding measured precipitation. One advantage of the technique used in NOAA Atlas 14 was the statistical grouping of rain gauges into HHAs. Bonnin et al. (2004) used the L-moments statistical technique to identify areas within the Great Basin that showed similar statistical characteristics. Analysis of hyetographs derived for these HHAs can be further evaluated to identify homogeneity as was done in preparation of NOAA Atlas 14. Elevation of the rain gauge is also expected to exert an effect on the temporal distribution of rainfall as will the season and type of precipitation producing storm event.

2.2.4. Depth Area Reduction Factors

An accepted principle in hydrology is that "larger catchments are less likely than smaller catchments to experience high intensity storms over the whole of the catchment area" (Siriwardena and Weinmann, 1996). Therefore, the conversion of point precipitation into area-averaged precipitation is necessary whenever an area, large enough for rainfall not to be uniform, is to be modeled. However, while point precipitation has been well studied because of the availability of rain gauge data, areal precipitation cannot be measured, and its estimation has been a subject of research for the last few decades (U.S. Weather Bureau 1957, 1958a, 1958b, 1959, 1960, 1964; Rodriguez-Iturbe and Mejia, 1974; Frederick et al., 1977; Omolayo, 1993; Srikathan, 1995; Bacchi and Ranzi, 1996; Siriwardena and Weinmann, 1996; Sivapalan and Blöschl, 1998; Asquith and Famiglietti, 2000; De Michele et al., 2001; Durrans et al., 2002; Olivera et al., 2005 and 2008; and Guo, 2011).

A number of approaches for converting point precipitation into areal precipitation are based on observed precipitation data from rain gauges or radar. DARF-estimation algorithms can be grouped into two categories, 1) geographically fixed DARFs, and 2) storm-centered DARFs. Algorithms used to calculate geographically fixed DARFs can be sensitive to the configuration of the network, particularly in the geographically-fixed approach where the point rainfall is compared to areal averages for non-concurrent storm events. That is to say, where areal and point precipitation are not derived from the same event in TP-29, but rather, DARFs are computed from annual maxima and annual averages. While statistically expedient, within-storm distribution of rainfall may be masked by the approach taken in TP-29 and other derivative works.

DARFs have been estimated using radar technology for the last three decades beginning with Austin and Houze (1972). More recently, Durrans et al. (2002) developed DARFs using the Arkansas Basin River Forecast Center (ABRFC) Multi-sensor Precipitation Estimates (MPE), which is gauge-adjusted in production of radar rainfall estimates. Their results were similar to the previous NWS analyses, but suffered from documented MPE biases (Young, 2002; Looper and Vieux, 2012). Olivera et al. (2005) performed a similar study for the state of Texas utilizing the West Gulf River Forecast Center (WGRFC) MPE dataset. The estimates of drainage area reduction factors, from the WGRFC dataset, were significantly larger (more reduction) than found in TP-29. Olivera et al. (2005) explained that the reduction could be due to the analysis only comparing each individual grid cell to the surrounding area rather than the statistical

expediency represented by TP-29.

One aspect of radar rainfall estimation is that the assumed empirically derived relationship between reflectivity, Z, and rainfall rate, R, called a Z-R relationship, must effectively be dealt with. If the DARF is considered as a non-dimensional relationship between point to areal ratios, then the bias introduced by an assumed Z-R relationship is immaterial. Frederick et al. (1977) observed that because DARFs are expressed as dimensionless ratios of areal point precipitation to areal average precipitation, the uncertainty in the Z-R relationships found in radar data is removed. They also observe that DARFs have not been possible to derive for areas larger than 1,000 km^2 using rain gauge networks, which limitation is obviated by the high-resolution coverage over large areas afforded by radar. Bacchi and Ranzi (1996) also identified radar data as being more efficient than typical rain gauge networks in capturing the spatial distribution of storms and estimating DARFs.

The storm-centered approach is well suited for using continuous (i.e., surface) precipitation data such as radar data. In this case, DARFs are calculated for individual events for which they describe their areal properties, and are equal to the ratio of the average precipitation depth over an area to the concurrent point precipitation depth in the storm center. Because storm-centered DARFs are estimated for individual events, they can capture the anisotropy of the rainfall field (i.e., the storm shape and orientation) and the seasonal effect of atmospheric processes such as the jet stream affecting speed and direction of storms. As with any method, the storm-centered approach can depend heavily on the sample size and types of storms included. Srikathan (1995) and Olivera et al. (2005 and 2008), emphasize that the expected storm characteristics and seasonal trends may not be represented by their storm sample from only 2 years of data even though a large geographical area was covered, i.e. 265,000 mi^2.

A variant to the storm-centered approach is one that centers on individual storm cells captured in each ~5-min duration radar scan. These storm cells have movement and with sufficient elapsed time, produce a storm total. Curtis (2001, 2007) applied the storm-cell method using the TITAN software package (Dixon and Wiener, 1993) designed for targeting storms. The storm-cell approach was used by Curtis to develop DARFs for urban stormwater management applications, and specifically for the City of Colorado Springs, CO (City of Colorado Springs, 2013). The areal reduction found was much higher than those obtained from storm total maps of any duration greater than the 5-min radar scan intervals. This deviation in approach from well-accepted methodologies is presented by Curtis as an equivalent means to obtain DARFs for a storm total, which is not supportable. The *cell-centered*, i.e. each volume scan, approach applied by Curtis does not have applicability to basin hydrology or the intended usage envisioned in this project, and is not considered further.

A component of probable maximum precipitation (PMP) studies is an estimate of the depth area reduction factor. The approach developed for PMP application involves distributing point rainfall to areas by means of concentric ellipses. These ellipses are assumed to have a major to minor axis ratio of 2.5:1 elongated in the direction of storm movement (as in Hydrometeorological Reports 51 and 52). Depth area duration curves are utilized to determine the PMP depth for a given area and duration. The events that are typically used for PMP studies are usually more intense than storms typically used for highway design purposes. However, they do provide another independent dataset that can be used for verification purposes. Events specified in

Hydrometeorological Report 49 (Hansen et al., 1984) will be compared with the derived DARFs from this research project. Recently, Wright et al. (2014) provided a critical review of the use of DARFs based on the TP-29 methodology, and showed that classifying storm types has a large impact on the DARF relationships. Storm classification is an important component of developing a list of storms for analysis and will be evaluated during selection. Schaefer (2013) presented research on PMP studies that could be relevant to DARF estimation. His research emphasizes the use of the "isopercentile" method that uses climatological rainfall patterns to adjust the spatial distribution of rainfall interpolated for severe events used in PMP studies. Riley and Moore (2014) use a similar method to adjust historic storms based on elevation and dewpoint. However, *moisture maximization* is a common element of PMP storm development, but has less applicability to this project. The influence of elevation on the DARF relationship will be identified during Task 2 of this project.

The question of whether the depth-area relationship changes for a given depth and its corresponding return period is motivated from the application of the DARF to design problems where rainfall depth of specific return period is used to model and design infrastructure such as bridges carrying transportation routes. Asquith (1999) and Asquith and Famiglietti (2000) found dependency of the DARFs on geographic location and increasing values as the storm recurrence interval increased. Allen and DeGaetano (2005) analyzed rain gauge networks in New Jersey and North Carolina, and found statistically-significant variation in DARFs with return period, though somewhat slight. Higher return periods associated with greater rainfall depths exhibited greater reduction, which is in agreement with the results of Bell (1976, 1987), Omolaya (1993), and Asquith and Famiglietti (2000).

Representation of the precipitation field as isotropic ignores storm movement, and in particular direction. Statistical analysis often ignores this characteristic because they are largely based on geographically-fixed DARFs derived from rain gauge networks that cannot adequately detect storm movement over a small area of point measurements within the network. Rodriguez-Iturbe and Mejia (1974) proposed that DARFs depend solely on correlation between the precipitation depths at two randomly chosen points, which does not address potential anisotropy present in rainfall depth fields. Sivapalan and Blöschl (1998) proposed constructing intensity-duration-frequency (IDF) curves from an extreme value distribution. De Michele et al. (2001) calculate DARFs of extreme rainfall events from their spatial and temporal scaling and statistical self-affinity.

Radar data has proven to be useful in characterizing storm structure for hydrologic applications. Durrans et al. (2002a, b, c) relied on a methodology similar to TP-29 but using NEXRAD data to derive DARFs over a 7-year period. Gill (2005) calculated DARFs for different regions of Texas, storm durations, storm areas, precipitation depths, storm shapes and orientations, and seasons using radar. Vieux and Associates, Inc. (VAI) has been utilizing radar rainfall for hydrologic applications since 1992. Operational systems include the Florida Rain Gauge Network Optimization study (Vieux, 2005), City of Austin Flood Early Warning System (Looper et al., 2012), the Flood Alert System for the Texas Medical Center (Bedient et al., 2003; Vieux and Bedient, 2004; Looper and Vieux, 2013). VAI has utilized NEXRAD data to refine design storms used for sizing hydraulic structures for the Metropolitan Sewer District of Greater Cincinnati (Mosio and Vieux, 2013) the City of Baltimore (Vieux, 2012), and the Hampton

Roads Sewer District (Vieux, 2014). The latter study involved developing DARFs from radar storm totals that showed greater reductions than found in TP-29.

In general, it can be observed that geographically-fixed DARFs are the result of statistically processing precipitation data from rain gauges, and then calculating DARF values. In contrast, storm-centered DARFs are the result of processing spatially continuous data, e.g. radar, and calculating DARF values for each storm to find a statistically reliable relationship of point to area rainfall depths. Depending on the statistical analysis, the DARF obtained from radar may be similar to TP-29 reduction values, as with Durrans et al. (2002a, b, c); or the DARFs may exhibit greater reductions when individual storm structure are considered.

3. RECOMMENDED APPROACH

Our approach will focus on each HHA and identify the temporal and spatial distribution specific to storms in Nevada affecting NDOT drainage structures. Potential benefits of the approach include improved sizing of culverts and bridges based on design storms that are representative of the local hydrometeorological conditions. The recommended storm analysis approach can be divided into temporal and spatial distribution of rainfall described as follows.

3.1 Temporal Distribution

The approach to developing temporal distributions from available rain gauge networks will rely on grouping by HHA for distribution in areas where gauges do not exist. The boundaries of the HHAs from the NOAA Atlas 14 will then be compared to the additional rain gauge networks to ensure that the boundaries take into account hydrologically significant physiography such as watershed boundaries and elevation. Next, storms will be determined for each of the HHAs using all available rain gauge networks available in each HHA. Storm properties such as depth, duration, intensity, and temporal distribution will be calculated from the historic gauge record. Dimensionless hyetographs will then be created using the temporal distribution for each storm event centered at its maximum intensity. The median of these centered hyetographs will be computed to obtain the most representative hyetograph for each HHA.

3.2 Spatial Distribution

Development of point-to-area reduction will rely on storm totals developed for areas where coverage exists from radar. Evaluation of representative DARFs will be based on a storm-centered approach using a large number of individual storms classified by type, season, and elevation. Seasonal variations will be accounted for by segmenting and analyzing storm characteristics from summertime convective periods, and wintertime storms. The anisotropy of storms will be evaluated from radar storm total imagery and appropriate recommendations made. DARFs for storms will be aggregated by HHAs in an effort to account for elevation and geographic location within Nevada. Actual storm areal distributions will be used to identify orographic enhancement and its effects on spatial distribution or rainfall. Finally, DARFs will be compared to actual storm events and previous studies to ensure the factors are representative of Nevada's storm characteristics.

4. REFERENCES

1. Adams, D.K., and A.C. Comrie, 1997. "The North American Monsoon." *Bull. Amer. Meteor. Soc.*, 78, 2197–2213.
2. Adams, J.L., and D.J. Stensrud, 2007. "Impact of tropical easterly waves on the North American monsoon." *J. Climate*, 20, 1219-1238.
3. Allen, R. J., and A. T. DeGaetano, 2005. "Areal Reduction Factors for Two Eastern United States Regions with High Rain-Gauge Density." *Journal of Hydrologic Engineering* 10 (4): 327–325.
4. Asquith, W. H., 1999. "Areal-Reduction Factors for the Precipitation on the 1-Day Design Storm in Texas." Water-Resources Investigations Report: 99–4267.
5. Asquith, W.H., and J. S. Famiglietti, 2000. "Precipitation Areal-Reduction Factor Estimation Using an Annual-Maxima Centered Approach." *Journal of Hydrology* 230 (1-2): 55–69.
6. Austin, P. M., and R. A. Houze, 1972. "Analysis of the Structure of Precipitation Pattern in New England." *Journal of Applied Meteorology* 11: 926–35.
7. Bacchi, B., and R. Ranzi, 1996. "On the Derivation of Areal Reduction Factors of Storms." *Atmospheric Research* 42: 123–35.
8. Bedient, P. B., A. Holder, J. A. Benavides, and B.E. Vieux, 2003. "Radar-Based Flood Warning System Applied to Tropical Storm Allison." *Journal of Hydrologic Engineering* 8 (6): 308–18.
9. Bedient, P. B., W.C. Huber, B.E. Vieux, 2013. *Hydrology and Floodplain Analysis.* Fifth Edition, Prentice-Hall, Inc., One Lake St., Upper Saddle River, NJ 07458. ISBN 0-13-256796-2. p. 801.
10. Bell, F. C., 1976. "The Areal Reduction Factors in Rainfall Frequency Estimation." NERC Report No. 35.
11. Bell, T. L., 1987. "A Space-Time Stochastic Model of Rainfall for Satellite Remote Sensing Studies." *Journal of Geophysical Research*: 9631–44.
12. Bonnin, G.M., D. Martin, B. Lin, T. Parzybok, M. Yekta, D. Riley, 2004. "Precipitation frequency atlas of the United States." NOAA Atlas 14, National Weather Service, Silver Spring, Maryland.
13. Brenner, I. S., 1974. "A surge of maritime tropical air—Gulf of California to the southwestern United States." *Mon. Wea. Rev.*, 102, 375–389.
14. Clark County Regional Flood Control District, 1999. "Hydrologic Criteria and Drainage Design Manual."
15. City of Colorado Springs, 2013. "Drainage Criteria Manual." Volume 1.
16. Curtis, D. C., 2001. "Storm Sizes and Shapes in the Arid Southwest." In Proceedings of the Arizona Floodplain Management Association, Fall 2001 Meeting, 10 (6): 785–97.
17. Curtis, D. C., 2007. "Evaluation of the Spatial Structure of Storms and the Development of Design Storms." In World Environmental and Water Resources Congress 2007@ Restoring Our Natural Habitat, 1–10. ASCE. http://ascelibrary.org/doi/abs/10.1061/40927(243)286.
18. Daly, C. and K. Bryant, 2013. "The PRISM Climate and Weather System – An Introduction."
19. De Michele, C., N. Kottegoda, and R. Rosso, 2001. "The Derivation of Areal Reduction Factor of Storm Rainfall from Its Scaling Properties." *Water Resources Research* 37 (12):

3247–52.
20. Dixon, M., and G. Wiener, 1993. “TITAN: Thunderstorm Identification, Tracking, Analysis, and Nowcasting-A Radar-Based Methodology.” *Journal of Atmospheric and Oceanic Technology* 10 (6): 785–97.
21. Douglas, M. W., R. A. Maddox, K. Howard, and S. Reyes, 1993. "The Mexican monsoon." *J. Climate*, 6, 1665–1678.
22. Durrans, S. R., L. T. Julian, and M. Yekta, 2002. “Estimation of Depth Area Relationships Using Radar Data.” *Journal of Hydraulic Engineering* 7 (5): 356–67.
23. Frederick, R. H., V. A. Myers, and E. P. Auciello, 1977. “Storm Depth Area Relations from Digitized Radar Returns.” *Water Resources Research* 13 (3): 675–79.
24. Gill, T. D., 2005. “Transformation of Point Rainfall to Areal Rainfall by Estimating Areal Reduction Factors, Using Radar Data, for Texas”. Master of Science Thesis Submitted to Texas A&M University Civil Engineering.
25. Guo, J., 2011. “Storm Centering Approach for Flood Predictions from Large Watersheds.” *Journal of Hydrologic Engineering* 17 (9): 960–64.
26. Hales, J. E. 1972. "Surges of maritime tropical air northward over the Gulf of California." *Mon. Wea. Rev.*, 100, 298–306.
27. Hansen, E. M., L. C. Schreiner, and J. F. Miller, 1982. “Application of Probable Maximum Precipitation Estimates, United States East of the 105th Meridian.” Hydrometeorological Report No. 51.
28. Hansen, E. M., F.K. Schwarz, and J.T. Riedel, 1984. “Probable Maximum Precipitation Estimates, Colorado River and Great Basin Drainages”. Hydrometeorological Report No.49.
29. Hansen, E. M., D. D. Fenn, L. C. Schriner, R. W. Stodt, and J. F. Miller, 1988. “Probable Maximum Precipitation Estimates - United States between the Continental Divide and the 103rd Meridian.” Hydrometeorological Report No. 55A.
30. Hershfield, D. M., 1961a. “Estimating the Probable Maximum Precipitation.” Proceedings ASCE, Journal of Hydraulics Division 87: 99–106.
31. Hershfield, D. M., 1961b. “Rainfall Frequency Atlas of the United States for Durations from 30 Mins to 24 Hours and Return Periods from 1 Year to 100 Years.” Tech. Memo 40.
32. Higgins, R. W., Y. Yao, and X. L. Wang, 1997. "Influence of the North American monsoon system on the U.S. summer precipitation regime." *J. Climate,* 10, 2600–2622.
33. Higgins, R. W., K. C. Mo, and Y. Yao, 1998. "Interannual variability of the U.S. summer precipitation regime with emphasis on the southwestern monsoon." *J. Climate*, 11,2582–2606.
34. Ho, F. P., and J. T. Reidel, 1980. “Seasonal Variation of 10 Sq. Miles, Probable Maximum Precipitation Estimates - United States East of the 105th Meridian.” Hydrometeorological Report No. 53.
35. Houghton, J. G., 1969. "Characteristics of Rainfall in the Great Basin." Desert Research Institute, Reno, 205 pp.
36. Houghton, J. G, C. M. Sakamoto, and R. O. Gifford, 1975. Nevada’s Weather and Climate. Vol. 2. NV Bureau of Mines & Geology.
37. Jeton, A. E., S. A. Watkins, T. J. Lopes, and J. Huntington, 2014. “Evaluation of Precipitation Estimates from PRISM for the 1961-90 and 1971-2000 Data Sets, Nevada.” Accessed February 24. http://pubs.usgs.gov/sir/2005/5291/.

38. Kaplan, M.L., C.S. Adaniya, P.J. Marzette, K. C. King, S.J. Underwood, J.M. Lewis, 2009. "The Role of Upstream Midtropospheric Circulations in the Sierra Nevada Enabling Leeside (Spillover) Precipitation. Part II: A Secondary Atmospheric River Accompanying a Midlevel Jet." *J. Hydrometeor.*, 10, 1327–1354
39. Koutsoyiannis, D., 1999. "A Probabilistic View of Hershfield's Method for Estimating Probable Maximum Precipitation." *Water Resources Research* 35 (4): 1313–22.
40. Li, J., R. A. Maddox, X. Gao, S. Sorooshian, K. Hsu. 2003. "A Numerical Investigation of Storm Structure and Evolution during the July 1999 Las Vegas Flash Flood." *Mon. Wea. Rev.*, 131, 2038–2059.
41. Looper, J. P, and B. E. Vieux, 2012. "An Assessment of Distributed Flash Flood Forecasting Accuracy Using Radar and Rain Gauge Input for a Physics-Based Distributed Hydrologic Model." *Journal of Hydrology* 412: 114–32.
42. Looper, J. P, B. E. Vieux, and M. A. Moreno, 2012. "Assessing the Impacts of Precipitation Bias on Distributed Hydrologic Model Calibration and Prediction Accuracy." *Journal of Hydrology* 418: 110–22.
43. Looper, J. P., and B. E. Vieux, 2013. "Distributed Hydrologic Forecast Reliability Using Next-Generation Radar." *Journal of Hydrologic Engineering*.
44. Lopes, T. J., and K. K. Allander, 2009a. Hydrologic Setting and Conceptual Hydrologic Model of the Walker River Basin, West-Central Nevada. US Geological Survey. http://pubs.usgs.gov/sir/2009/5155/.
45. Lopes, T. J., and K. K. Allander, 2009b. Water Budgets of the Walker River Basin and Walker Lake, California and Nevada. US Geological Survey. http://pubs.usgs.gov/sir/2009/5157/.
46. Lundquist, J. D., J. R. Minder, P. J. Neiman, and E. Sukovich, 2010. "Relationships between Barrier Jet Heights, Orographic Precipitation Gradients, and Streamflow in the Northern Sierra Nevada." *Journal of Hydrometeorology* 11 (5): 1141–56. doi:10.1175/2010JHM1264.1.
47. Maddox, R. A., F. Canova, and L. R. Hoxit, 1980. "Meteorological characteristics of flash flood events over the western United States." *Mon. Wea. Rev.*, 108, 1866–1877.
48. Miller, J. F., R. H. Frederick, and R. J. Tracey, 1973. "NOAA Atlas 2, Precipitation-Frequency Atlas of the Western United States".
49. Mosio, S. and B. Vieux, 2013. "Design Storm Analysis and Storm Builder." Technical Memorandum. Metropolitan Sewer District of Greater Cincinnati.
50. Nevada Department of Transportation (NDOT), 2006. "Drainage Manual." 2nd Edition. Prepared by: Hydraulics Section. December 2006.
51. National Climatic Data Center, 2014."Storm Events Database." 2014. Accessed March 14. https://www.ncdc.noaa.gov/stormevents/.
52. National Oceanic and Atmospheric Administration (NOAA), 1985. "Narrative Summaries, Tables and Maps for Each State with Overview of State Climatologist Programs Third Edition. Volume 1: Alabama-New Mexico, Volume 2: New York-Wyoming." 1985 - Gale Research Company.
53. Olivera, F., J. Choi, D. Kim, and M. Li, 2005. *Calculation of Areal Reduction Factors using NEXRAD Precipitation Estimates.* College Station, TX. Texas Transportation Institute. FHWA/TX-07/0-4642-3.
54. Olivera, F., J. Choi, D. Kim, and M.Li, 2008. "Estimation of Average Rainfall Areal Reduction Factors in Texas Using NEXRAD Data." *Journal of Hydrologic Engineering*

13 (6): 438–48.
55. Omolayo, A.S., 1993. “On the Transposition of Areal Reduction Factors for Rainfall Frequency Estimation.” *Journal of Hydrology* 145 (1): 191–205.
56. Peck, E.L. and E.A. Richardson, 1962. An Analysis of the Causative Factors of the February 1962 Floods in Utah and Eastern Nevada." *Mon. Wea. Rev.*, 90, 407–413.
57. Parzybok, T. W., and E. M. Tomlinson, 2006. “A New System for Analyzing Precipitation from Storms.” *Hydro Review*, Vol. XXV, No. 3, 58-65.
58. Randerson, D., 1976. "Meteorological analysis for the Las Vegas, Nevada, flood of 3 July 1975." *Mon. Wea. Rev.*, 104, 719–727.
59. Riley, R. C., and J. N. Moore, 2014. “Storm Distribution Developed from World Curve Data and It’s Potential Areal Application.” Accessed February 24. https://www.nrcs.usda.gov/Internet/FSE_DOCUMENTS/16/nrcs143_014770.pdf.
60. Rodriguez-Iturbe, I., and H. M. Mejia, 1974. “On the Transformation of Point Rainfall to Areal Rainfall.” *Water Resources Research* 10 (4): 729–35.
61. Schaake, J., A. Henkel, and S. Cong, 2004. “Application of PRISM climatologies for hydrologic modeling and forecasting in the western U.S.” Proc., 18th Conf. on Hydrology, American Meteorological Society, Boston, 5.3.
62. Schaefer, M, 2013. “Regional Precipitation-Frequency Analysis and Extreme Storms Including PMP Current State of Understanding/Practice.” NRC Workshop- Probabilistic Flood Hazard Assessment.
63. Siriwardena, L., and P. E. Weinmann, 1996. “Development and Testing of Methodology to Derive Areal Reduction Factors for Long Duration Rainfalls.”
64. Sivapalan, M., and G. Blöschl, 1998. “Transformation of Point Rainfall to Areal Rainfall: Intensity-Duration Frequency Curves.” *Journal of Hydrology* 204 (91): 150–67.
65. Srikanthan, R, 1995. “A Review of the Methods for Estimating Areal Reduction Factors for Design Rainfalls.” Cooperative Research Center for Catchment Hydrology 3 (3): 1–15.
66. Underwood, S. J., M.L. Kaplan, K.C. King, 2009. "The Role of Upstream Midtropospheric Circulations in the Sierra Nevada Enabling Leeside (Spillover) Precipitation. Part I: A Synoptic-Scale Analysis of Spillover Precipitation and Flooding in a Leeside Basin." *J. Hydrometeor.*, 10, 1309–1326.
67. U.S. Weather Bureau, 1957. “Rainfall Intensity-Frequency Regime - Part 1: The Ohio Valley”, Technical Paper No. 29 (TP-29), Washington, D.C.
68. U.S. Weather Bureau, 1958a. “Rainfall Intensity-Frequency Regime - Part 2: The Southeastern United States”, Technical Paper No. 29 (TP-29), Washington, D.C.
69. U.S. Weather Bureau, 1958b. “Rainfall Intensity-Frequency Regime - Part 3: The Middle Atlantic Region”, Technical Paper No. 29 (TP-29), Washington, D.C.
70. U.S. Weather Bureau, 1959. “Rainfall Intensity-Frequency Regime - Part 4: The Northeastern United States”, Technical Paper No. 29 (TP-29), Washington, D.C.
71. U.S. Weather Bureau, 1960. “Rainfall Intensity-Frequency Regime - Part 5: The Great Lakes Region”, Technical Paper No. 29 (TP-29), Washington, D.C.
72. U.S. Weather Bureau, 1964. “Two to Ten Day Precipitation for Return Periods of 2 to 100 years in the Contiguous United States”, Technical Paper No. 49 (TP-49), Washigton, D.C.
73. Vieux, B.E., and P.B. Bedient, 2004. “Assessing Urban Hydrologic Prediction Accuracy through Event Reconstruction.” *Journal of Hydrology* 299 (3): 217–36.

74. Vieux, B.E., and J.E. Vieux, 2005. “Statistical Evaluation of a Radar Rainfall System for Sewer System Management.” *Atmospheric Research* 77 (1): 322–36.
75. Vieux, B.E., 2012. "Development of a Local Design Storm for the City of Baltimore, Maryland." Technical Memorandum. City of Baltimore, Maryland.
76. Vieux, B. E., 2014. "Design Storm Analysis and Storm Event Characterization." Technical Memorandum. Hampton Roads Sanitation District.
77. Welborn, T., 2013. “USGS Nevada Water Science Center — Nevada Flood Chronology.” Accessed March 10, 2014. http://nevada.usgs.gov/crfld/.
78. Wright, D. B., J. A. Smith and M. L. Baeck, 2014. “A critical examination of areal reduction factors, J. of Hydrological Engineering”, in press.
79. Young, C. B., 2002. “Comparing NEXRAD Operational Precipitation Estimates and Raingage Observations of Intense Precipitation in the Missouri River Basin.” In AGU Spring Meeting Abstracts, 1:17.
80. Zorn, R. J., 2013. “Nevada.” Encyclopedia Britannica Online. Retrieved 10 March, 2014, from http://www.britannica.com/EBchecked/topic/411016/Nevada.

TECHNICAL MEMORANDUM

To: Dr. Annjanette Dodd, Ph.D., P.E.
Kimley-Horn and Associates

From: Dr. Baxter Vieux, Ph.D., P.E.
Vieux & Associates, Inc.

Date: October 6, 2014

Re: Nevada Department of Transportation, Research Project No. P530-13-803
Streamlining Hydrologic Prediction Processes Using New and More Accurate Techniques and Methods. – Design Storm Hyetograph

1 Purpose

This Technical Memorandum (TM) is the third in a series of TM's being generated for the Nevada Department of Transportation research project (Project) titled, "*Streamlining Hydrologic Prediction Processes Using New and More Accurate Methods*" (#P530-13-803). The overall purpose of the Project is to streamline hydrologic prediction for design of NDOT drainage infrastructure by establishing a design storm that is more representative of storms across the state of Nevada. The purpose of this Technical Memorandum is to present the methodology and results used to derive the design storm hyetographs for the study area from the temporal distribution for each storm event recorded at the relevant precipitation gauges.

2 Methodology

2.1 Precipitation Gauge Data

Rain gauge and radar data sources were identified in the Data Plan TM. The Data Plan summarized the available rain gauge and radar sources available for both the summer and winter periods for Nevada. The storm events culled from these sources were further evaluated here to determine the applicability for deriving design storm hyetographs.

2.2 Design Storm Hyetograph Development

The methodology for developing design storm hyetographs was presented in the first TM, *Review of Past Methods and Recommended Approach*. The approach relies on assembling data by Hydrometeorological Homogeneous Area (HHA). Within these HHA groupings, rain gauges exhibit similar statistical characteristics. Figure 1 shows the HHAs and rain gauge networks used for analysis. Storm events were determined from the gauges in each HHA. A storm event is

defined as having an accumulation of at least 0.01 inches and no rainfall for a period greater than 6 hours between events. Incremental rainfall data, for each gauge, were used for segmentation into discrete storm periods with a minimum inter-event time of 6 hours. A cumulative hyetograph was developed for each storm event, consisting of accumulated rainfall depth versus time for the event duration. These hyetographs were then made dimensionless by dividing each depth by the total depth, and each time step by the total duration. The resulting dimensionless hyetograph represents the percentage depth versus percentage duration. Each hyetograph was then classified according to the quartile - the quarter of the event duration during which the maximum accumulation of rainfall occurred. Each storm event was then characterized by quartile, duration, depth, average intensity, and maximum hourly accumulation.

In order to make comparisons of hyetograph shapes between HHAs, the 50^{th} (median) and 90^{th} percentile hyetographs were determined from the multitude of storm event hyetograph shapes for every gauge in each HHA. This was done by shifting each storm event hyetograph in time so that the 50% depth point is the same for each event. The 50% depth point is the time when 50% of the overall precipitation has accumulated for that event. This aligns the events, capturing the peak rainfall intensities for each event at the same time. The result is a group of hyetographs that can be used to determine a median hyetograph that will be representative of the significant storms at a gauge. Once shifted, a median or greater percentile can be computed without smoothing of the data. Another method used by Huff (1990) divided storms into quartiles, in an attempt to mitigate smoothing of irregular shaped cumulative hyetographs. However, the shifting of specific hyetographs effectively reduces such smoothing associated with computation of median hyetographs. Each median hyetograph was then normalized to a depth and duration between 0 and 1 (i.e., made dimensionless). The dimensionless median hyetograph can then be analyzed for the more significant storms, i.e. those that accumulate more than some threshold amount, i.e. 0.25 or 0.5 inches.

A key characteristic of the dimensionless hyetograph is the maximum slope (maximum increase in percentage depth versus percentage duration), which is when the maximum intensity occurred during that event. For a dimensionless median hyetograph this maximum intensity is referred to as the median maximum intensity (MMI). The MMI was used to evaluate the seasonality of the storm events in the study area to identify whether summertime convection dominates everywhere or if higher intensities in northern latitudes occur during the winter. The monthly dimensionless median hyetograph with the steepest slope is assumed the controlling month that would result in the greatest rainfall intensities for that gauge location. From a hydrologic design standpoint, months with lesser intensities were not viewed as important.

The design hyetograph duration is defined by the watershed characteristic's governing the peak discharge runoff response. These durations are related to the *time of concentration* of runoff in a particular drainage network. The applicable design storm duration was determined based on the

time of concentration for the Nevada watersheds intersecting NDOT primary roads. The duration, quartile, and MMI, among other descriptive statistics, are investigated to develop representative hyetographs in Nevada, as described in the following sections.

3 Results

3.1 Precipitation Gauge Data

This section summarizes the precipitation gauge networks used to determine the storm event properties and hyetograph characteristics. Incorporating a diversity of rain gauge networks was necessary to cover the state geographically.

The main rain gauge networks used in this study are operated by the National Weather Service (NWS), Federal Aviation Administration (FAA), the Department of Defense (DOD), US Forest Service, the Bureau of Land Management, and Clark County Regional Flood Control District (CCRFCD).

The NWS Cooperative Observer Program (COOP) program is a nationwide observation network established in 1890. COOP data are recorded on a sub-hourly to daily basis, and sent to the National Climatic Data Center (NCDC) for archival storage. Hourly and sub-hourly COOP gauge data were compiled at gauges that had reliable rainfall information. Compiling sub-hourly data, at 15-minute increments was necessary to determine an accurate hyetograph shape for shorter duration events.

The Automated Surface Observing System (ASOS) gauges are located mainly at airports and are operated by the NWS, FAA, and DOD. Although the ASOS gauges tend to have a shorter and more recent period of record available for download, they are generally a reliable network and provide valuable data for this study.

Besides the COOP and ASOS gauge networks, the other networks used were the Remote Automated Weather Stations (RAWS) operated by the US Forest Service and Bureau of Land Management, as well as rain gauges in and around Clark County in southern Nevada operated by CCRFCD.

Other networks considered, but not used due to data limitations, include California Data Exchange Commission (CDEC), the Nevada Department of Transportation (NDOT) Road Weather Information System (RWIS), the National Resources Conservation Service (NRCS) observing stations known as SNOwpack TELemetry or SNOTEL, National Oceanic and Atmospheric Administration (NOAA) Special Operations and Research Division (ARL-SORD), Community Environmental Monitoring Program (CEMP), Desert Research Institute (DRI), and the Hydrometeorological Automated Data System (HADS).

There are a total of 371 unique gauge locations, in or Near Nevada, applicable to this study (Table 1). The records at each of these gauges were evaluated and it was determined that of these 371 gauges, only 147 have sufficiently reliable records with hourly or sub-hourly interval data. In the case of the CCRFCD gauges, those used here were chosen based on both spatial

distribution and a representative range of elevation from 400 to 9000 ft. msl. The precipitation data derived from the rain gauge networks are mostly at hourly intervals (COOP, ASOS, and RAWS) with some at 5-minute (CCRFCD) or 15-minute intervals (COOP).

Table 1 summarizes the gauge sources that were available in the project along with the maximum period of record possible for each gauge source. Figure 1 shows the location of gauges used from the COOP, ASOS, RAWS, and CCRFCD networks. Appendices A-1 through A-3 contain detailed information on the gauge networks. Considering the 147 gauges selected and the total area of Nevada at 110,567 square miles, the network density is approximately one gauge per 752 sq. mi., or an average spacing of 27 mi., neglecting local variations associated with clustering.

Table 1 Period of record for gauge sources in Nevada

Gauge Source	Description	Continuous Period of Record	No. of Gauges Possible	No. of Gauges Used
COOP Hourly	The National Weather Service (NWS) Cooperative Observer Program	1948 - 2012	68	20
COOP 15-min	The National Weather Service (NWS) Cooperative Observer Program	1971 - 2013	59	48
ASOS	Automated Surface Observing System	1996 - 2012	11	6
CCRFCD	Clark County Regional Flood Control District	1988 - 2014	177	24
RAWS	Remote Automated Weather Stations	1997 - 2014	56	49
		Totals =	371	147

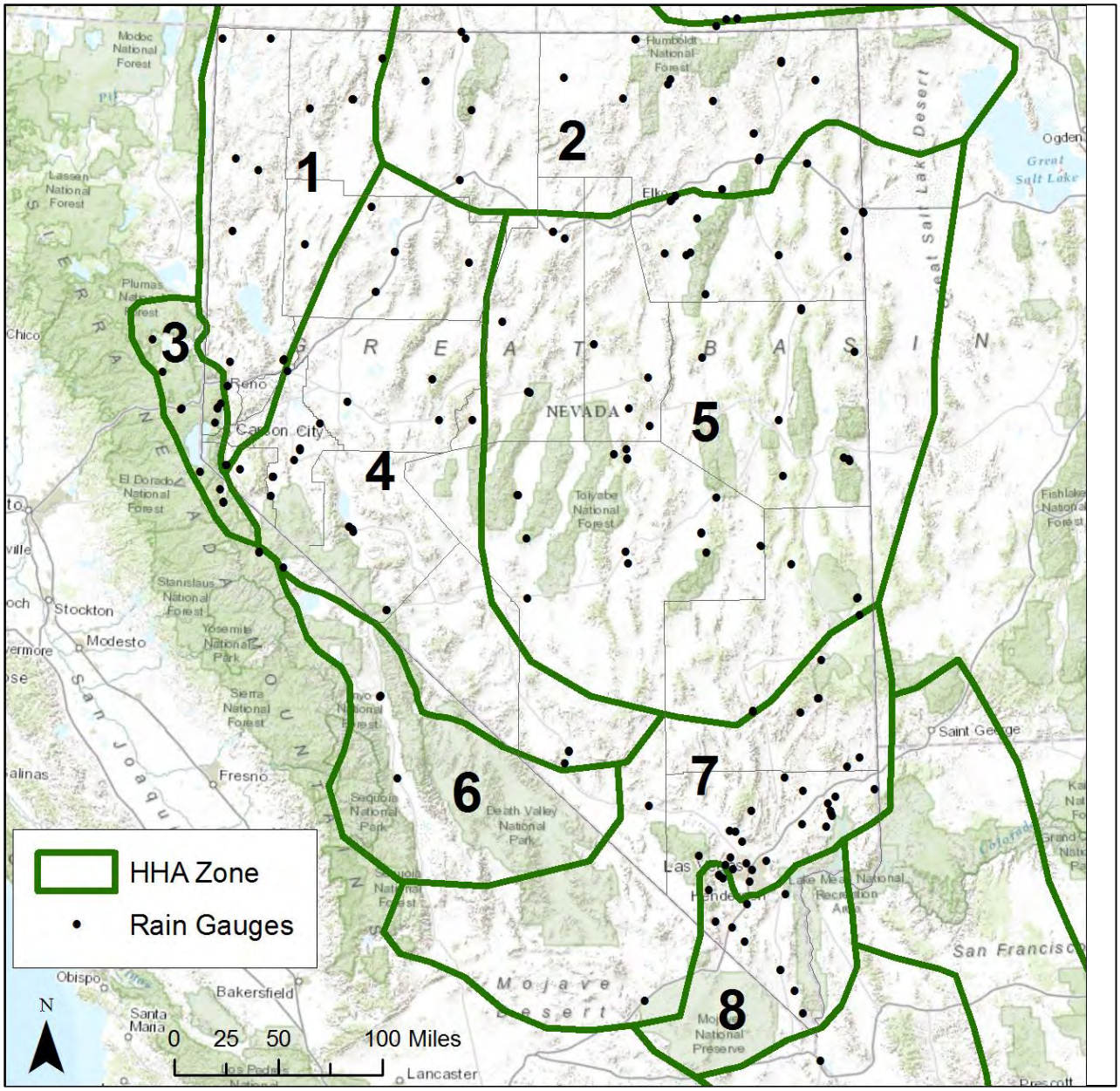

Figure 1 Combined precipitation gauges from COOP, ASOS, RAWS, and CCRFCD networks

Any given rainfall event over a specific HHA can be widespread or isolated, affecting multiple gauges or only one gauge. To get an idea of the approximate number of unique events across each HHA, the individual event lists for storm events accumulating more than 0.25 inches for each hourly COOP and ASOS gauge were merged together into a single chronology of events. Figure 2 shows the monthly distribution of storm events accumulating more than 0.25 inches found in HHA 1 and 8. The seasonal pattern of storm events differs among the HHAs with a pronounced summertime resurgence in July and August in HHA 7 and 8, which happens to coincide with the peak months of the North American Monsoon (NAM). The northern HHAs, such as 1 and 3, show a larger number of events in winter compared to summer when Pacific Systems tend to dominate precipitation generation. These and the other HHA distributions are in

Appendix A-4. The seasonal histograms indicate that most of the rainfall events with accumulations ≥ 0.25 inches are more likely to occur across western Nevada during the winter months, while eastern Nevada is more likely to be impacted by summertime convection during the NAM season.

Figure 3 is a plot of the annual number of events during the period of record for hourly ASOS and COOP gauges in HHA 1 and 8. These plots and those from the remaining HHAs are in Appendix A-5. While the total number of events for a given year can be impacted by the number of gauges available, a cyclic tendency is observed, particularly in HHA 1. The evident decrease in the number of events during the last half of the period compared to the first across HHA 2 is likely because less hourly gauges were available in the most recent period. In all HHAs, while the number of events is variable, there appears to be an adequate number of years to capture rainfall statistics.

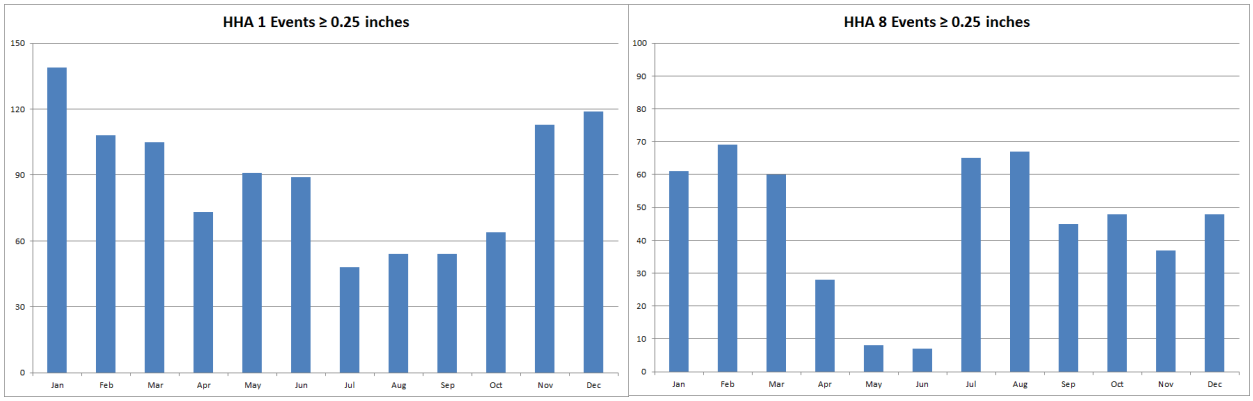

Figure 2 Distribution of storms by month for HHA 1 and 8, based on hourly COOP and ASOS gauge data.

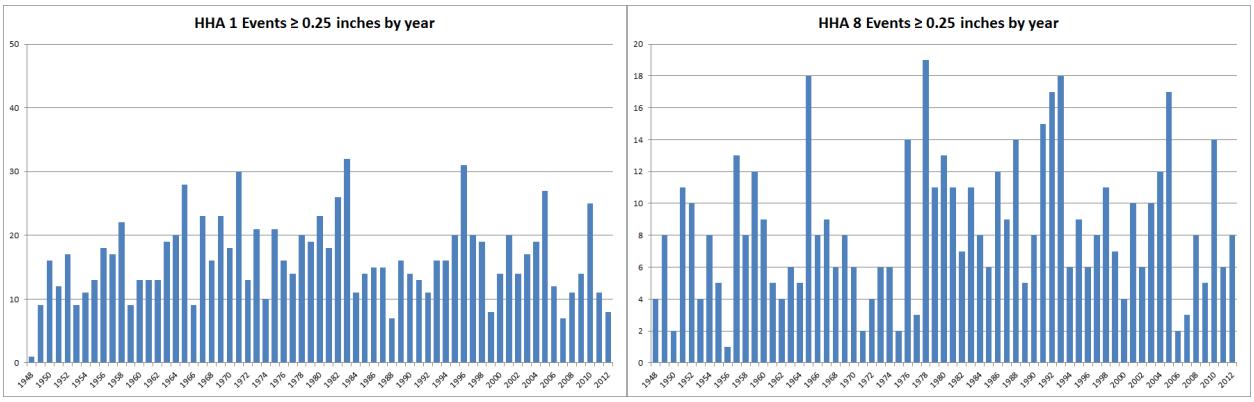

Figure 3 Annual number of storms distributed over the period of record for HHA 1 and 8, based on hourly COOP and ASOS gauge data.

Table 2 shows the total number of events ≥ 0.25 inches for each HHA based on the COOP, ASOS, RAWS, and CCRFCD gauge networks as a whole. The total number of events can be

impacted by factors such as climatology, location, the size of the zone, the number of gauges in the zone, and the period of record of the gauges. The number of events for any specific gauge is likely to be much less than the overall total since a single gauge will not be affected by every rainfall event that impacts a given HHA.

Table 2 Total number of rainfall events ≥ 0.25 for each HHA

HHA	No. of Events
1	3802
2	5764
3	8063
4	4166
5	12424
6	617
7	4497
8	2591

3.2 Storm Event Descriptive Statistics

The 5-minute, 15-minute, and hourly gauge data were compiled for events that had at least 0.25 inches, and period of no rainfall greater than 6 hours. There were a total of 41,924 events with rainfall greater than 0.25 inches. After investigating the shape of the dimensionless hyetographs for these events, it was decided that a larger threshold of 0.50 inches and a duration of at least one hour for sub-hourly gauges and four hours for hourly gauges would be more appropriate. This higher threshold was necessary to ensure that the dimensionless hyetographs were not being overly influenced by small rainfall events, considered not relevant to design storm applications.

Using this increased threshold reduced the number of storm events to 16,771 and the total number of gauges to 147. Table 3 provides the descriptive statistics for the events used to calculate the dimensionless hyetographs. The mean depths range from 0.8 to 1.2 inches with a mean duration between 12.7 and 18.5 hours. These statistics were compiled for hourly data, thus, minimum duration was 1 hour, except in HHA 6, which was 3.25 hrs. The storm event maximum duration ranged from 73 to 198 hours, and maximum depth from 10.5 to 20.0 inches. The storm event threshold of 0.5 inches is roughly half of the mean event rainfall depth statewide.

Table 3 Descriptive statistics for events used to calculate dimensionless hyetographs

HHA	No. of Gauges	No. of Events	Mean Depth (in)	Median Depth (in)	Min Depth (in)	Max Depth (in)	Mean Duration (hrs)	Median Duration (hrs)	Min Duration (hrs)	Max Duration (hrs)
1	14	1371	0.8	0.7	0.5	10.5	15.3	13.0	1	83
2	16	1747	0.8	0.65	0.5	12.4	14.9	13.0	1	80
3	10	4445	1.2	0.8	0.5	13.1	18.5	15.0	1	181
4	20	1502	0.8	0.7	0.5	15.1	12.7	11.0	1	65
5	45	4206	0.8	0.66	0.5	20.0	13.5	11.5	1	76
6	2	304	1.1	0.78	0.5	5.9	15.8	13.0	3.25	73
7	27	1986	0.9	0.75	0.5	10.7	14.4	12.9	1	143
8	13	1210	1.0	0.8	0.5	10.9	14.2	12.0	1	198
Statewide	147	16771	0.9	0.7	0.5	20.0	15.2	13	1	198

3.3 Dimensionless Median Hyetograph Development

Dimensionless hyetographs were developed for each gauge as follows:

1) Cumulative hyetographs were compiled for all storm events at a gauge with rainfall accumulation $\geq$ 0.5 inches. An example is summarized in Figure 4a.
2) The cumulative hyetographs were then shifted in time so that the 50% depth point was the same for each event. An example is summarized in Figure 4b.
3) The shifted cumulative hyetographs were then normalized by depth and duration to create a group of dimensionless hyetographs. Figure 5a shows the same hyetographs as Figure 4a, but normalized by depth and duration.
4) Finally, the dimensionless median hyetograph was determined by computing the median and greater percentile depths at each time, from 0-1. An example median hyetograph is shown in Figure 5b.

The monthly dimensionless median hyetographs were then grouped by each HHA and the MMI was determined for each month. The resulting monthly dimensionless median hyetographs and corresponding MMIs are summarized in Figure 6 by HHA.

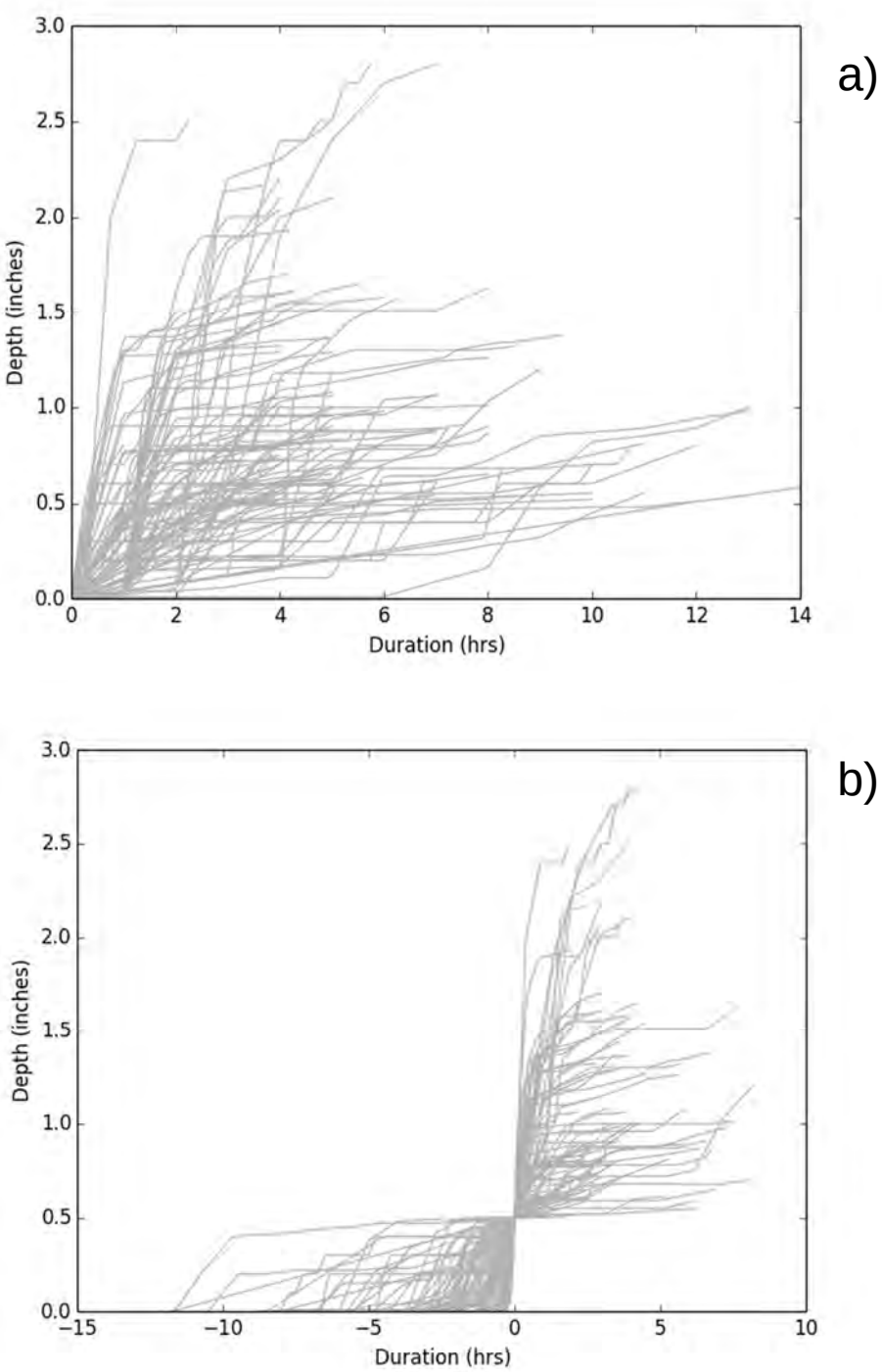

Figure 4 a) Cumulative depth hyetographs derived from rain gauge and b) shifted cumulative depth hyetographs with 50% depth centered on zero hour duration

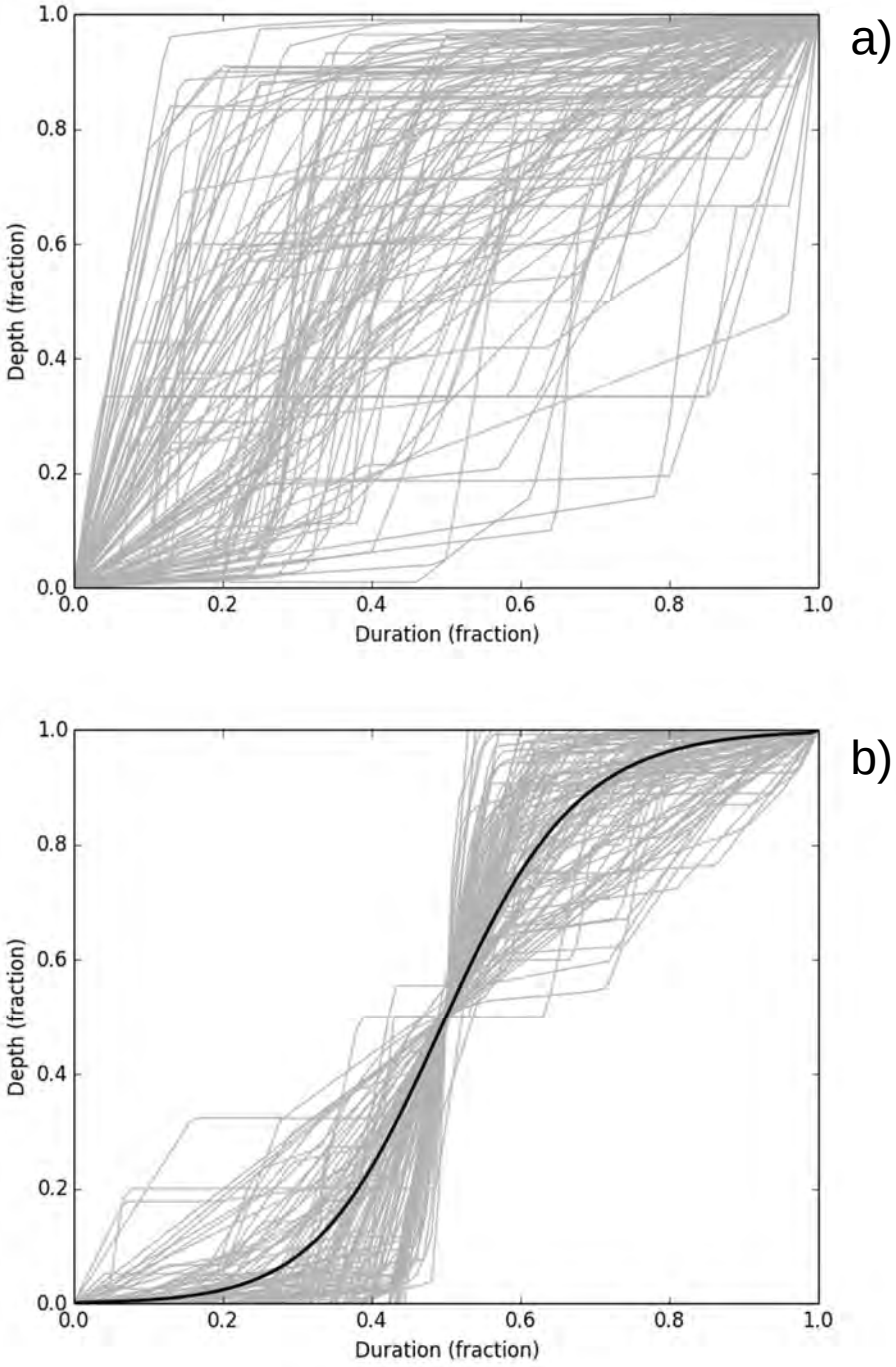

Figure 5 a) Normalized hyetographs by both depth and duration and b) shifted in time by 50% depth and median hyetograph overlaid as dark black line.

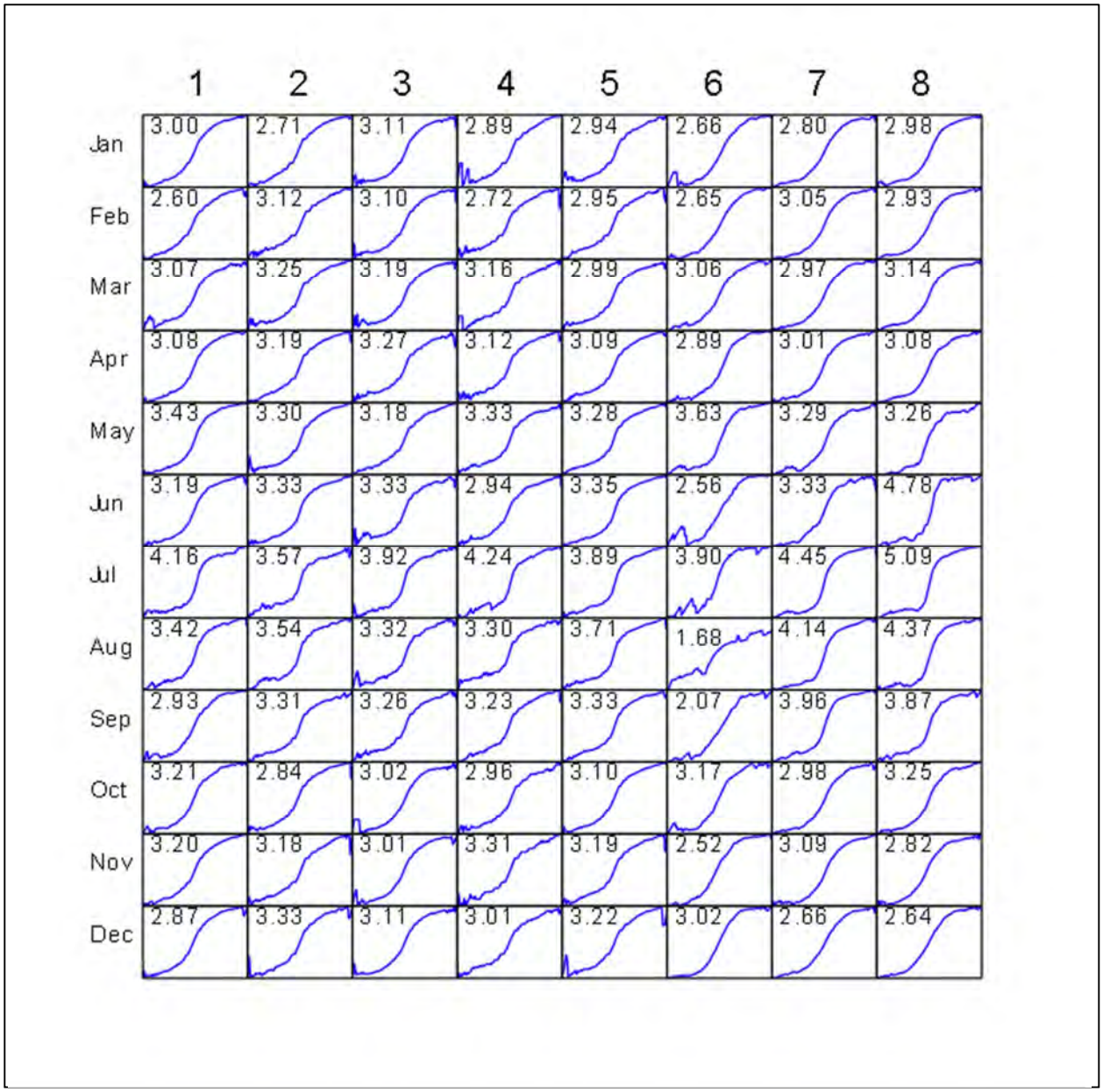

Figure 6 Median dimensionless hyetographs grouped by HHA (columns) and month (rows) with MMI shown in each panel

4 Discussion

Monthly dimensionless median hyetographs and MMIs were developed for each HHA. Since the goal here is to determine design storm hyetographs, it is important to understand how the storm events used vary in space and time in order to develop a standard hyetograph or hyetographs for the region.

4.1 Hyetograph Duration

The time of concentration was determined for major watersheds intersecting NDOT primary roads. Figure 7a shows the location of watershed areas intersecting these roads within the State

of Nevada. The time of concentration computed for these drainage areas is summarized in Figure 7b, where, except for one watershed with a very large area and time of concentration greater than 40 hours, the watersheds intersecting primary roads in Nevada have a time of concentrations of the order of 24 hours or less. The Mean and Median durations for storm events ≥ 0.5 inches range from 11 hours to 18.5 hours (Table 3). Thus, the dimensionless hyetographs derived from these events are applicable to the design storm application.

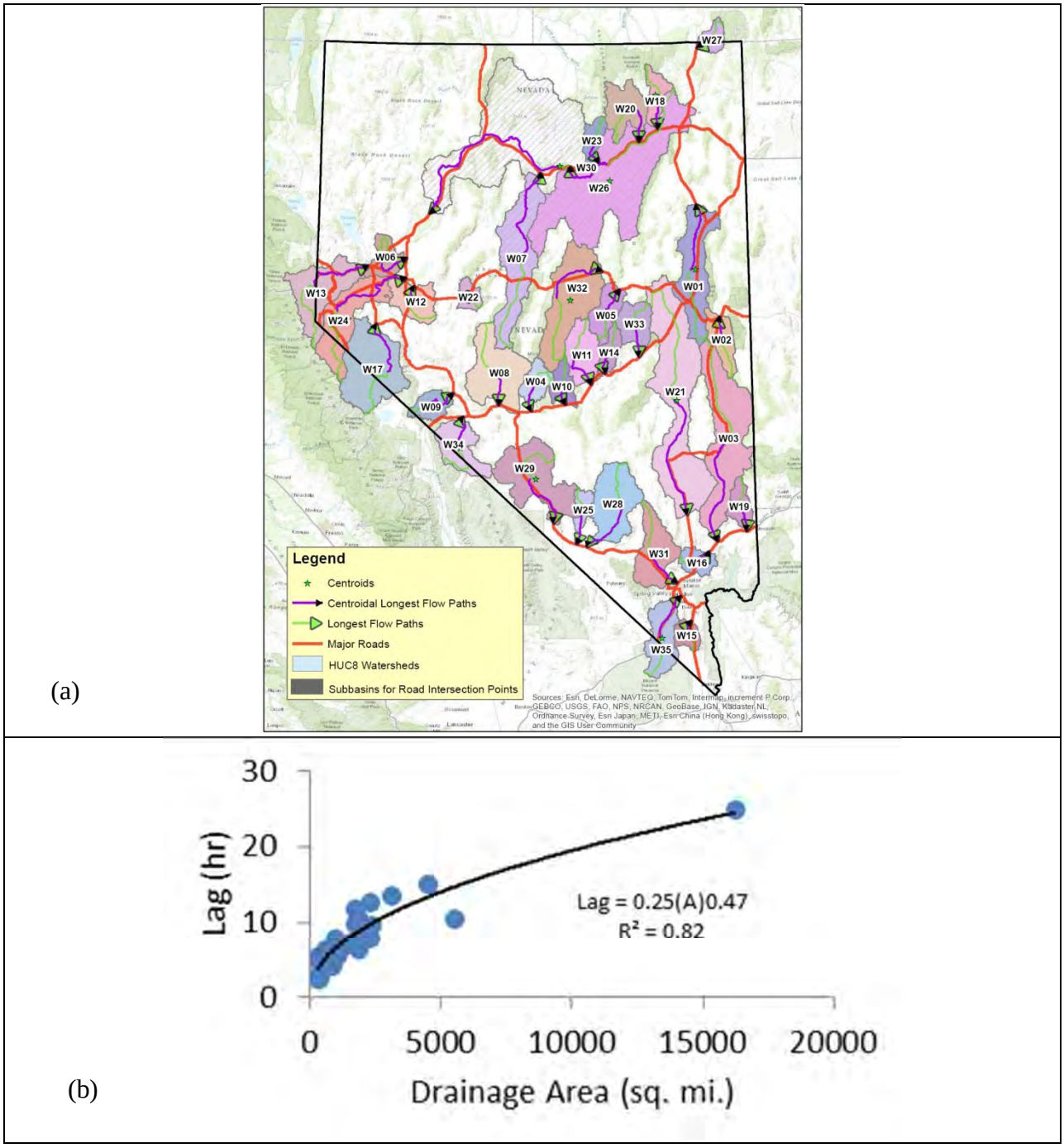

Figure 7 a) Major drainage areas intersecting NDOT primary roads and b) relationship between time of concentration and drainage area for the major drainage areas.

4.2 Relationship between MMI and Duration

To determine if the MMI is influenced by storm event duration, MMIs were computed for a range of storm durations from 1 hour to 200 hours. The results are plotted in Figure 8, which shows there is little difference for storms < 24 hours. However, there is a noticeable and progressive decrease in the maximum intensity for storms >24 hours. Presumably, storms longer than 24 hours are less intense, while storms less than 24 hours show no significant change in MMI with duration. Other characteristics are not considered important since MMI will likely govern the hydrologic response. Therefore, in terms of maximum intensity, one hyetograph will suffice for all storms shorter than 24 hrs.

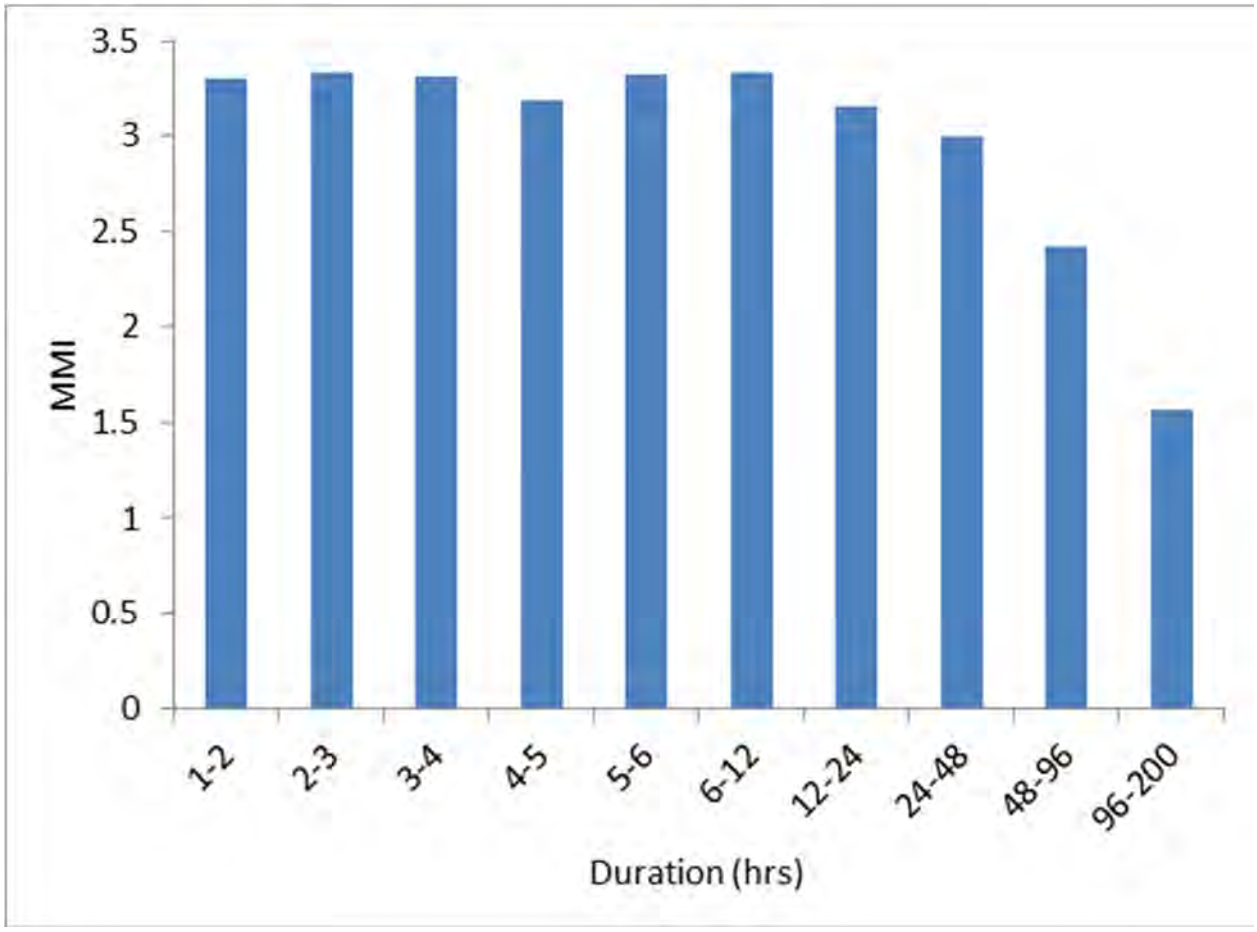

Figure 8 Dimensionless maximum intensity versus storm duration

4.3 Verification of Controlling Quartile

The period during the storm when the most accumulation occurred was evaluated for each storm to identify dominant quartile. As seen in Figure 9, the second and third quartile events have the higher MMIs considering all HHAs and seasons. The MMI in the second quartile, is more intense than the third quartile storms, and was selected as the controlling quartile.

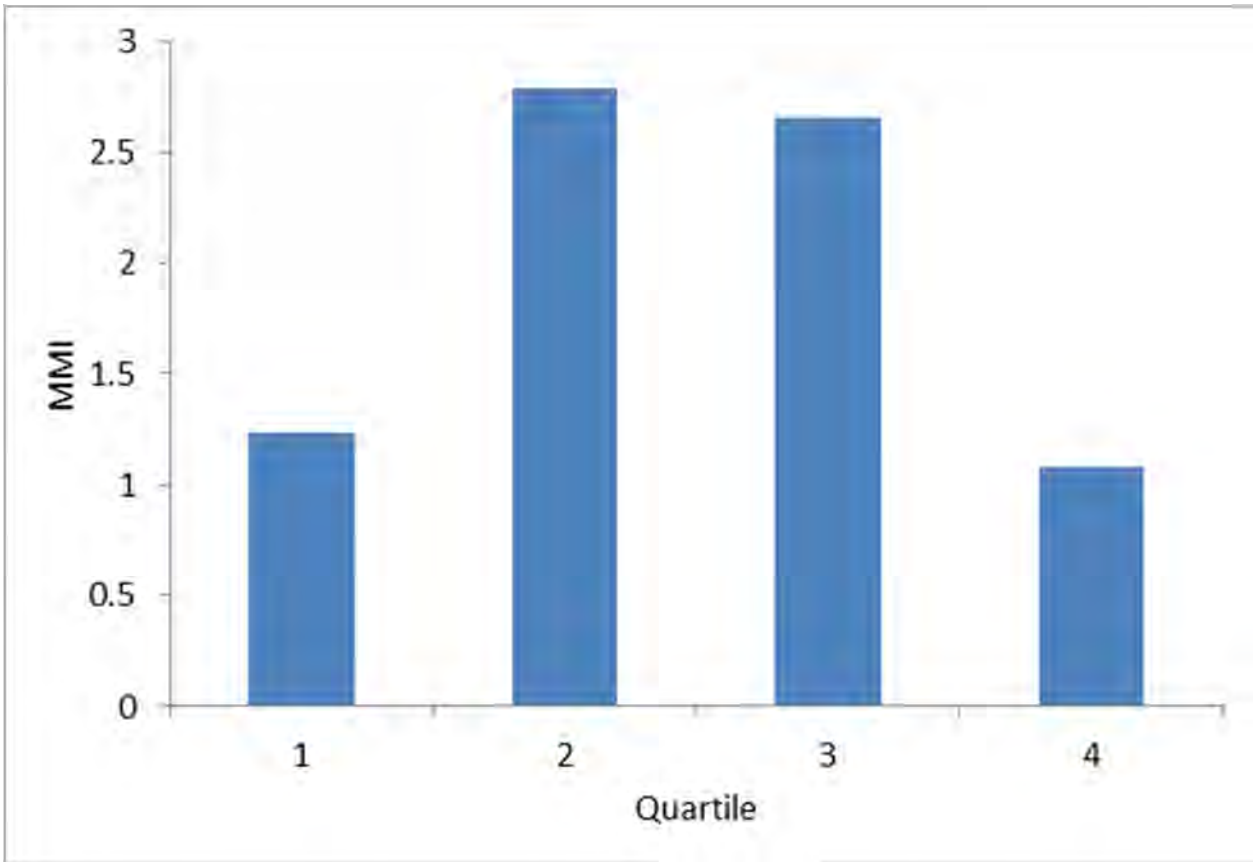

Figure 9 Dimensionless maximum intensity versus quartile

4.4 Seasonal Variability of MMI

As seen in Figure 6, the MMI varies by month. In this Figure, the MMI and the dimensionless median hyetograph (columns) for each month (rows) are provided. The values in each of the panels on Figure 6 represent the maximum intensity of each hyetograph taken from the maximum increase located within 5% of the 50% accumulated depth. Across the state, MMI ranges from a low of 1.68 (% depth/% duration) for August in HHA 6, to a high of 5.09 for July in HHA 8. This indicates that the expected intensity (median) is the highest in the southern portion of Nevada during July, one of the peak months of the North American Monsoon. This seasonal variation is also illustrated in Figure 10 for HHA 1 and HHA 8.

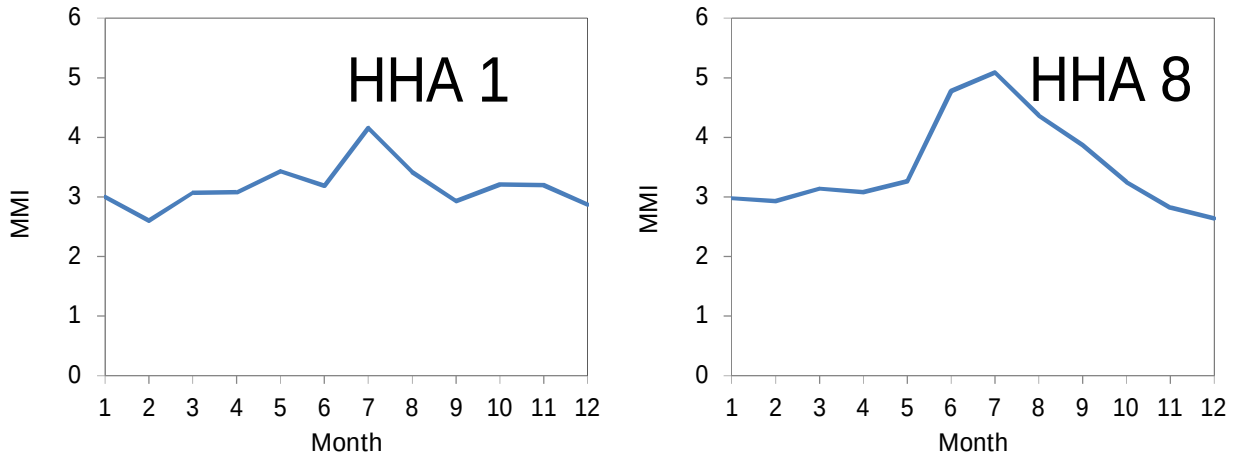

Figure 10 Seasonal variation of maximum dimensionless intensity for HHA 1 (left) and HHA 8 (right)

The controlling MMI for each HHA is averaged from the gauges falling within its boundary to gain an idea of the seasonal and geographic distribution of this key hyetograph characteristic. Scanning across months for each HHA, the MMI is greatest in July for all HHAs. In the northwest, HHA 1, the highest expected intensity is in July as well, indicating that summertime convection is strong there too and outweighs the wintertime intensity. The same tendency towards higher intensity in summertime (July) is observable in HHA 2, as well, though its difference compared to its wintertime intensity is less pronounced. The MMI for each month was selected as the maximum value in each HHA as shown in Figure 11. From this seasonal and geographic distribution, it is clear that any HHA has a maximum intensity in summertime, i.e. July, which indicates that convective storms dominate even in Northwestern Nevada. Thus, the MMI associated with summertime convection (July) dominates regardless of location across the state.

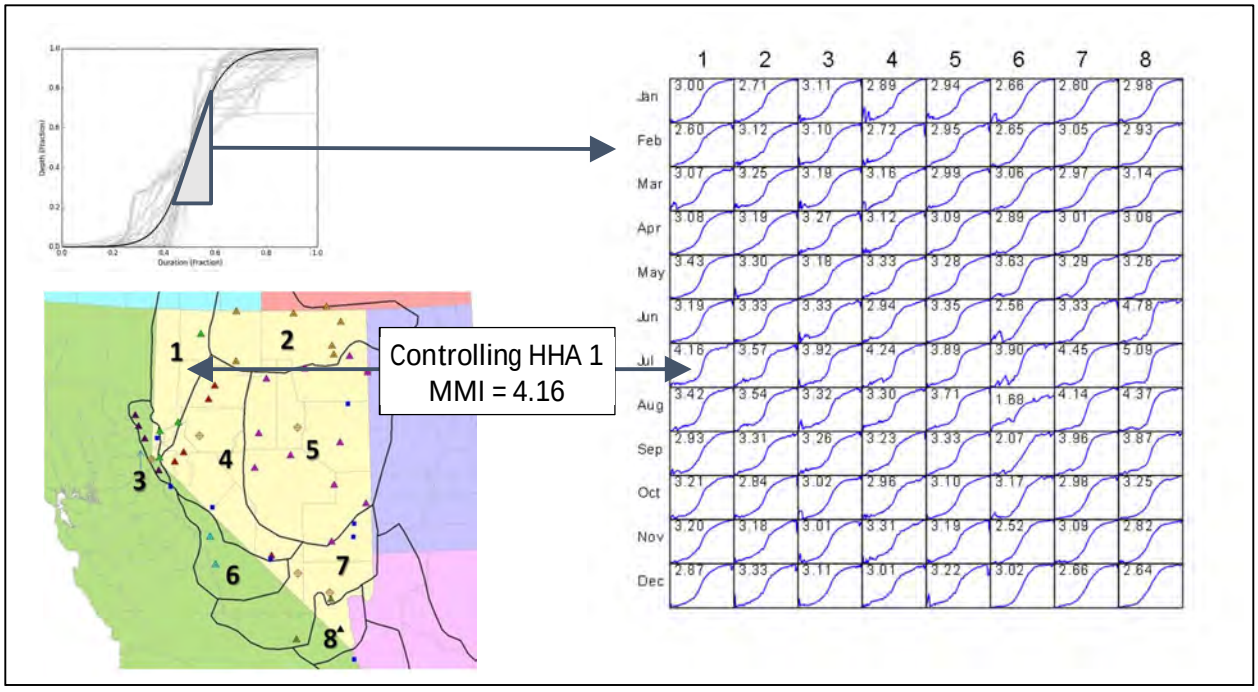

Figure 11 Method for selecting controlling intensity for each HHA

4.5 Geographic Distribution of Hyetograph Intensities

Review of the MMI interpolated surface revealed some irregularities between closely spaced gauges that had similar elevation, but dissimilar MMI values. After review, some of the sub-hourly gauges were excluded because they had a short period of record and relatively few events, which produced unreliable spatial patterns. Upon removal of the short period-of-record gauges, the total number of gauges used to interpolate the surface was reduced from 147 to 110. In Figure 12, the controlling MMI was mapped using the natural neighbor interpolation (Sibson, 1981), which is part of the ESRI ArcGIS software package. The maximum intensity mapped by this method falls within the classes from 1.7 to 6.7 throughout the state. More variability is present in the mapped MMI because these values represent at-gauge values, whereas the MMI presented in Figure 11 above is averaged within each HHA. The values in Figure 11 represent the MMI across each of the HHA zones, but the values in Figure 12 represent the MMI at each individual gauge location. The peak MMI for a gauge was 6.7 while the peak MMI for a HHA was 5.09.

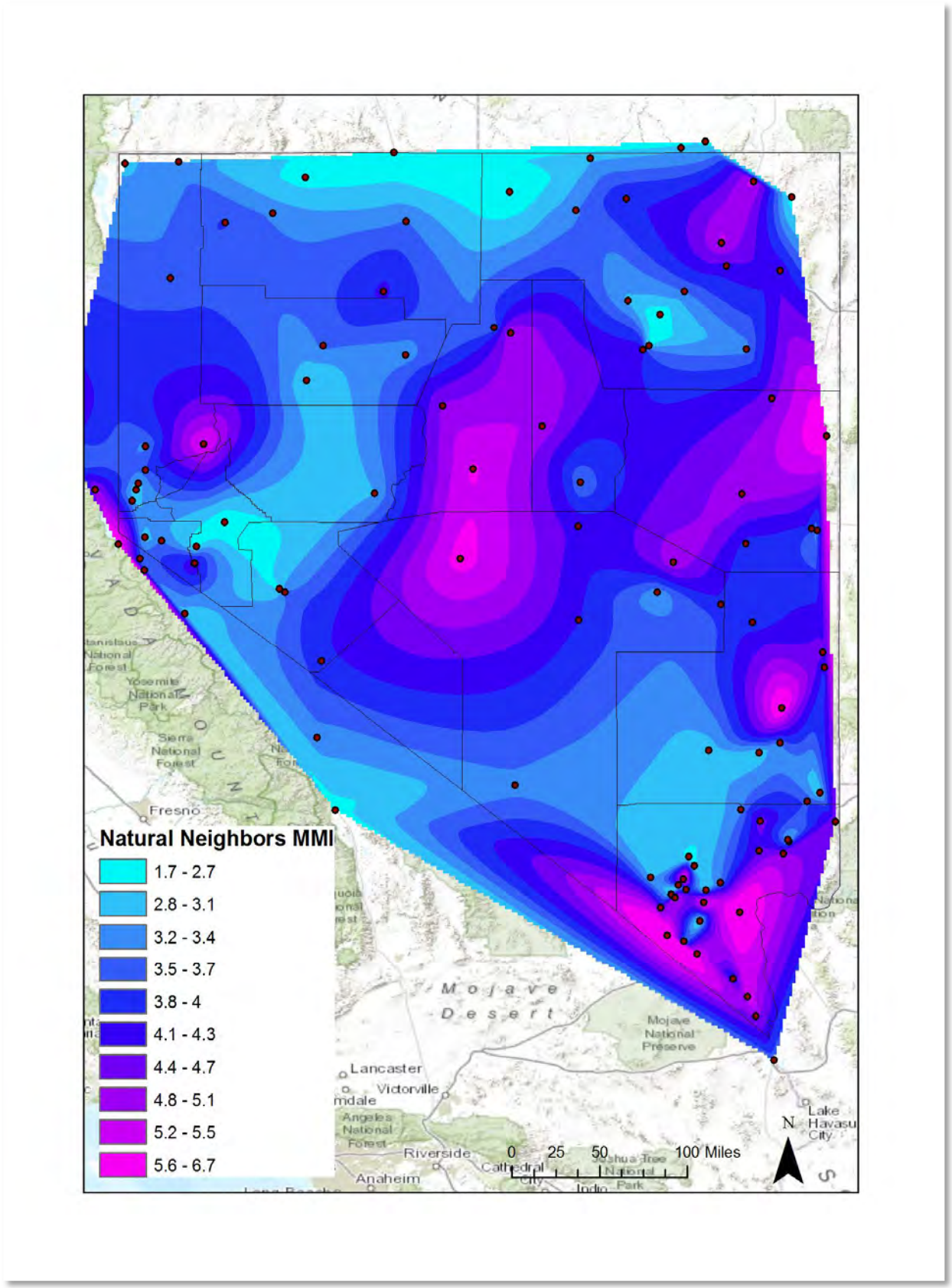

Figure 12 Map of controlling MMI using natural neighbors interpolation

Recognizing that the gauge network is somewhat sparse, advanced interpolation was applied to the MMI point values using climate-aided interpolation (CAI) similar to PRISM. This creates a smoother surface based on the gauge data and the climate characteristics. Three CAIs were conducted using climate maps represented by 1) the annual normal precipitation, 2) the normal precipitation for July, and 3) the 1-hour, 100-year rainfall depth map from NOAA Atlas 14, Volume 1. Of the climate maps tested, the 1-hour, 100-year CAI had the lowest mean error between the gauges and the interpolated surface. Further, the 1-hour, 100-year CAI interpolation produced a map of MMI that appears more consistent with terrain and associated orographic enhancement. Figure 13 shows the 1-hour, 100-year CAI interpolation for the MMI. Alternatively, the 1-hour, 100-year CAI for the 90^{th} percentile maximum intensity is presented in Figure 14. The graphs of mean error for these two surfaces are presented in Appendix A-6. The scatterplot shown in the Figure A-6-1 shows that the surface reproduces the observed (at-gauge) values well, with a relative bias that is less than 5% for the MMI, and 4% for the 90^{th} percentile maximum intensity. The MMI and the 90^{th} percentile maximum intensity maps aggregated by 12-digit hydrologic unit code (HUC-12) watersheds are also provided in Appendix A-6.

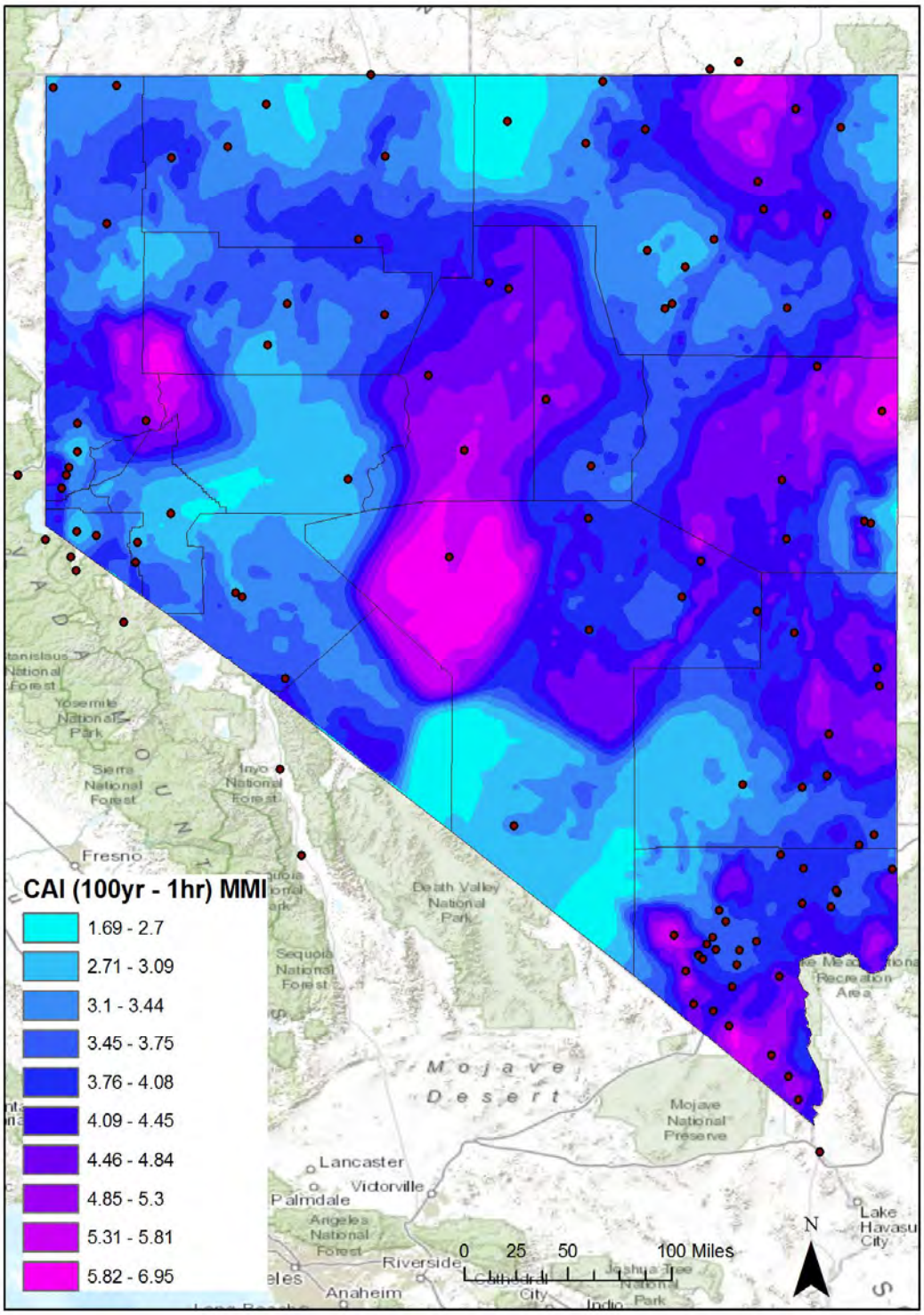

Figure 13 CAI(100yr-1hr) interpolated surface of MMI

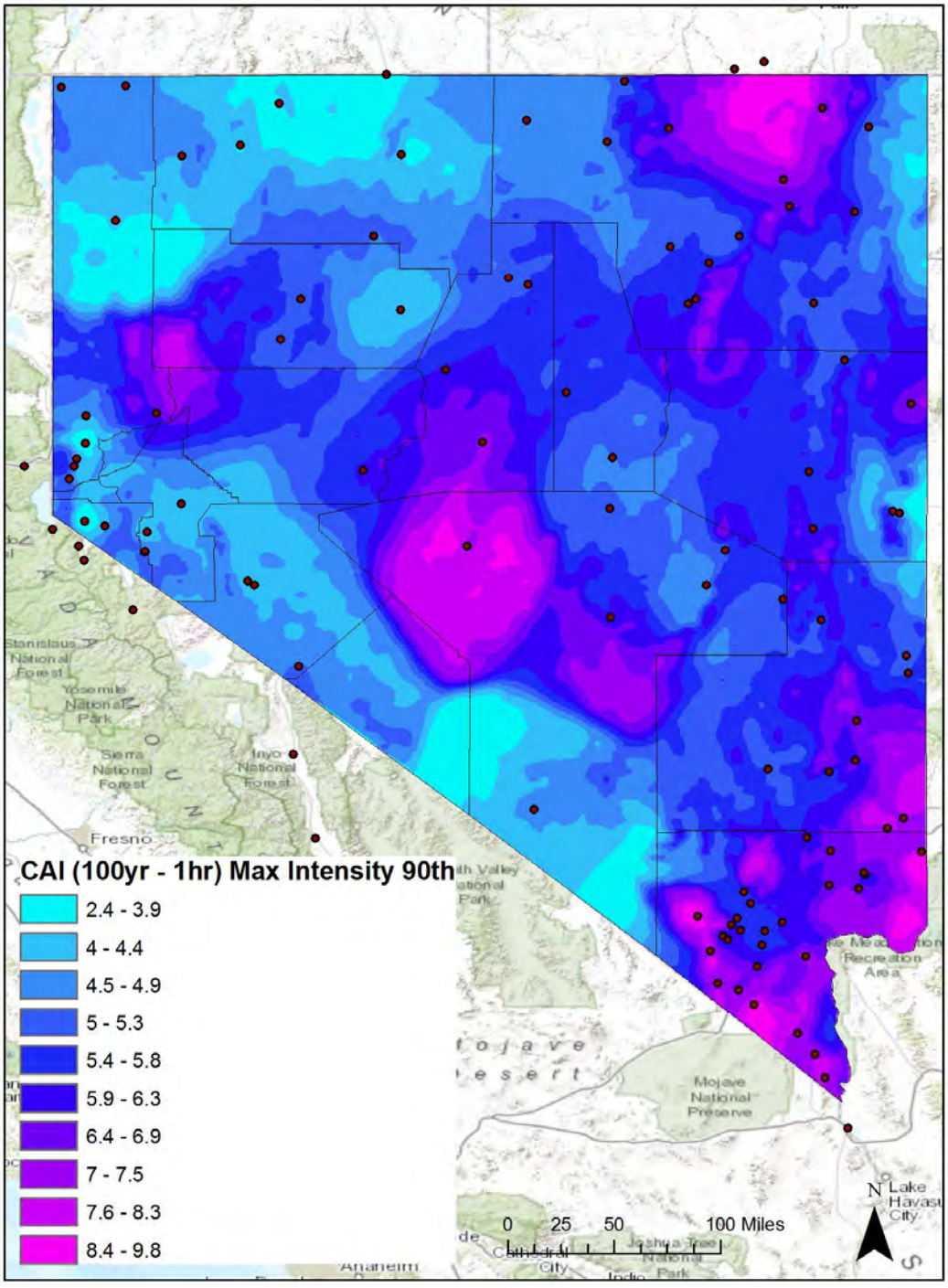

Figure 14 CAI (100yr-1hr) 90th percentile MI

4.6 Hyetograph Comparative Analysis

The hyetographs derived in this analysis are compared with other published cumulative hyetograph on a dimensionless basis. Three comparisons are made, namely 1) NOAA (see Bonnin, 2004), Huff (taken from Huff, 1990), SCS Type II (presented in Kent, 1968), and CCRFCD (see CCRFCD, 1999). In the following comparisons, the peak intensity portion of the cumulative hyetograph, MMI is plotted. The slope of the line presented in the following comparisons represents the MMI in units of % depth versus % time, or (%/%). The values shown are from HHA 8 with an MMI of 5.08 (%/%).

4.6.1 NOAA

The NOAA hyetograph is selected from the 6-hr, 2nd Quartile Convective Area (Bonnin et al., 2004) for comparison with the coincident area, HHA 8. In Figure 15, the NOAA 14 Vol. 1 hyetograph from the convective precipitation area is shown with the HHA-8 MMI = 5.08 (%/%) plotted. The NOAA hyetograph is less intense than either the MMI or 90th percentile hyetographs. However, this may be expected since NOAA averages together all storms for the region, and for all seasons, both winter and summer.

4.6.2 Huff

As seen in Figure 16, Comparison of the HHA 8 MMI with Huff (1990) shows that the Huff hyetograph is less intense. The Huff hyetograph shown is 2nd Quartile. The 2nd Quartile corresponds with the majority of events used to derive the MMI.

4.6.3 SCS

The SCS Type II (Kent, 1968) distribution hyetograph is shown in Figure 17, and is more intense than the HHA 8 MMI=5.08 (%/%). The SCS Type II hyetograph is the only one tested that exceeds the MMI for HHA 8, the maximum intensity statewide.

4.6.4 CCRFCD

The CCRFCD 6-hr hyetograph is presented with the MMI, overlaying with nearly identical slope seen in Figure 18. The specified hyetograph is SDN3 for drainage areas less than 8 sq. mi. are defined in Table 503 found in CCRFCD (1999, after p. 510). The MMI = 5.09 (%/%) for HHA 8 is very close to the CCRFCD maximum intensity of, 7.20 (%/%). The long rise in accumulation is evident in the CCRFCD hyetograph, gaining nearly 25% of the storm total before the maximum intensity occurs at 55% of duration, i.e. 3rd Quartile.

4.6.5 Norbert

Remnants of Hurricane Norbert produced extreme flooding in southern Nevada, with particularly heavy precipitation and flooding near Moapa, in Clark County (Figure 20). Several Clark County rain gauges were examined that had the greatest accumulation. Weiser Wash is an ALERT rain gauge that received 4.59 inches in about 3.5 hours from 1:29 to 4:09:00 PM PDT on September 8, 2014. Figure 15 shows the dimensionless hyetograph and MMI of 5.08 (%/%) for the HHA 8

in which the rainfall occurred. The dimensionless intensity of the recorded hyetograph was 2.94 (%/%) which is less than the median for HHA 8. Part of the severe flooding experienced during this event and the consequent erosion of the highway embankment on I-5 could be attributable to the volume of rainfall and secondarily to the intensity.

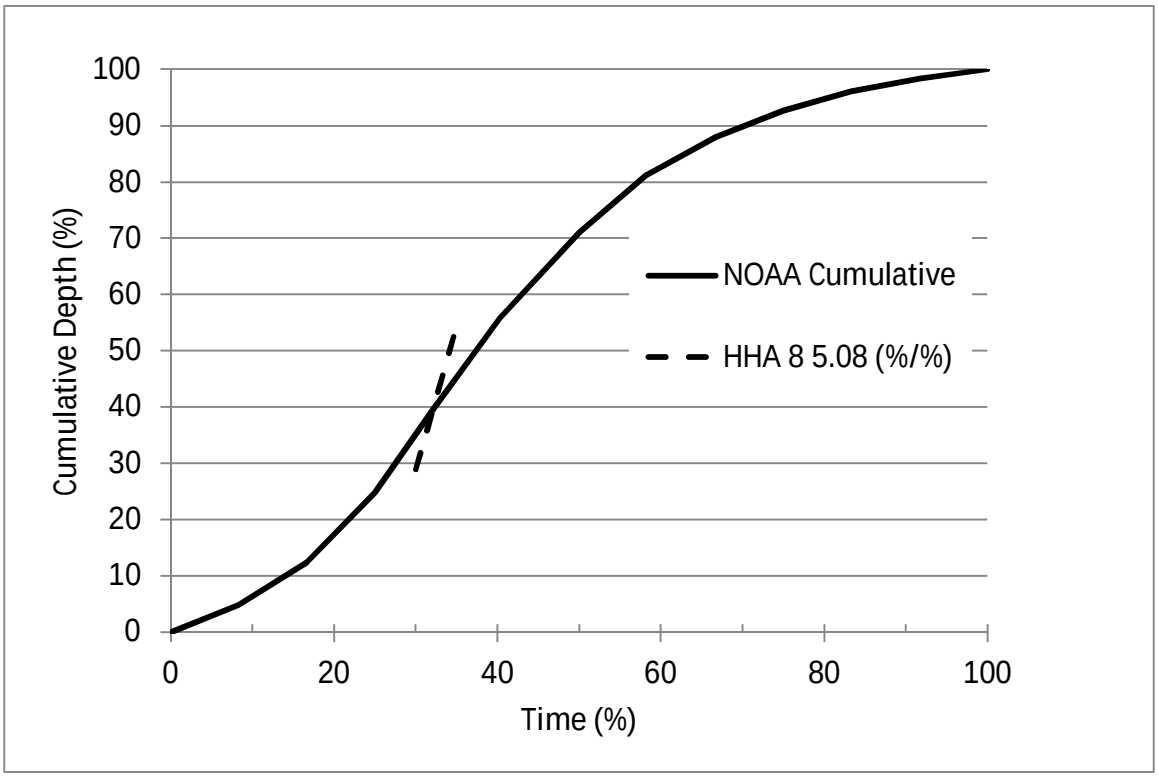

Figure 1516 Comparison of NOAA 14 Vol. 1 hyetograph with MMI

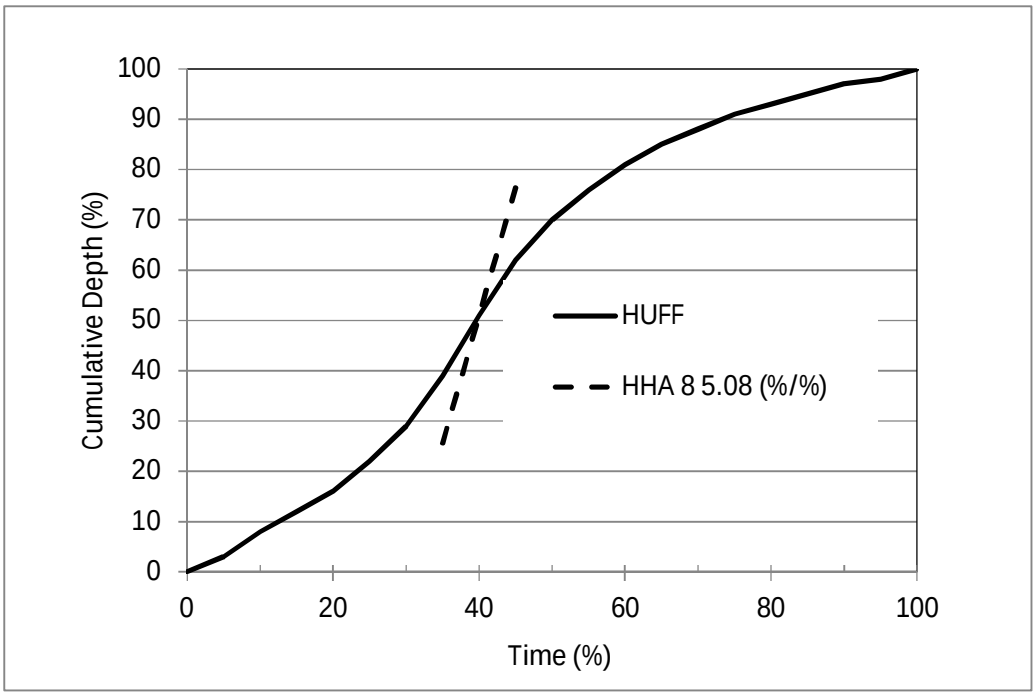

Figure 16 Comparison of Huff hyetograph with MMI

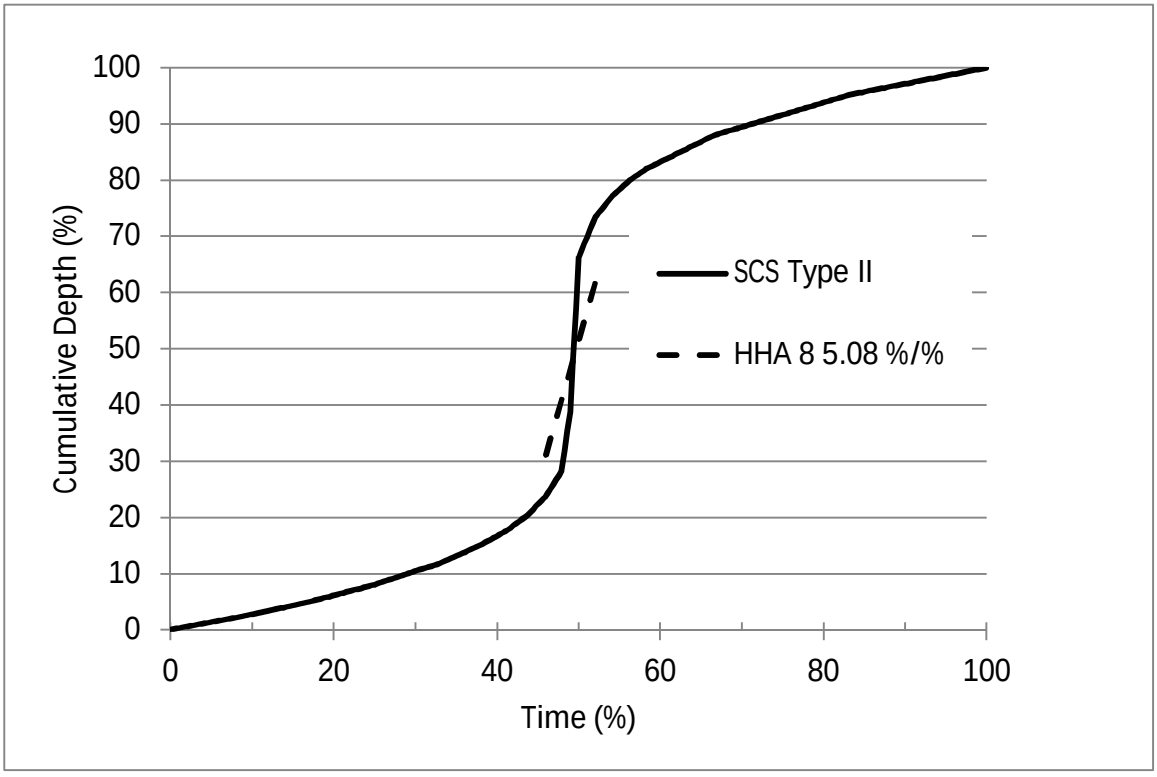

Figure 17 Comparison of SCS Type II hyetograph with MMI

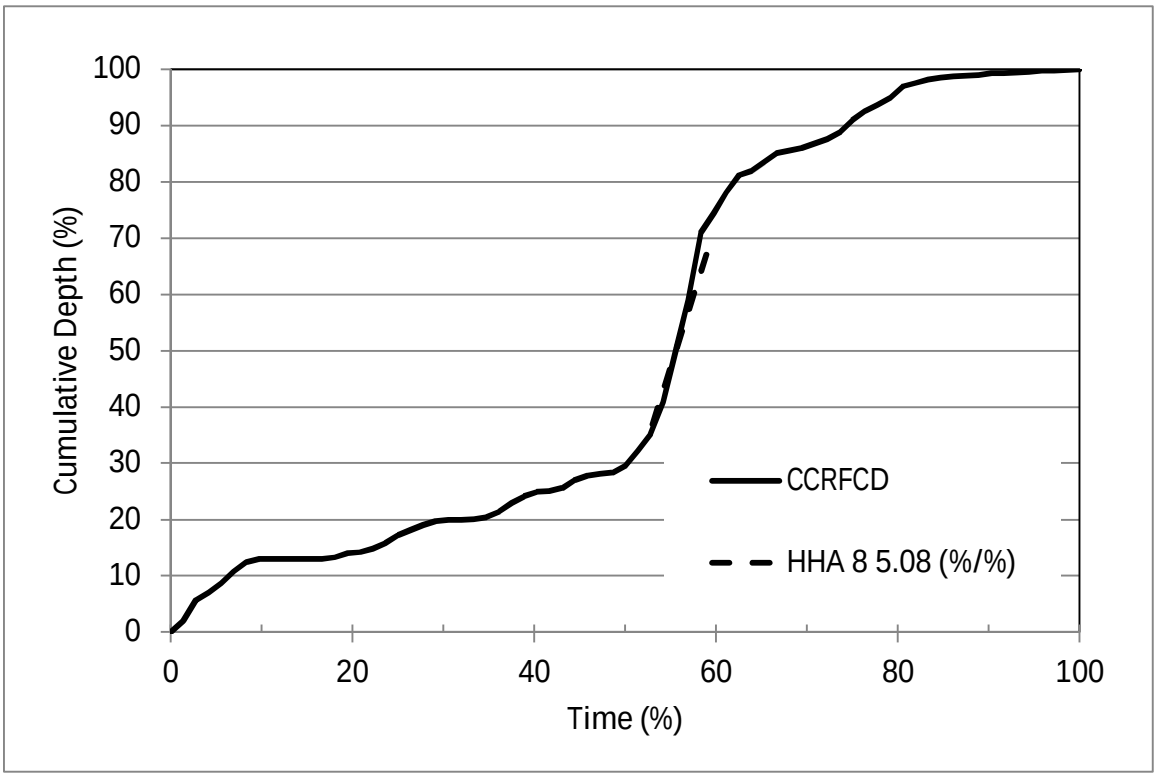

Figure 18 Comparison of the CCRFCD hyetograph and MMI

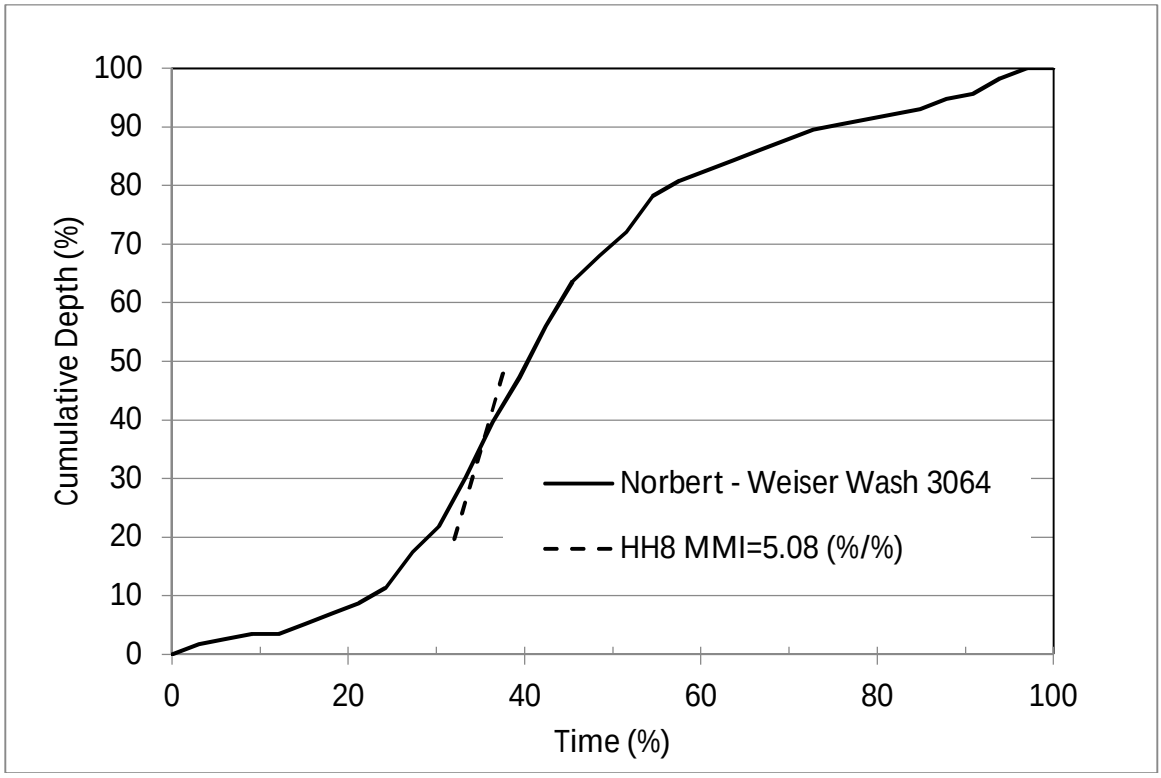

Figure 19 Comparison of the remnants of Hurricane Norbert hyetograph and MMI

5 Summary

Design storm hyetographs were developed for the state of Nevada using point rain gauge measurements for the period of record available at each gauge. The approach relies on rain gauge networks that have hourly or 5-minute/15-minute interval data. The data sources considered are within Nevada or nearby, and consist of 371 gauges among four networks. Of these gauges, 147 had a sufficiently reliable record, with data recorded at intervals less than daily, i.e. hourly or 5-minute/15-minute; or were selected based on spatial distribution and a representative range of elevations. The 147 gauges cover a range of elevations, falling between 480 and 9000 feet. From the combination of four networks across the state, the average spacing of the selected rain gauge locations is roughly 27 miles. Review of unreliably short periods of record further reduced this number to 110 for purposes of spatial interpolation of hyetograph intensities over the state.

The rain gauge data were processed into events defined by a 6-hr interval during which no rain fell. These events were further segregated into events with more than 0.5 inches in depth to focus on storms with well-defined hyetograph shape and excluding those with small or only trace amounts that would likely not produce a hydrologic response. As a result, there were 16,771 events analyzed that met this threshold. Dimensionless hyetographs were then shifted to a common starting time in order to compute median characteristics. These events averaged 0.9 inches with a duration of 15 hours statewide. Rather than identify the most frequent quartile, the quartile with the highest intensity was selected, and found to be the 2nd Quartile. To identify whether hyetographs needed to be further segregated, correlations to depth, duration, or quartile were evaluated. However, the main hyetograph characteristic, the maximum intensity was found to be invariant for storm duration up to 24 hours. Similarly, no strong relationship with depth was found, which would suggest that storms with greater depths would require a different hyetograph. To focus hyetograph shape on storms with more significant depths, segregation was performed, resulting in hyetographs for storms greater than 0.5 inches.

Storm event characteristics derived from gauges were then grouped by HHA for purposes of statistical evaluation and characterizing the controlling hyetograph by month and geographic distribution. Once the controlling hyetograph intensity was determined, it was mapped over the state using a spatial interpolation technique that considers the nearest neighbors. The intensities mapped are the dimensionless hyetograph intensity, MMI (%/%) that are controlling, i.e. the greatest for any month. In every HHA, the controlling intensity occurs during July, even in the northern parts of the state, where climatologically, wintertime has the greatest total precipitation. Since watersheds follow topographic divides, it is likely that many watersheds contain a range of elevation from higher values upstream to lower downstream. With the aid of the 100-yr 1-hr precipitation map that represents climate, the MMI and 90th percentile maximum intensity were interpolated from gauge values producing a map of these values. Their geographic distribution follows terrain due to orographic enhancement and other effects present in the predictor map used in the CAI interpolation. These interpolated MMI and 90th percentile maximum intensity

values were also averaged by HUC-12 watersheds found in Appendix A-6.

The intended use of this map is to identify the hyetograph maximum intensity expected at any given location and the range of intensities that can be expected within a watershed. Comparison of the MMI for HHA 8 reveals that median intensity is more than the published hyetographs by NOAA or Huff, but less intense than the SCS Type II. The maximum intensity in the CCRFCD hyetograph was 8.9 versus 5.08 (%/%). While the CCRFCD hyetograph is slightly more intense compared with HHA 8, the CCRFCD 6-hr hyetograph agrees quite well with HHA 8 in terms of maximum hyetograph intensity.

6 References

1. Bonnin, G.M., D. Martin, B. Lin, T. Parzybok, M. Yekta, D. Riley, 2004. "Precipitation frequency atlas of the United States." Volume 1 Version 5.0: Semiarid Southwest (Arizona, Southeast California, Nevada, New Mexico, Utah).
2. CCRFCD, 1999. Clark County Regional Flood Control District. *Hydrologic Criteria and Drainage Design Manual*. Adopted August 12, 1999. Available on the Internet at: http://www.ccrfcd.org/ (Last checked, July 30, 2014).
3. Huff, F.A., 1990. Time Distributions of Heavy Rainstorms in Illinois. Illinois State Water Survey ISWS/CIR-173/90, Circular 173. Available on the Internet at: http://www.isws.illinois.edu/pubdoc/C/ISWSC-173.pdf (Last checked 7/30/2014).
4. Kent, K.M. 1968. *A method for estimating volume and rate of runoff in small watersheds*. SCS-TP-149 U.S. Department of Agriculture, Soil Conservation Service, Washington, D.C.
5. Sibson, R., 1981. A Brief Description of Natural Neighbor Interpolation. Chapter 2 in *Interpolating Multivariate Data*, John Wiley & Sons, New York, pp. 21-36.

7 Appendices

APPENDIX A-1 List of COOP and ASOS gauges

APPENDIX A-2 List of RAWS gauges

APPENDIX A-3 List of CCRFCD gauges

APPENDIX A-4 Seasonal distribution of events for each HHA determined by the COOP and ASOS gauge networks

APPENDIX A-5 Annual distribution of events for each HHA determined by the COOP and ASOS gauge networks

APPENDIX A-6 MMI and 90^{th} Percentile Maximum Intensity Mean Error and Watershed Averages

APPENDIX A-1 – List of COOP and ASOS gauges

HHA	ID	Name	Hourly	15-min	Elevation (ft)	Source
1	26-4527	LEONARD CREEK RANCH	Yes	Yes	4239	COOP (NOAA Atlas 14)
1	26-5191	MINDEN	Yes	Yes	4709	COOP (NOAA Atlas 14)
1	26-6779	RENO WSFO AIRPORT	Yes	No	4410	COOP (NOAA Atlas 14)
1	26-8838	WADSWORTH 4 N	Yes	Yes	4000	COOP (NOAA Atlas 14)
1	26-2840	FERNLEY	Yes	No	4203	COOP (NOAA Atlas 14)
2	26-9072	WILD HORSE RSVR	Yes	Yes	6239	COOP
2	26-7397	SEVENTY ONE RCH	Yes	No	5453	COOP
2	26-1905	CONTACT	Yes	Yes	5350	COOP (NOAA Atlas 14)
2	26-4935	MCDERMITT	Yes	Yes	4430	COOP (NOAA Atlas 14)
2	26-5092	METROPOLIS	Yes	Yes	5800	COOP (NOAA Atlas 14)
2	26-5869	OWYHEE	Yes	Yes	5397	COOP (NOAA Atlas 14)
2	26-8988	WELLS	Yes	Yes	5700	COOP (NOAA Atlas 14)
2	26-9171	WINNEMUCCA WB CITY	Yes	No	4296	COOP (NOAA Atlas 14)
2	10-9119	THREE CREEK	Yes	Yes	5460	COOP (NOAA Atlas 14)
2	10-6250	MURPHY DESERT HOT SPRINGS	No	Yes	5159	COOP
3	26-5441	MT ROSE CHRISTMAS TREE	Yes	Yes	7235	COOP
3	04-8355	SONORA JUNCTION	Yes	Yes	6886	COOP
3	04-5356	MARKLEEVILLE	Yes	Yes	5530	COOP (NOAA Atlas 14)
3	04-7085	PORTOLA	Yes	No	4850	COOP (NOAA Atlas 14)
3	04-8218	SIERRAVILLE R S	Yes	No	4975	COOP (NOAA Atlas 14)
3	04-9043	TRUCKEE RS	Yes	Yes	5823	COOP (NOAA Atlas 14)
3	04-9775	WOODFORDS	No	Yes	5668	COOP
3	KTVL	Lake Tahoe Airport	Yes	No	6263	NWS ASOS
4	26-0714	BEATTY	Yes	No	3304	COOP
4	26-5362	MONTGOMERY MTNC STN	Yes	Yes	7100	COOP

4	26-3512	HAWTHORNE	Yes	Yes	4330	COOP
4	26-2477	EASTGATE	Yes	No	5023	COOP
4	26-9234	YERINGTON 2	Yes	No	4383	COOP
4	04-1076	BRIDGEPORT RANGER STATION	No	Yes	6439	COOP
4	26-0718	BEATTY 8 N	Yes	Yes	3550	COOP (NOAA Atlas 14)
4	26-4698	LOVELOCK	Yes	Yes	3975	COOP (NOAA Atlas 14)
4	26-7192	RYE PATCH DAM	Yes	Yes	4135	COOP (NOAA Atlas 14)
4	26-7612	SMITH 6 N	Yes	Yes	5000	COOP (NOAA Atlas 14)
4	26-8822	WABUSKA 6 SE	Yes	Yes	4300	COOP (NOAA Atlas 14)
4	26-3515	HAWTHORNE AP	Yes	Yes	4219	COOP (NOAA Atlas 14)
4	26-8977	WELLINGTON RS	Yes	No	4843	COOP (NOAA Atlas 14)
4	KNFL	Fallon Naval Air Station	Yes	No	3934	NWS ASOS
5	26-4341	LAGES	Yes	Yes	5960	COOP
5	26-0961	BLUE JAY HIGHWAY STATION	No	Yes	5320	COOP
5	26-2570	ELKO	No	Yes	5234	COOP
5	26-2820	FERGUSON SPRINGS HMS	No	Yes	5841	COOP
5	26-3964	INDIAN CREEK RANCH	No	Yes	7498	COOP
5	26-4095	JIGGS 8 SSE ZAGA	No	Yes	5763	COOP
5	26-4394	LAMOILLE YOST	No	Yes	5891	COOP
5	26-0507	AUSTIN	Yes	Yes	6780	COOP (NOAA Atlas 14)
5	26-0691	BATTLE MOUNTAIN AP	Yes	Yes	4505	COOP (NOAA Atlas 14)
5	26-2573	ELKO FCWOS	Yes	Yes	5030	COOP (NOAA Atlas 14)
5	26-2631	ELY WSO AIRPORT	Yes	No	6262	COOP (NOAA Atlas 14)
5	26-5880	PAHRANAGAT W L REFUGE	Yes	Yes	3334	COOP (NOAA Atlas 14)
5	26-6148	PEQUOP	Yes	Yes	6033	COOP (NOAA Atlas 14)
5	26-7620	SMOKEY VALLEY	Yes	Yes	5647	COOP (NOAA Atlas 14)
5	26-7640	SNOWBALL RANCH	Yes	Yes	7160	COOP (NOAA Atlas 14)
5	26-7750	SPRING VALLEY ST PK	Yes	Yes	5950	COOP (NOAA Atlas 14)

5	26-7908	SUNNYSIDE	Yes	Yes	5297	COOP (NOAA Atlas 14)
5	42-9382	WENDOVER AWOS	Yes	No	4237	COOP (NOAA Atlas 14)
5	26-0955	BLUE EAGLE CURRANT 12S	Yes	Yes	4780	COOP (NOAA Atlas 14)
5	26-2860	FISH CREEK RCH	Yes	No	6053	COOP (NOAA Atlas 14)
5	26-3340	GREAT BASIN NP	Yes	Yes	6830	COOP (NOAA Atlas 14)
5	26-4086	JIGGS 3 N	Yes	No	5423	COOP (NOAA Atlas 14)
5	26-8170	TONOPAH AIRPORT	Yes	No	5430	COOP (NOAA Atlas 14)
5	KP68	Eureka	Yes	No	5945	NWS ASOS
5	KENV	Wendover Airforce Aux Field	Yes	No	4237	NWS ASOS
6	04-0822	BISHOP WSO AIRPORT	Yes	Yes	4102	COOP (NOAA Atlas 14)
6	04-4232	INDEPENDENCE	Yes	No	3950	COOP (NOAA Atlas 14)
7	26-1358	CALIENTE	Yes	No	4379	COOP
7	26-2557	ELGIN	Yes	Yes	3422	COOP
7	26-4436	LAS VEGAS WSO AIRPORT	Yes	No	2131	COOP (NOAA Atlas 14)
7	04-0436	BAKER	Yes	No	962	COOP (NOAA Atlas 14)
7	26-4651	LOGANDALE	Yes	Yes	1322	COOP (NOAA Atlas 14)
7	26-5846	OVERTON	Yes	Yes	1250	COOP (NOAA Atlas 14)
7	KVGT	North Las Vegas Airport	Yes	No	2205	NWS ASOS
7	KDRA	Desert Rock Airport	Yes	No	3310	NWS ASOS
8	04-6115	NEEDLES	Yes	No	480	COOP
8	26-7369	SEARCHLIGHT	Yes	Yes	3540	COOP (NOAA Atlas 14)

APPENDIX A-2 – List of RAWS gauges

HHA	ID	Name	Elevation (ft)	Source
1	NBAR	BARREL SPRINGS	5731	RAWS
1	NBLU	BLUEWING MOUNTAIN	4570	RAWS
1	NBUF	BUFFALO CREEK	3940	RAWS
1	NCAT	CATNIP MOUNTAIN	5750	RAWS
1	NDRY	DRY CANYON	4900	RAWS
1	NDSS	DESERT SPRINGS	5280	RAWS
1	NFOX	FOX MOUNTAIN	6890	RAWS
1	NJUN	JUNIPER SPRINGS	5536	RAWS
1	NTEX	TEXAS SPRINGS	5760	RAWS
2	NANT	ANTELOPE LAKE	5460	RAWS
2	NDOU	DOUBLE H	6380	RAWS
2	NLON	LONG HOLLOW	5820	RAWS
2	NMOR	MOREY CREEK	5500	RAWS
2	NROC	ROCK SPRING CREEK	5427	RAWS
2	NSTA	STAG MOUNTAIN	6790	RAWS
3	NLIT	LITTLE VALLEY (WRCC)	6310	RAWS
4	NCHV	CHERRY VALLEY	7622	RAWS
4	NDEA	DEAD CAMEL MOUNTAIN	4490	RAWS
4	NDES	DESATOYA MOUNTAIN	6152	RAWS
4	NFIS	FISH SPRINGS	5230	RAWS
4	NMAJ	MAJUBA	5293	RAWS
4	NSIA	SIARD	4600	RAWS
5	NALL	ALLIGATOR RIDGE	6675	RAWS
5	NCCP	CATTLE CAMP	7025	RAWS
5	NCED	CEDAR PASS	7314	RAWS
5	NCOI	COILS CREEK	6745	RAWS
5	NCOM	COMBS CANYON	6590	RAWS

HHA	ID	Name	Elevation (ft)	Source
5	NCRA	CRANE SPRINGS	6414	RAWS
5	NCUR	CURRANT CREEK	5750	RAWS
5	NCYW	COYOTE WASH	5770	RAWS
5	NIMM	IMMIGRATION WASH	6230	RAWS
5	NPAN	PANCAKE	5165	RAWS
5	NQPK	QUIMA PEAK	7984	RAWS
5	NREB	RED BUTTE	5026	RAWS
5	NRUB	RUBY LAKE	5970	RAWS
5	NSPG	SPRING GULCH	5470	RAWS
5	NSPM	SPRUCE MOUNTAIN	6296	RAWS
5	NSVM	SEVEN MILE	7725	RAWS
5	NTIM	TIMBER MTN	9000	RAWS
7	NDNW	DESERT NWR	7120	RAWS
7	NKAN	KANE SPRINGS	4382	RAWS
7	NKYL	KYLE CANYON	7200	RAWS
7	NYUC	YUCCA GAP	3180	RAWS
8	NMOU	MOUNTAIN SPRINGS	5600	RAWS
8	NRER	RED ROCK	3756	RAWS

APPENDIX A-3 – List of CCRFCD gauges

HHA	ID	Name	Elevation (ft)	Source
7	2664	Mesquite 2	2475	CCRFCD
7	2754	Bunkerville	2715	CCRFCD
7	3034	Halfway Wash	2812	CCRFCD
7	3134	California Wash 3	1974	CCRFCD
7	3234	Wildcat Wash	2533	CCRFCD
7	3244	Mormon Mesa 2	1900	CCRFCD
7	3264	Moapa	1710	CCRFCD
7	3284	Silica Dome	2062	CCRFCD
7	4014	Fossil Ridge	3600	CCRFCD
7	4044	Castle Rock (1 & 2)	3180	CCRFCD
7	4054	Lone Mountain/Hualpai	3020	CCRFCD
7	4109	Nellis AFB South	1730	CCRFCD
7	4209	Summerlin NW	3632	CCRFCD
7	4224	Angel Park West	2812	CCRFCD
7	4274	Downtown Las Vegas	2102	CCRFCD
8	4314	Blue Diamond Ridge North	4823	CCRFCD
8	4324	Red Rock Canyon	3625	CCRFCD
8	4704	Sloan at I-15	2687	CCRFCD
8	4854	Boulder City	3440	CCRFCD
8	4924	Goodsprings 1	4927	CCRFCD
8	4954	Jean Airport	2711	CCRFCD
8	4964	Jean SE	4099	CCRFCD
8	5134	CalNevAri	2902	CCRFCD
8	5224	Laughlin 1	2590	CCRFCD

APPENDIX A-4 – Seasonal distribution of events for each HHA determined by the COOP and ASOS gauge networks

APPENDIX A-5 – Annual distribution of events for each HHA determined by the COOP and ASOS gauge networks

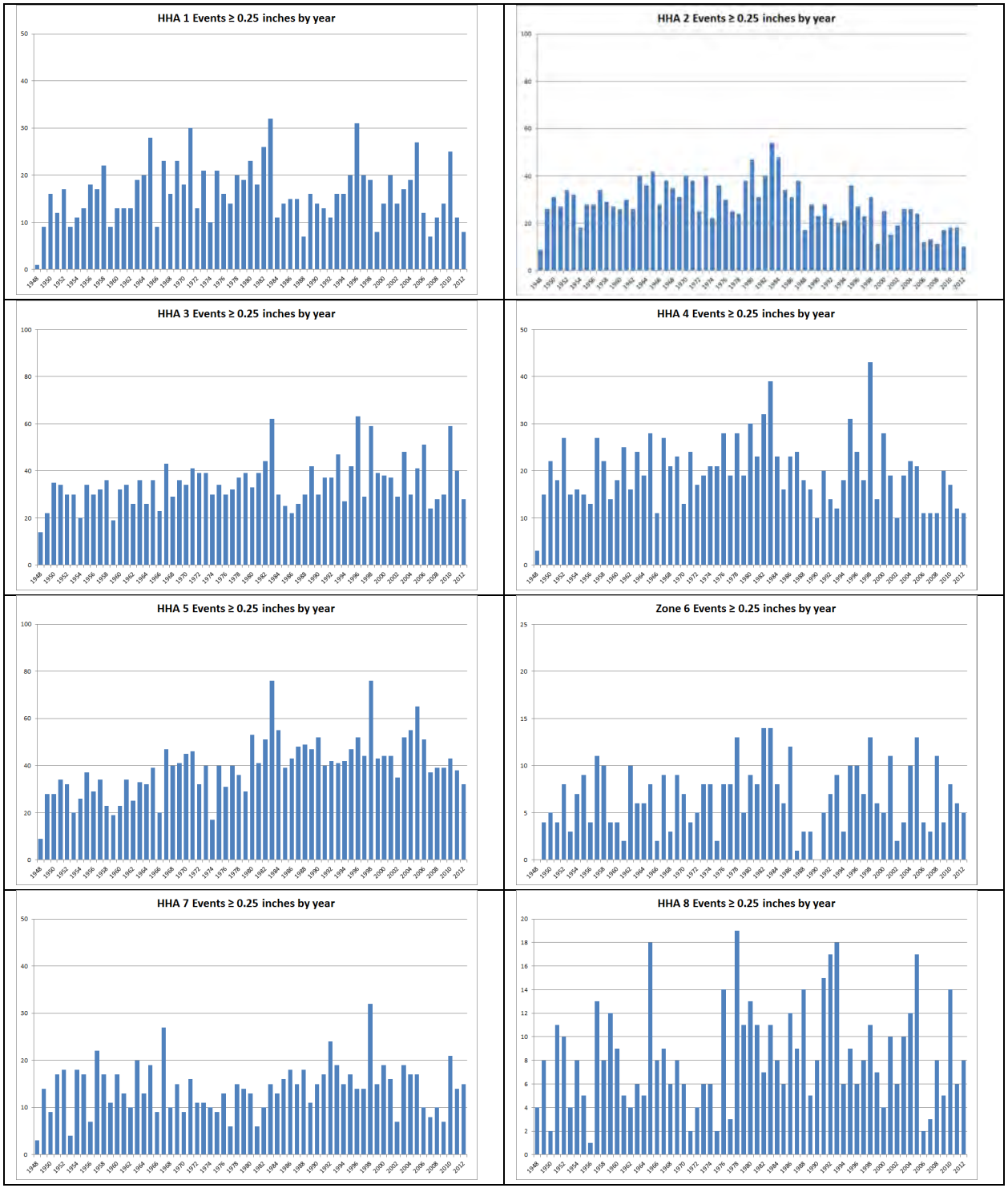

APPENDIX A-6 MMI and 90th Percentile Maximum Intensity Mean Error and Watershed Averages

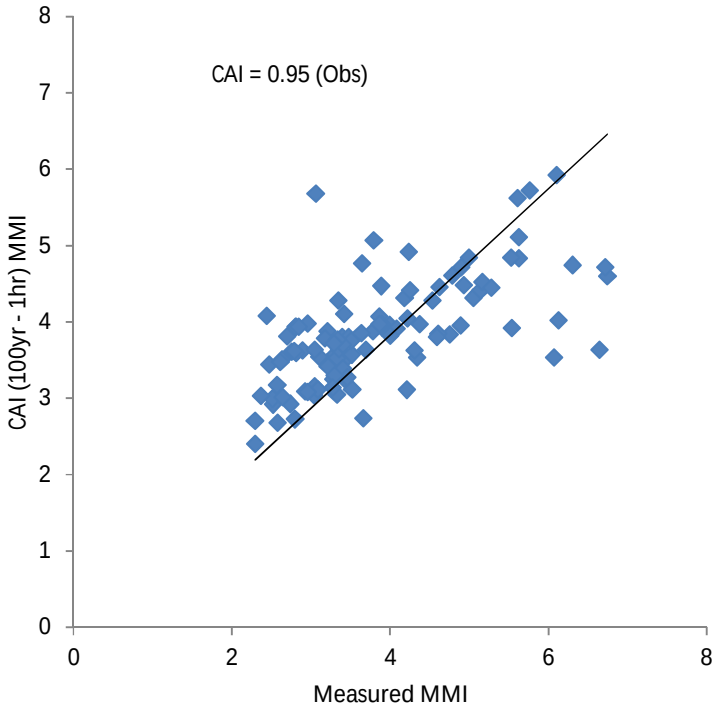

a)

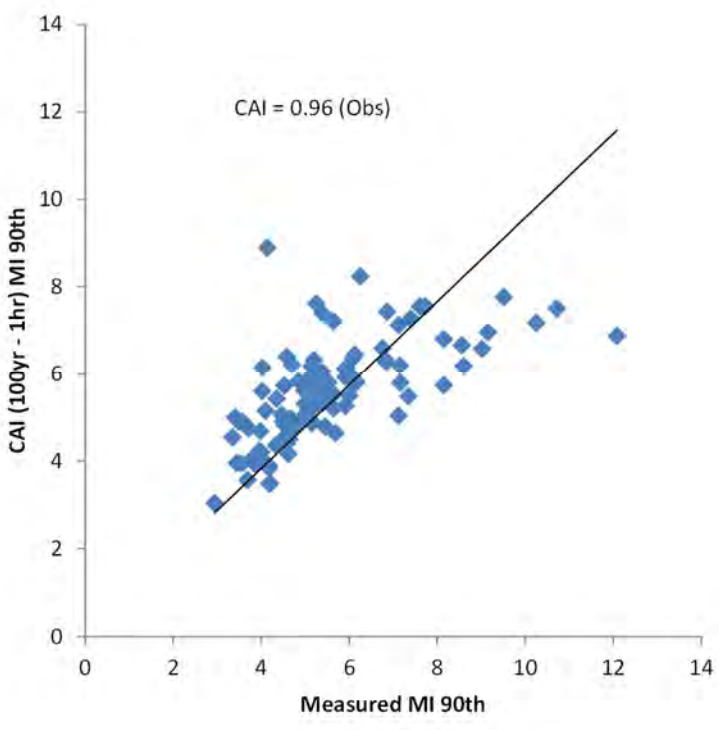

b)

Figure A-6-1 Mean error of interpolated surfaces, a) MMI and b) 90th Percentile Maximum Intensity

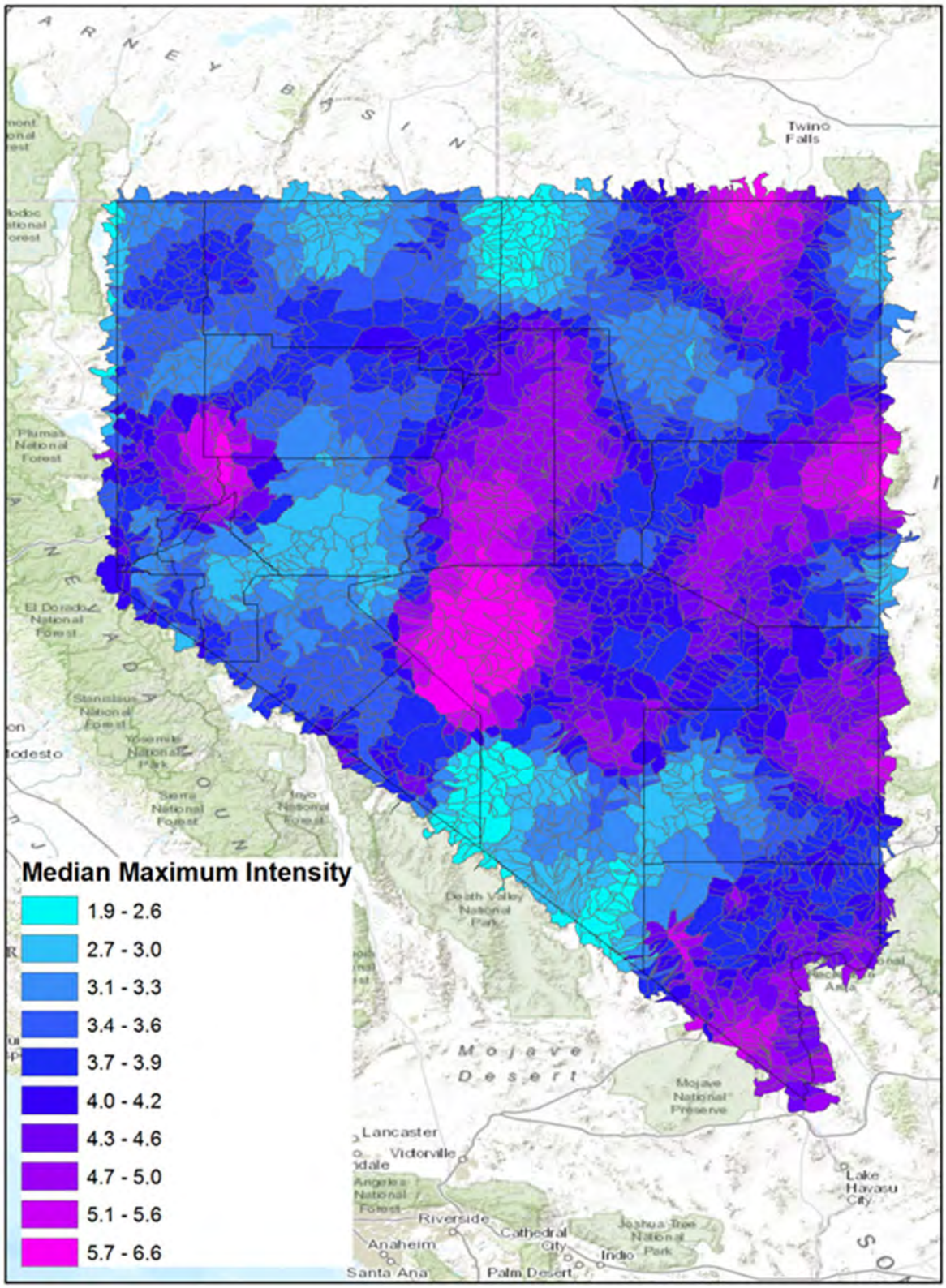

Figure A-6-2 MMI averaged by HUC-12 watershed boundaries

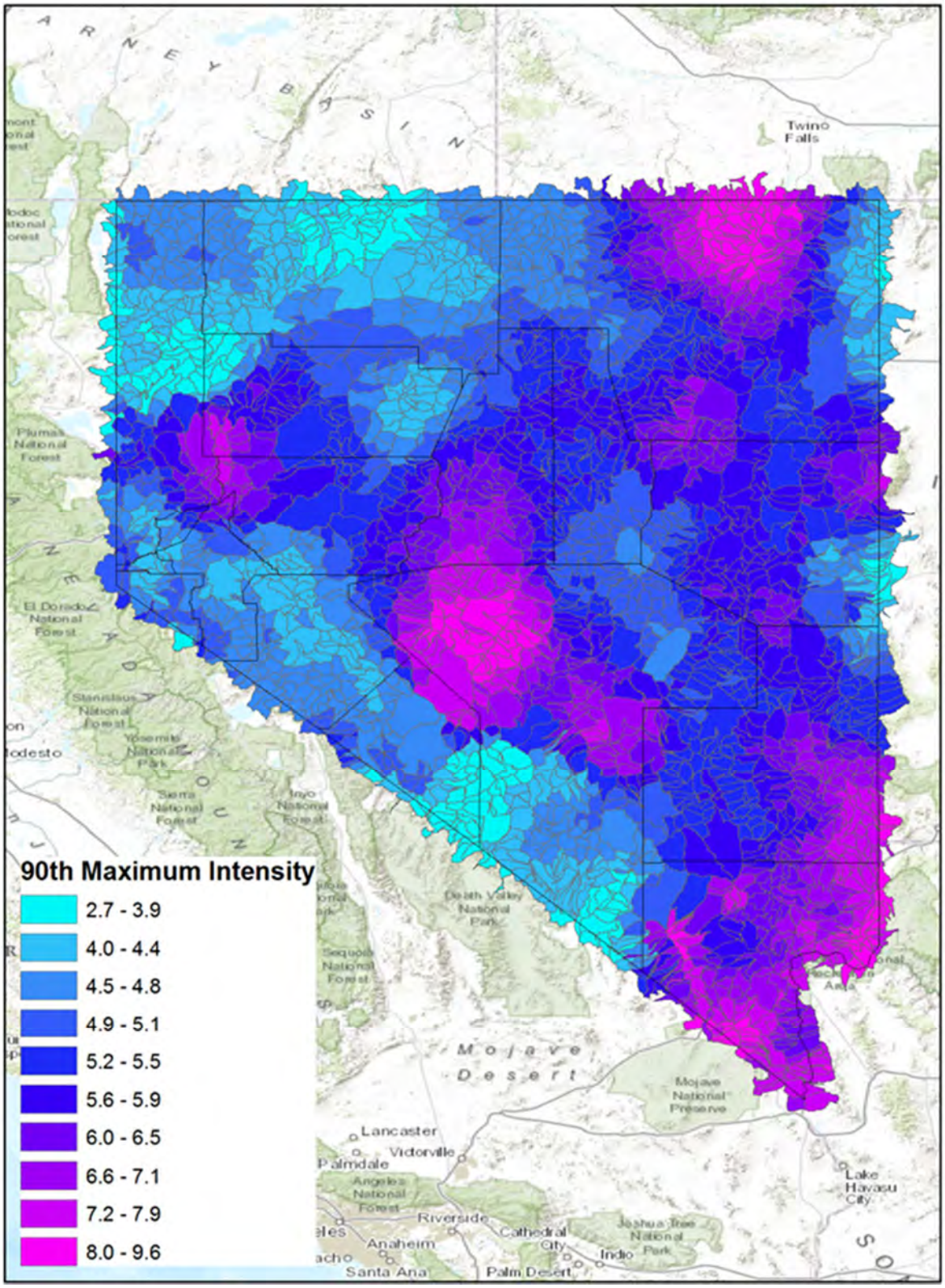

Figure A-6-3 MMI averaged by HUC-12 watershed boundaries

TECHNICAL MEMORANDUM

To: Dr. Annjanette Dodd, Ph.D., P.E.
Kimley-Horn and Associates

From: Dr. Baxter Vieux, Ph.D., P.E.
Vieux & Associates, Inc.

Date: December 23, 2014

Re: Nevada Department of Transportation, Research Project No. P530-13-803
Streamlining Hydrologic Prediction Processes Using New and More Accurate Techniques and Methods - Technical Memorandum No. 4

1. Introduction

This Technical Memorandum (TM) Number (No.) 4 presents the Depth Area Reduction Factor (DARF) Analysis for characterizing the spatial distribution of rainfall to be used for design purposes by the Nevada Department of Transportation (NDOT). The motivation of the proposed research is to improve the accuracy of design storms used as input to hydrologic models for hydraulic structure design. Principal components of a design storm consist of applying a temporal distribution to point rainfall depth based on duration and return frequency, distributing this depth according to a temporal distribution, and distribution spatially based on a DARF for the drainage area. The design storm approach is divided into two main parts: 1) the temporal distribution defined by the hyetograph shape, which was the subject of TM No. 3; and 2) the spatial distribution defined by representative DARFs, the subject of this Technical Memorandum No. 4.

2. Background

A principle of hydrology is that larger catchments are less likely than smaller catchments to experience high intensity storms over the whole of the catchment area (Siriwardena and Weinmann, 1996). Therefore, the conversion of point precipitation into area-averaged precipitation is necessary whenever an area, large enough for rainfall not to be uniform, is to be modeled. DARFs are commonly used for this conversion.

DARF-estimation algorithms can be grouped into two categories, 1) geographically fixed (GF) using rain gauges, and 2) storm-centered (SC) using radar. GF DARF-estimation using high-density rain gauge networks has been well studied for the last few decades, and the main findings are presented in a series referred to as Technical Paper No. 29 (TP-29) (U.S. Weather Bureau

1957, 1958a, 1958b, 1959, 1960, 1964). Additional references are reviewed in TM No. 2 pertaining to DARF analysis.

A number of approaches for converting point precipitation into areal precipitation are based on observed precipitation data from rain gauges (GF) or radar (SC). Algorithms used to calculate GF reduction factors can be sensitive to the configuration of the network, particularly in the GF approach where the point rainfall is compared to areal averages for non-concurrent storm events. That is to say, where areal and point precipitation values are not derived from the same event in TP-29, but rather, DARFs are computed from annual maxima and annual averages. While statistically expedient, within-storm distribution of rainfall may be masked by the approach taken in TP-29 and other derivative works.

Radar technology has been used for DARF analysis in the last three decades beginning with Austin and Houze (1972), and more recently, Durrans et al. (2002) and Olivera et al. (2005). One aspect of radar rainfall estimation is that the empirically derived relationship between reflectivity, Z, and rainfall rate, R, called a Z-R relationship, must effectively be determined. If the DARF is considered as a non-dimensional relationship between point-to-areal ratios, then the bias introduced by an assumed Z-R relationship is immaterial. Frederick et al. (1977) observed that because DARFs are expressed as dimensionless ratios of point precipitation to areal average precipitation, the uncertainty in the Z-R relationships found in radar data is removed. They also observe that it is not possible to derive DARFs for areas larger than 1,000 km^2 (386 sq. mi.) using rain gauge networks. However, this limitation is avoided by radar, which has a high-resolution coverage over large areas. Bacchi and Ranzi (1996) also identified radar data as being more efficient than typical rain gauge networks in capturing the spatial distribution of storms and estimating DARFs.

The SC approach is well suited for using spatially continuous (i.e., surface) precipitation estimates derived from radar reflectivity. In this case, DARFs are calculated for individual events for which areal properties are described, and are equal to the ratio of the average precipitation depth over an area to the concurrent point precipitation depth in the storm center. Because SC DARFs are estimated for individual events, they can capture the anisotropy of the rainfall field (i.e., the storm shape and orientation) and the seasonal effect of atmospheric processes such as the jet stream affecting speed and direction of storms. As with any method, the SC approach can depend heavily on the sample size and the distribution of storms included in the sample. Srikathan (1995) and Olivera et al. (2005 and 2008) emphasize that the expected storm characteristics and seasonal trends may not be represented by their storm sample from only 2 years of data even though a large geographical area was covered, i.e. 265,000 mi^2.

Dependence of the depth-area relationship with storm maximum rainfall depth was investigated by Asquith (1999) and Asquith and Famiglietti (2000), who found that the percent reduction

increased as depth (storm recurrence interval) increased. Allen and DeGaetano (2005) analyzed rain gauge networks in New Jersey and North Carolina, and found statistically-significant variation in DARFs with return period, though somewhat slight. Higher return periods associated with greater rainfall depths also exhibited greater reduction, which is in agreement with the results of Bell (1976 and 1987), Omolaya (1993), and Asquith and Famiglietti (2000). TM No. 2 contains further details on other published studies in DARF analysis.

Houghton et al. (1975) found that despite the arid to semi-arid nature of much of Nevada, both flooding and flash flooding occurs throughout Nevada. Significant flash flood events are often associated with a westward-moving, inverted trough tracking across the southwestern United States. Under these conditions, torrential downpours and resultant flash flooding have been documented, particularly in Southern Nevada (Randerson, 1976; Li et al., 2003; Maddox et al. 1980). Flash flooding is a significant threat during the warmer months as convection, especially during the monsoon season, known as the North American Monsoon (NAM), generally reaches its peak across the Southwestern United States from July through early September (Hales, 1972; Brenner, 1974; Douglas et al., 1993; Higgins et al., 1997; Adams and Comrie, 1997; Higgins et al., 1998; Adams and Stensrud, 2007). During the NAM, short-duration, high-intensity rainfall is produced by atmospheric moisture surging northward from the Gulf of California. Another mechanism, atmospheric rivers, can produce significant floods in summer and winter, particularly in Northwestern Nevada. Even areas that have a very low annual average precipitation can still experience cloudburst storms when conditions are favorable. National Climatic Data Center (NCDC, 2014) reports indicate that flash flooding can occur across Nevada at any time of year, but mainly from July – September, coinciding with the peak of the NAM.

In summary, the following have been observed:

- Many DARF studies are based on only a few storms or in some cases one storm that is particularly severe. A large number of storms that are geographically distributed are needed to help ensure reliable results that can be generalized for the target area.
- Significant storms should be considered since the DARF is related to depth. Thus, storms associated with flash flood reports or flood advisories are good candidates for DARF analysis.
- Since the rain gauge network is very sparsely distributed in Nevada, many of the storms considered do not have rain gauge accumulations. Thus, it is not possible to select storms of known frequency or return period depth. However, radar that is not bias corrected can be used to determine depth-area relationships provided it is expressed as a percentage or decimal fraction relative to the peak depth.
- Rainfall area is related to the duration of the storm with longer duration events covering a larger area, thus making duration an important factor for consideration of the DARF relationship.

3. Methodology

The methodology to develop DARFs used to transform point precipitation estimates into distributed rainfall estimates for drainage design purposes is discussed here. Actual storm events, observed by radar, were used to determine the DARFs throughout Nevada. These events were grouped based on flooding potential and Hydrometeorological Homogeneous Area (HHA) (Figure 3) and aggregated by rainfall duration.

3.1. Establishment of Storm Event List

Rainfall data used for determining the depth-area relationship were taken from the National Weather Service (NWS) NEXRAD (Next Generation Radar) data. Data from four radar stations were used in this analysis spanning a period from 2005 - 2014: KRGX (Reno, NV), KLRX (Elko, NV), KESX (Las Vegas, NV) and KICX (Cedar City, UT) (Figure 3). Given the large geographic extent, the relatively sparse rain gauge network, and number of radars, the events selected for analysis were aggregated based on those events for which the NWS issued a flash flood warning or flood advisory.

Starting in 2007, flash flood warnings have been typically issued for an area defined by a polygon, where flash flooding is either imminent or occurring. Flood advisories are issued for nuisance type events where rainfall is not expected to reach the warning level. Prior to 2007, most flash flood warnings and flood advisories were issued on a county-by-county basis, making it difficult to locate spatially the storm of interest. Thus, the storm list is generally oriented to flood producing events after 2007. This focus implies that the storms are likely more convective in nature than synoptic scale events predominant in wintertime and northern latitudes of Nevada, since flash floods occur with more frequency during the summertime.

The seasonal distribution of the flash flood reports from NCDC **2005-2014** is shown in Figure 1. The number of events (flash flood reports) found for this period was **138**. The distribution of flash flood producing events is dominated by convective storms during the peak NAM months, with 83% falling in July–September. Storms from the NCDC database for 2005 and 2006 were used to supplement the flash flood warning and flood advisory polygons, specifically across HHAs with a smaller number of available events.

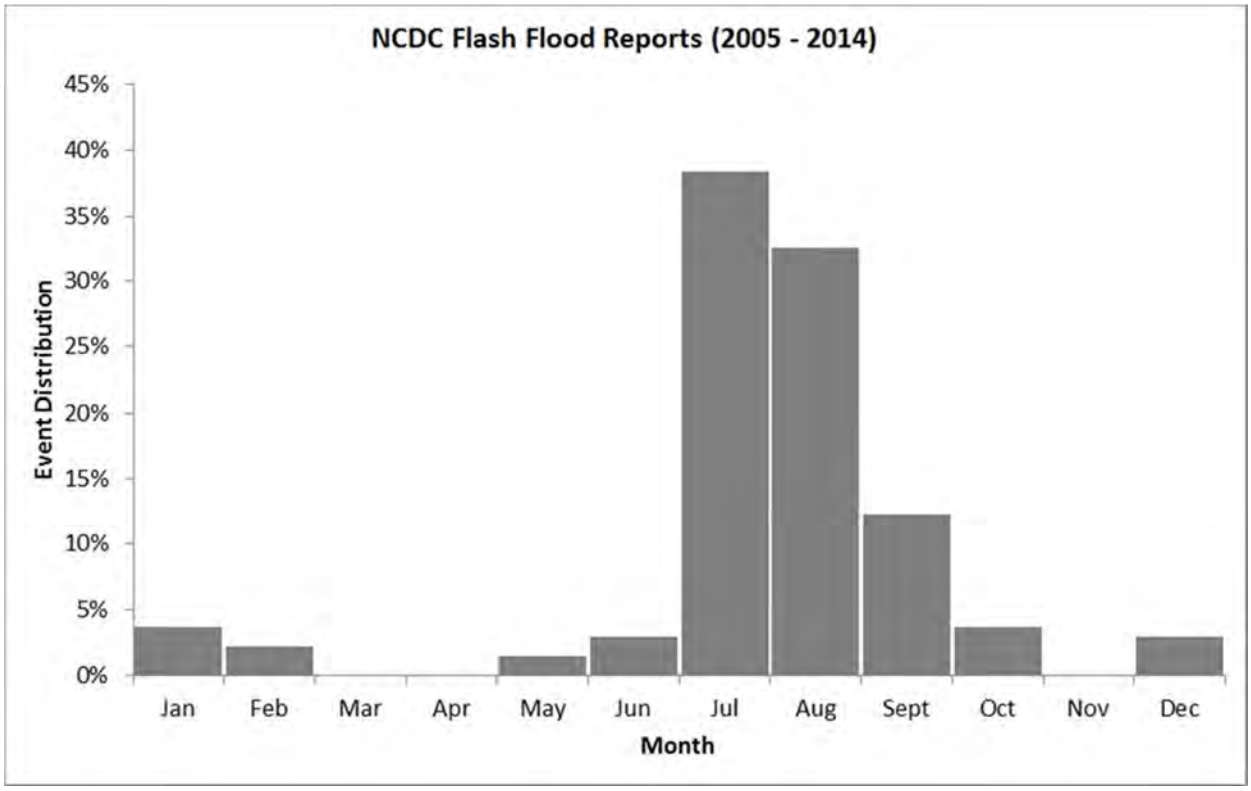

Figure 1 Monthly distribution of NCDC flash flood reports (2005-2014)

Flash flood reports, classified as either *flood warnings* or *flood advisories*, sometimes overlapped more than one HHA. In these cases, the polygon was assigned to the HHA containing the center of the warning/advisory. In addition, those flash flood events that were remotely sensed by more than one radar station were assigned to the dominant or closest radar for each HHA based on location of the peak rainfall depth. Figure 2 shows the spatial distribution of storms considered for the DARF analysis.

After the individual flash flood warnings and flood advisories were assigned to each HHA based on the location of peak rainfall depth, a final storm event list was created from each radar station to develop the DARFs. Events with overlapping times of occurrence were merged into a single event to reduce the likelihood of a specific storm being counted more than once and given extra weight in the analysis warning/advisory polygons. As a result, a single event range could possibly contain more than one area where a flash flood warning or flood advisory was issued. To increase the probability of capturing the entire rainfall event, merged event ranges were given an additional 6-hour buffer on each side, with care taken to ensure no temporal overlap with subsequent events. Table 1 presents the number of storms considered per HHA while Appendix A contains the detailed list, totaling 547 events.

To further focus the analysis on each individual HHA, the radar grids were “masked” to include

areas in close proximity to the region of interest. This was accomplished by using only the radar data within a 10-km buffer of each HHA. It was necessary to expand the buffer to 25-km for HHA 3 due to its smaller size, and for HHA 6 due to its lack of radar coverage, increasing the odds of correctly identifying the storm associated with the flood polygons. Figure 3 illustrates the radar masks used for each HHA.

Table 1 Summary of storm events by HHA meeting the warning/advisory requirements

HHA	1	2	3	4	5	6	7	8	Total
No. of Events	39	48	36	42	103	34	144	101	547

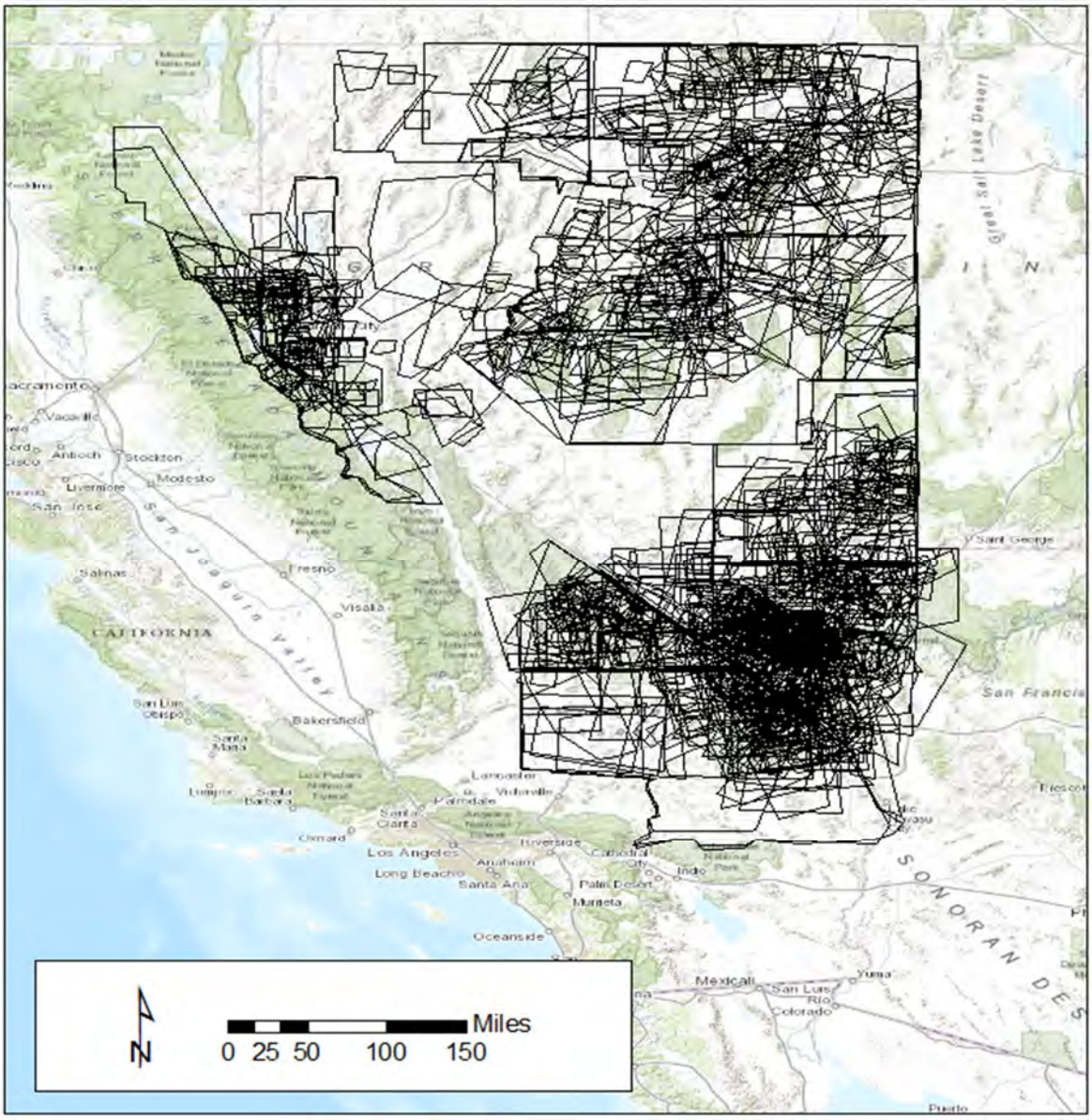

Figure 2 Distribution of flood warning/advisory polygon areas (black lines)

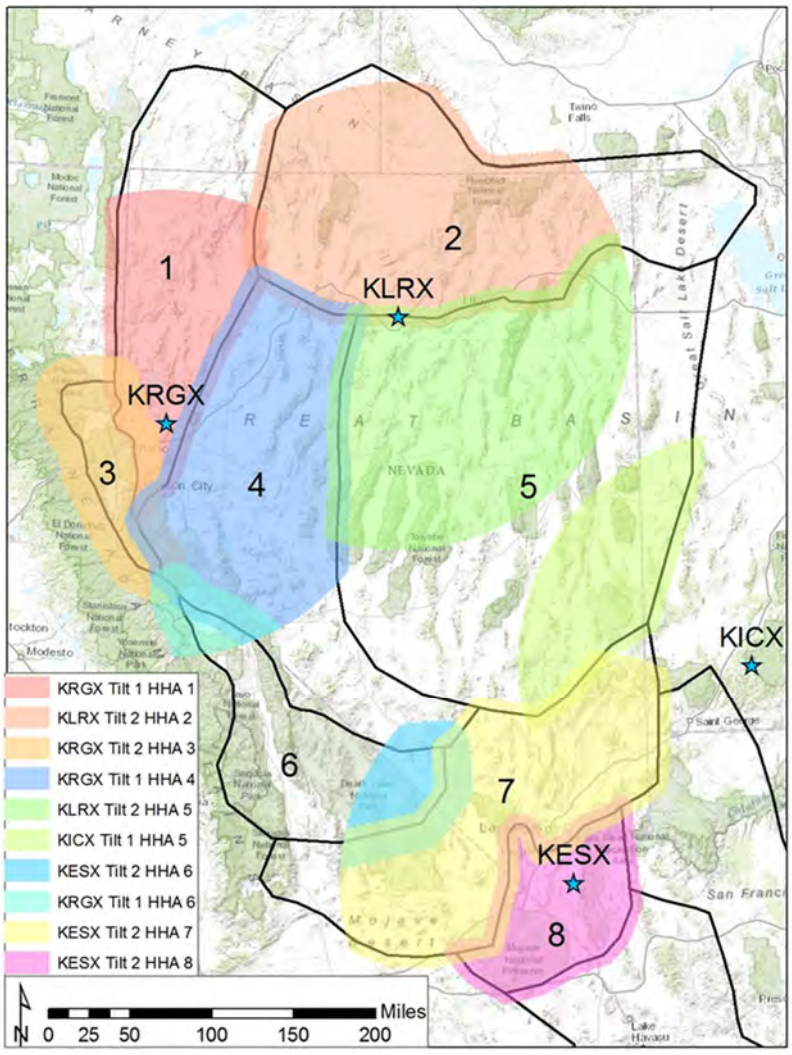

Figure 3 Radar masks used for each HHA (numbered black outlines)

After determining the event ranges and masking the radars, additional steps were taken to remove anomalous propagation (AP). AP is a false reflectivity echo on radar; an echo that is not precipitation. Radar return from AP is unpredictable, often contaminates precipitation measurements and can cause generation of erroneous rainfall estimates used in hydrology products. When possible, the second lowest radar tilt was used to avoid the most severe AP. The remaining areas of persistent APs, usually caused by terrain, were removed from the radar masks entirely, or were filled using information from surrounding radar bins. Further, attenuated or blocked radials were also filled by utilizing neighboring radar information.

Radar images were then generated for each event range for the peak 1-, 2-, 3-, 6-, 12-, and 24-hour durations, where applicable. Using the multiple durations, the individual events (Table 1)

were split into multiple duration-based events. Each radar image was then visually inspected to remove events that exhibited evidence of AP as well as those that did not indicate significant rainfall. An example is provided in Figure 4 illustrating AP from terrain during an event in HHA 1. Further, those events that showed significant rainfall were examined for bright-banding. Bright banding occurs when the radar beam encounters frozen layers in the atmosphere and can introduce anomalous reflectivity values that must be removed from the analysis. An example of this is provided in Figure 5 during an event in HHA 8. Figure 6 shows an ideal event that is devoid of AP and bright banding.

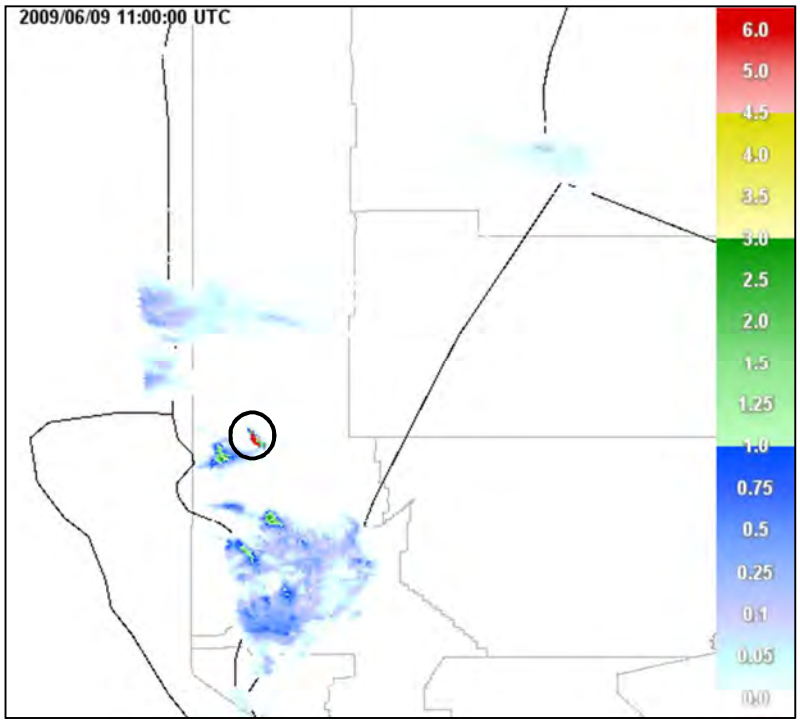

Figure 4 Example of terrain induced returns (AP) that occurred across HHA 1 during the 6/8/2009 event

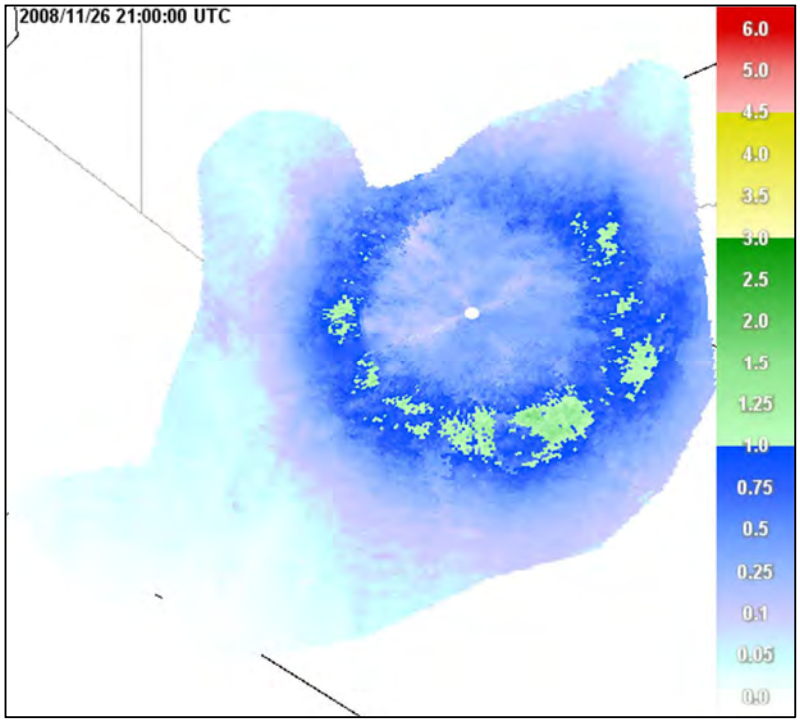

Figure 5 Example of radar bright banding that occurred across HHA 8 during the 11/26/2008 event

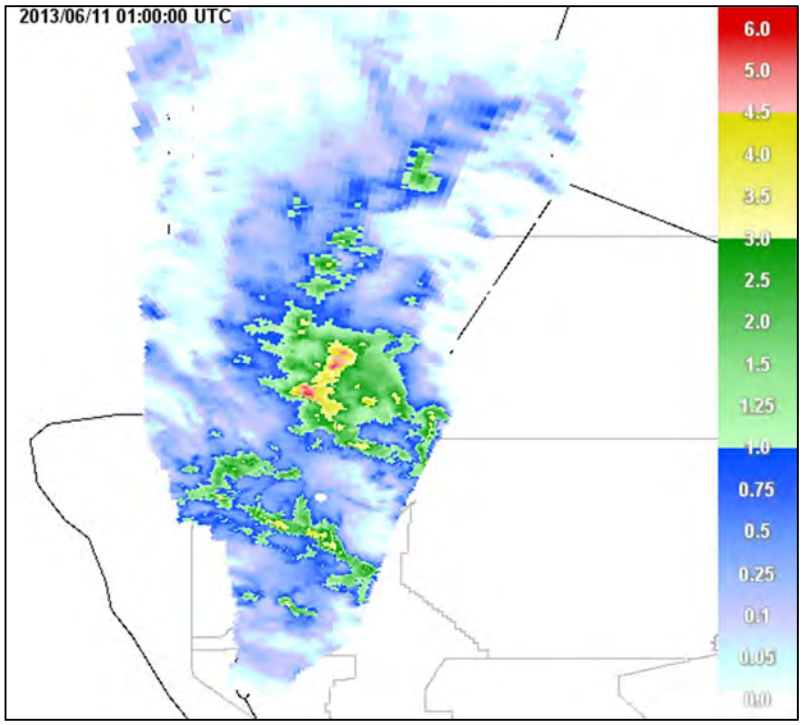

Figure 6 Example of an ideal radar event that occurred across HHA 11 during the 6/10/2013 event

For the 547 individual events, 2,797 duration-based storm totals were visually inspected for use in the analysis. This number exceeds that of the individual storms listed in Table 1 because, depending on the length, each event could represent multiple durations. After quality control

(QC) of the radar data, there remained 1,720 duration-based storm totals that met the standard for inclusion, having valid radar storm totals.

3.2.Analysis Steps

3.2.1. Convert Radar to Rainfall

Radar reflectivity (Z) data was converted to rainfall (R) by means of a convective Z-R relationship, $Z=300R^{1.4}$ (Bedient et al., 2013). The reflectivity measurements are in radial coordinates of 1-degree in azimuth and 1-km in radial dimensions. As discussed in Section 2, it is not necessary to correct rainfall totals for bias since they are considered relative for computation of point/area ratios.

3.2.2. Determine Duration-Based Storm Event Totals

Duration-based storm event totals were produced for 1-, 2-, 3-, 6-, 12-, and 24-hours by aggregation from the 1720 events discussed above. From these totals, the period with the maximum storm total, was selected. In Figure 7, the location of peak rainfall for the events analyzed is shown along with HHA boundaries. The distribution of these events depends on the location of the flood warning/advisory, which is expected to be associated with more intense or higher-depth events.

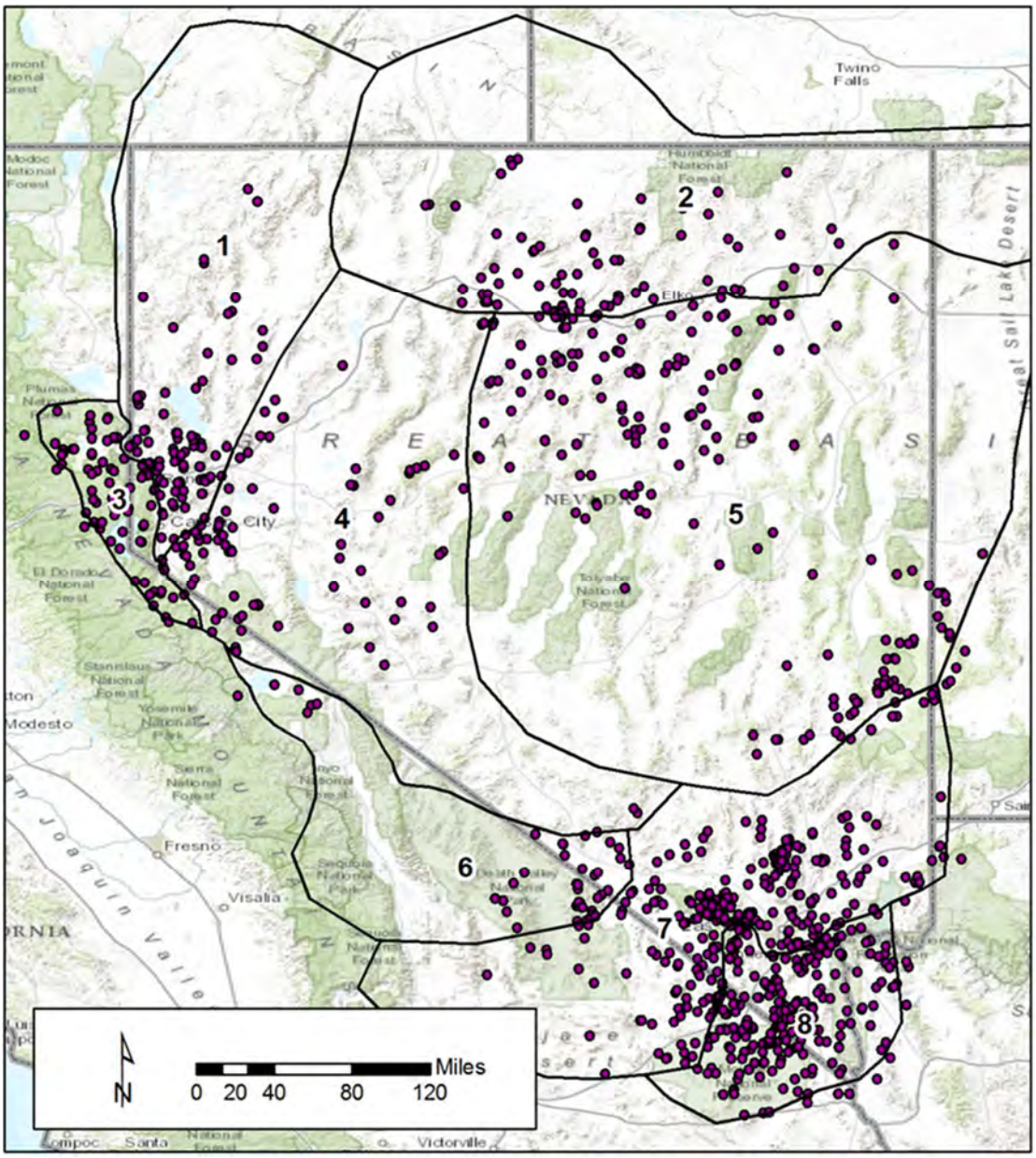

Figure 7 Distribution of duration-based storm event locations within HHAs (maroon filled circles)

3.2.3. Develop Depth-Area-Duration Values

From the storm event aggregations, depth-area-duration (DAD) values were computed. Area was determined for the average storm total depths in increments of 0.25-inches. For each event, the DAD period with the maximum depth was selected for DARF analysis.

3.2.4. Develop DARF Relationships

Once the rainfall peak depth was found, the rainfall depth and area were computed to produce a depth reduction for each area. For each area, the ratio of the average duration-based storm total depth divided by the peak storm total depth was determined. This produced a large number of

data points for each HHA and duration that can be used to fit a DARF relationship. Accounting for depth or elevation as factors affecting the DARF relationships was not performed since the storm total maps occur over a range of elevations and radar was not bias corrected.

There are multitudes of equations that can be fit to DARF data. Several were explored that involve exponential or hyperbolic functions. The hyperbolic form was found to have the best fit. The hyperbolic equation consists of three parameters, a, b, and c that are used to compute DARF as a function of area,

$$DARF = 1 - \frac{aA^c}{b+A^c} \quad [1]$$

where, *DARF* is the reduction expressed as a decimal fraction; A is area (sq. mi.), and the parameters, a, b, and c are fitting parameters that control the shape of the curve. The form of Equation 1 is similar to curves fit to intensity-duration-frequency (IDF) curves, except that instead of time, area is used (Meyer, 1928).

A nonlinear quantile model described by Koenker and Hallock (2001) was used to fit the data, and thereby obtain the 50th (median) and 90th percentile relationships for each HHA and duration. Time is not an explicit parameter in Equation 1 since the data were aggregated for specific durations from the DAD curves.

4. Results

4.1. Example DARF Curve for a Single Storm Event

As an example, a DARF curve for a single storm event is provided in Figure 8. Copious rainfall fell during several events during the NAM in 2014. The storm total ending at 7:00 UTC on August 21, 2014 is seen on the left, and the DARF curve on the right in Figure 8. A well-defined storm cell can be seen on the left, and on the right, depth-area pairs are plotted showing the relative reduction in depth as area increases. Multiple, lesser storm cells are also evident in Figure 8 on the left. These are included in the depth-area calculations. Multiple storm cells were present in many of the events analyzed. This is considered a typical rainfall pattern and their inclusion serves to increase the area of a given depth, thus reducing the percent reduction.

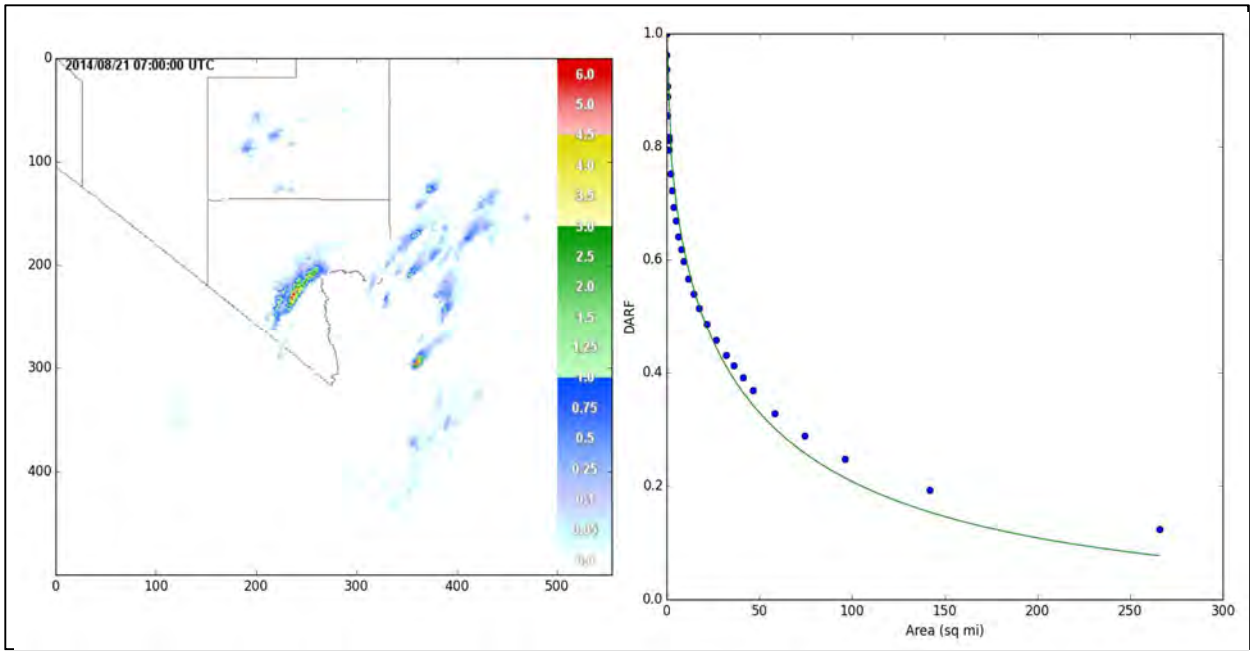

Figure 8 Storm total (left) and DARF curve (right) for storm ending on 2014/08/21 at 07:00 UTC

4.2.DARF Curves for each HHA and Duration

The DARF curve presented in Figure 8 represents a *single* storm event. When the DARF data are plotted for each duration and HHA, there is considerable spread (range of DARF values) for any given area, characterized by the "cloud" of points in Figure 9. (Note: The shape the DARF curve in Figure 8 is different than that in Figure 9 because of the different horizontal axis scales).

The fitted parameters for each duration 1-, 2-, 3-, 6-, and 12-hour and each HHA are summarized in Appendix C, Tables C-1 and C-2 for the median and 90th percentiles. The curves are provided in Appendix B. Examination of the DAD curves revealed that there were sometimes no significant increase in area beyond a given duration, between 12- and 24- hours. As a result, the corresponding DARF relationships for these two durations overlap. Further, the 24-hr duration did not contain sufficient data to make reliable estimates of the median or 90th percentile regression equations in any HHA, and as a result are not included.

The upper limit on area in this DARF analysis is limited to 500-sq. mi. even though larger areas were present in the data. The DARF relationships provided here should only be applied to areas up to 500-sq. mi. since this limit was imposed to aid in curve fitting and in meeting NDOT objectives (personal correspondence with Brian Wilson, NDOT Hydraulics Engineer). The limited extent helps focus the curve fitting to targeted areas useful for purposes of this analysis.

Figure 9 illustrates the data points and regression relationships for the median and 90th percentile for the 1-hr duration in HHA 8. From the shape of the data and regression curves, there is an evident small reduction for areas smaller than about 1 to 2sq. mi., beyond which, there is a

steady reduction with increasing area. Figure 10 shows the same, but for the 12-hr duration in HHA 8. There is a general shift to the right (larger area) for a given reduction because the storm covers a larger area as time progresses, i.e. for longer duration storms there is a smaller reduction.

In Figures 9 and 10, the median and the 90th percentile DARF relationships are shown for two target durations. As expected, the 90th percentile relationships show less reduction than the median DARF relationships. To apply the DARF relationship, Equation 1, for a particular HHA and duration, the model parameters are summarized in Appendix C by HHA and duration for the median and 90th percentiles. DARF curves for the target durations are presented in Figure 11 for HHA 1 for the median (left) and 90th (right) percentiles. As expected, the 90th percentile relationships on the right show less reduction than the median DARF relationships, which is evidenced by the upward shift (less reduction for a given area) in the plot on the right.

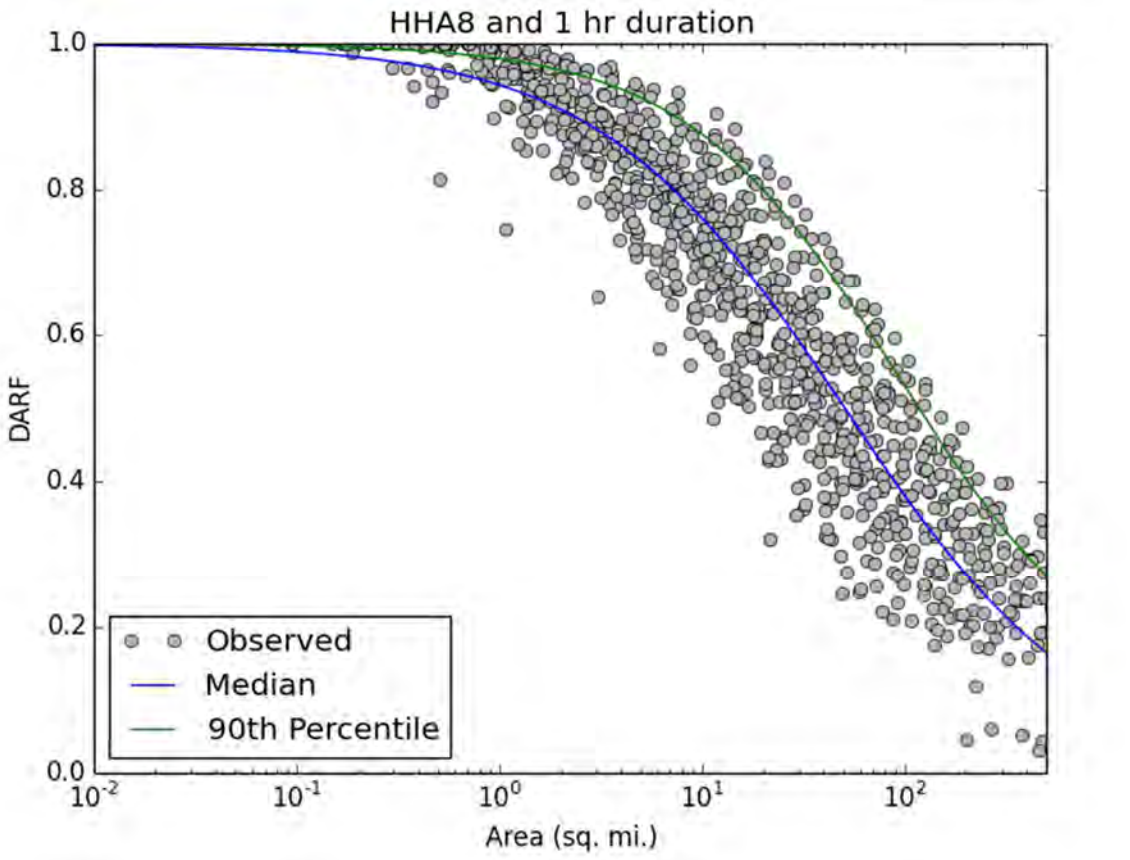

Figure 9 Observed DARF data points and fitted model for median and 90th for HHA 8 at 1-hr duration

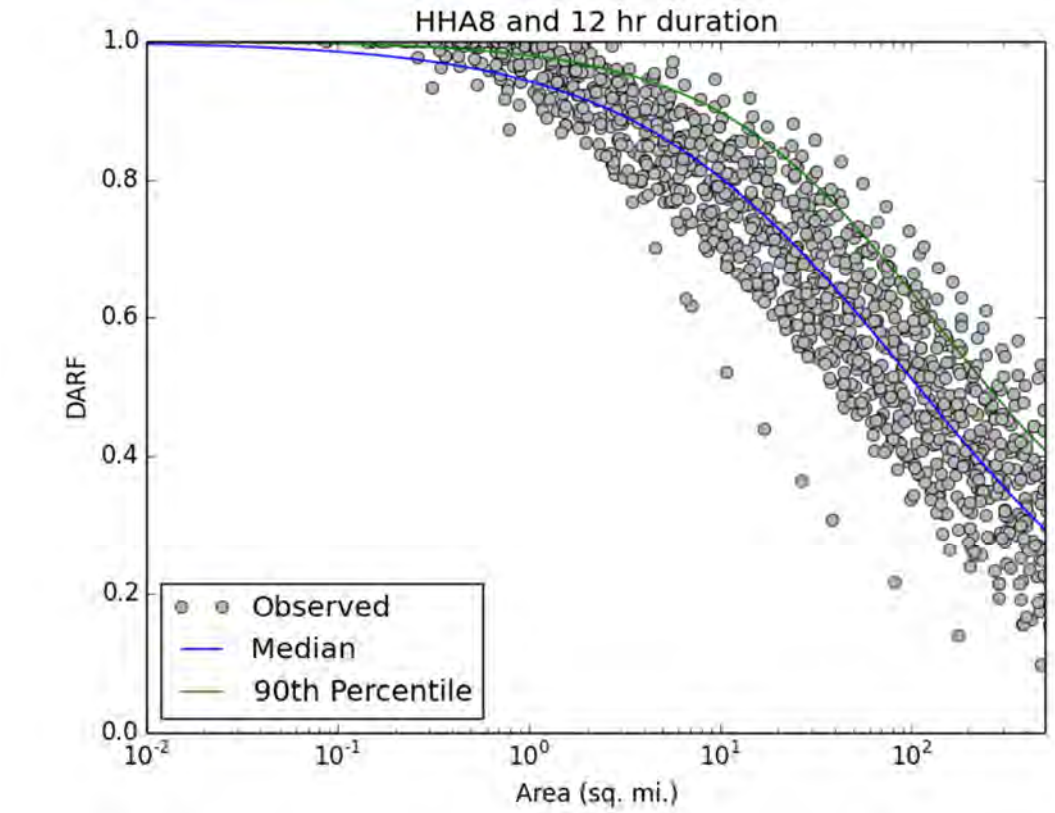

Figure 10 Observed DARF data points and fitted model for median and 90th percentile in HHA 8 at 12-hr duration

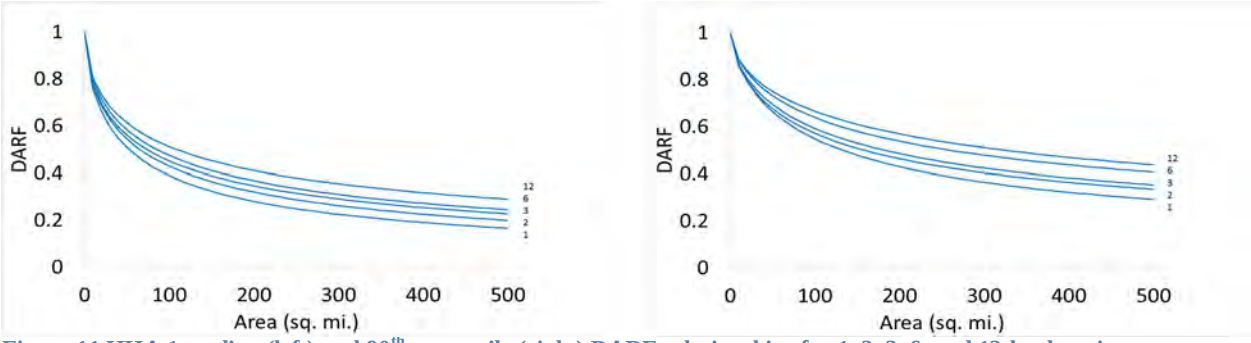

Figure 11 HHA 1 median (left) and 90th percentile (right) DARF relationships for 1, 2, 3, 6, and 12-hr durations

5. DARF Study Comparison

The following comparisons were made to identify similarities and differences between the results found using the radar in the storm centered (SC) framework presented here for the State of Nevada (referred to as, NDOT results) with other relevant SC and GF studies. The DARF studies used for comparison are those from NWS TP-29 (U.S. Weather Bureau, 1957-1960), Walnut Gulch (NOAA Atlas 2, Zehr and Myers, 1984), Clark County Regional Flood Control District (CCRFCD) (USACE, 1988), Texas Department of Transportation (TXDOT) (Olivera et al., 2005), Maricopa County (USACE, 1974), Durrans et al. (2002), and the Utah PMP (Jensen, 1995). Of these studies, only the TXDOT and Durrans et al. studies relied on radar (SC).

In the studies reviewed, reported DARF values are at various durations. Table 2 presents selected DARF values at multiple areas, where 0-sq. mi. represents a peak DARF value of 1.0 (no reduction), and at selected areas at 56-, 154-, and 303-sq. mi. These selected areas correspond to multiples of 4-km resolution so that comparisons can be made with the Durrans and TXDOT studies, which used NWS radar products at this resolution. Of the eight studies, five are in the Western U.S. (CCRFCD, Maricopa County, Utah PMP, and Walnut Gulch) and considered relevant even though they are GF, i.e. based on rain gauges. NDOT results were computed for the same durations and areas, and presented for both the median and 90th percentile. The median was used in all the comparison studies that included more than one storm, making the median NDOT values the most comparable to the results from the other studies. However, the NDOT 90th percentile is also relevant when comparing to single-storm DARF relationships, i.e. Maricopa County AZ, which is based on a single, though extreme storm event. Similarly, the Utah PMP study relies on a few extreme events with a DARF relationship published in Jensen (1995), which exhibits the greatest reduction. Walnut Gulch DARF values are published in a variety of publications including the NWS Technical Memorandum, Hydro 40 (Zehr and Myers, 1984) and used in NOAA Atlas 2. NOAA Atlas 2 has been superseded by NOAA Atlas 14; however, the planned addendum to NOAA Atlas 14 for areal reduction factors has not been published by the NWS as of the date of this TM No. 4. In most of the cases presented in Table 2, the NDOT DARFs result in a larger reduction. A detailed comparison between the NDOT results and the other studies is provided below.

Table 2 DARFs study results at selected durations and areas, with the statewide average of the median and 90th percentile values (average of HHA 1 through HHA 8)

Study	Study	Duration (Hr)	Area (Sq. Mi.)			
			0	56	154	303
			DARF			
NWS TP-29	GF	1	1.0	0.86	0.74	0.68
Durrans	SC	1	1.0	0.88	0.76	0.67
TXDOT	SC	1	1.0	0.79	0.61	0.49
NDOT Median	SC	1	1.0	0.49	0.31	0.21
NDOT 90th	SC	1	1.0	0.65	0.44	0.32
Utah PMP	GF	3	1.0	0.15	0.11	0.07
Walnut Gulch	GF	3	1.0	0.62	0.58	0.52
NDOT Median	SC	3	1.0	0.56	0.39	0.29
NDOT 90th	SC	3	1.0	0.70	0.53	0.41
CCRFCD	GF	6	1.0	0.68	0.55	0.46
Maricopa County	GF	6	1.0	0.88	0.83	0.81
Walnut Gulch	GF	6	1.0	0.63	0.59	0.55
NDOT Median	SC	6	1.0	0.60	0.44	0.34
NDOT 90th	SC	6	1.0	0.73	0.57	0.46

5.1.1. NWS TP-29

The DARF curves presented in NWS Technical Paper 29 (TP-29) (U.S. Weather Bureau, 1957 through 1960) were derived from dense rain gauge networks (GF-type analysis) located in the Midwest and Northeast U.S., none were in the Southwest U.S. DARF plots for selected drainage areas are shown in Figure 12 and are for comparison purposes only they should not be taken as the recommended shape of the DARF relationship (these are provided in the Appendices). The TP-29 DARFs exhibit much less reduction than those determined in this study (NDOT).

Even though the TP-29 DARFs were developed using storm data from the Midwest and Northeast, they have been used throughout the entire U.S. No geographical variation in DARF is presented in TP-29, making it less applicable in Nevada or other regions. Leclerc and Schaake (1972) characterized the TP-29 relationship between point and area depths as a double exponential curve containing a plateau at areas greater than about 500 sq. mi., implying that rainfall does not diminish for these large areas. Allen and DeGaetano (2005) considered the differences between SC and GF approaches, and found that the SC approach obtained from radar data typically shows 15-30% more reduction than GF results. The shape of the TP-29 DARF relationship, and its plateau for large areas, is a consequence of the GF method and statistical analysis used to derive the DARF, and perhaps related to climate. The TP-29 relationships were derived from a number of dense rain gauge networks, none of which was located in the

Southwestern U.S.

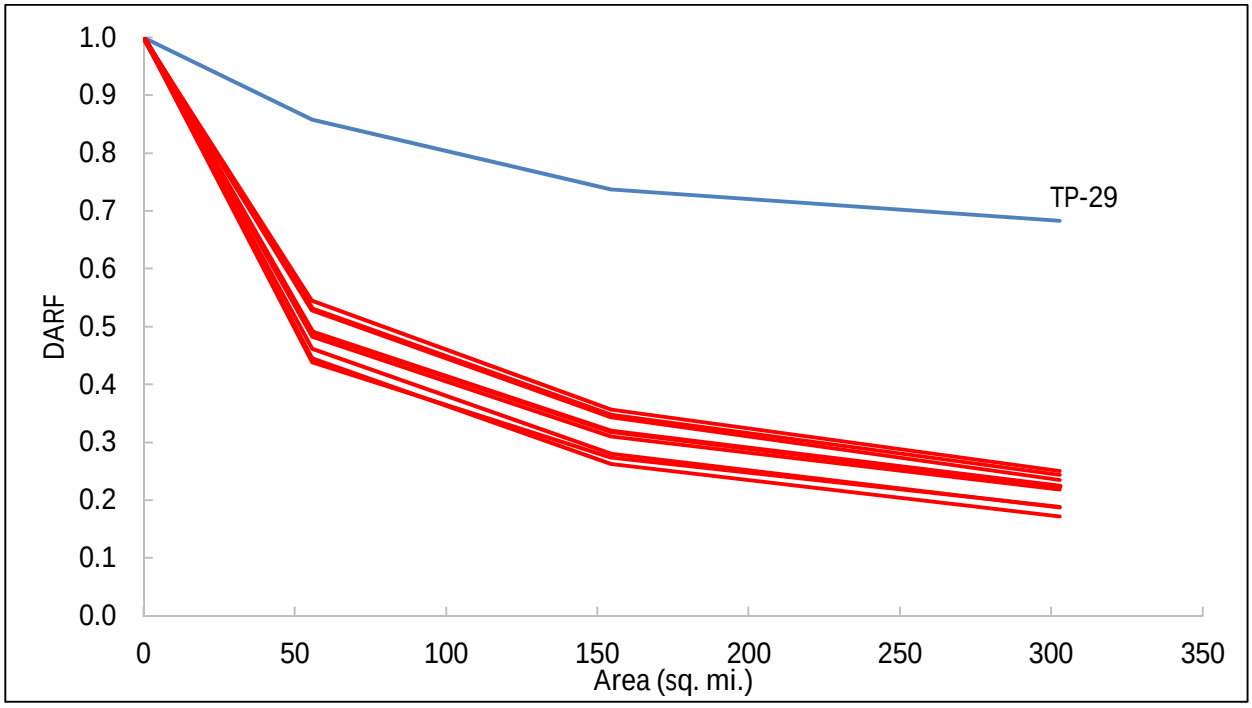

Figure 12 1-hr duration DARF curves from TP-29 (blue) and median DARF curves for HHA 1 through HHA 8 (red)

5.1.2. Walnut Gulch

NOAA Atlas 2 contained a GF-type analysis for a rain gauge network operated by the USDA Agricultural Research Service (ARS) in the Walnut Gulch watershed located near Tucson, AZ (Zehr and Myers, 1984). DARF plots for selected drainage areas are shown in Figure 13 for comparison purposes and indicate close agreement for areas from 0- to 100-sq. mi. In this range, the DARFs are coincident up to about 50 sq. mi., beyond which, the Walnut Gulch relationship begins to plateau, consistent with a GF analysis, while the radar-based (SC) analysis from the NDOT study continues to show reduction with larger areas.

The Walnut Gulch, AZ network consists of 107 gauges at an average elevation of 4,656-ft. msl. The Walnut Gulch rain gauge network only encompasses 150-sq. mi. and therefore, projections beyond this area would be an extrapolation. In fact, most of the reduction occurs by about 50-sq. mi., suggesting that this encompasses the spatial scale of the rainfall in this locale with its arid climatological conditions.

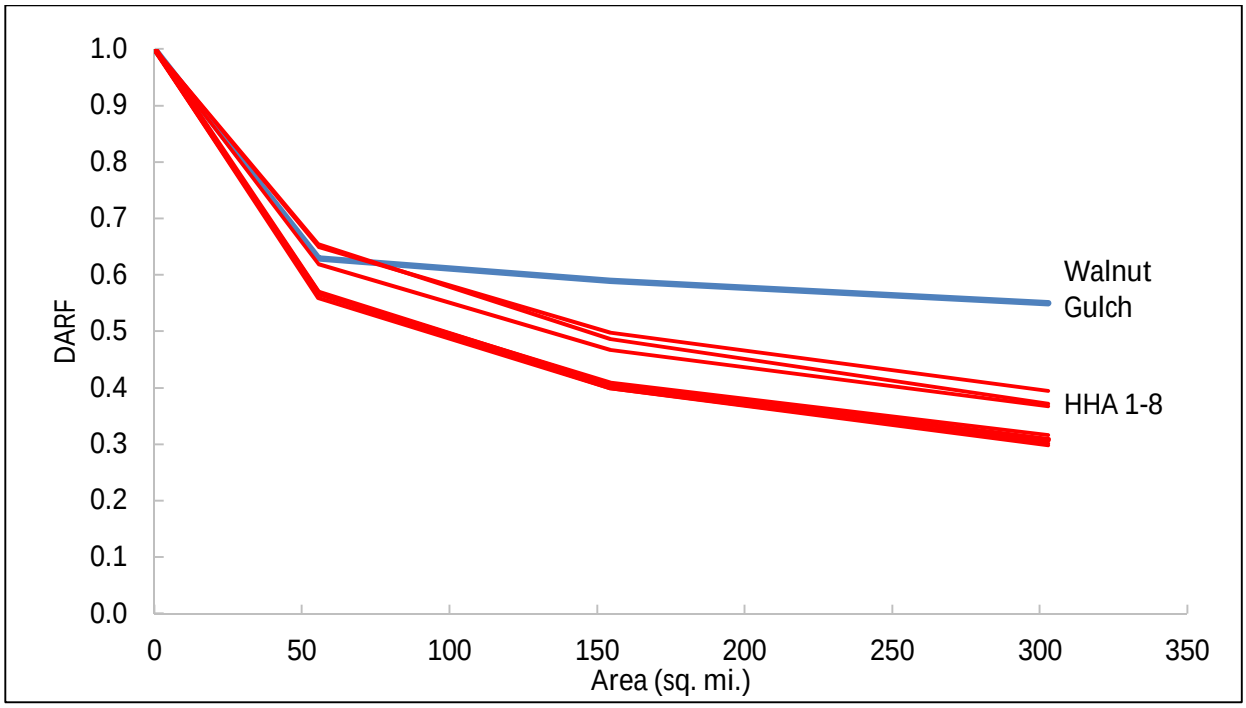

Figure 13 6-hr duration DARF curves for Walnut Gulch (blue) and median DARF curves for HHA 1 through HHA 8 (red)

5.1.3. CCRFCD

The Clark County Regional Flood Control District (CCRFCD) requires a specific design DARF that is based on DARFs determined by the U.S. Army Corps of Engineers (USACE), Los Angeles District for 6-hr duration (see USACE, 1988). In determining the DARFs, the USACE used storms from Los Angeles, CA and Las Vegas, NV. CCRFCD requires the factors presented in Table 3 for all stormwater design in the CCRFCD region. Figure 14 shows the results of DARF analysis from this study compared to the 6-hr duration CCRFCD DARF. The median curve falls slightly below the CCRFCD curve, while the 90th percentile DARF is nearly coincident with the CCRFCD curve.

Table 3 6-hour CCRFCD DARFs (USACE, Los Angeles District)

Area (sq. mi.)	0	0.5	1	2	4	6	8	10	20
DARF	1.00	0.98	0.97	0.93	0.91	0.90	0.88	0.86	0.79
Area (sq. mi.)	30	50	100	150	200	300	400	500	
DARF	0.74	0.68	0.60	0.55	0.51	0.46	0.42	0.39	

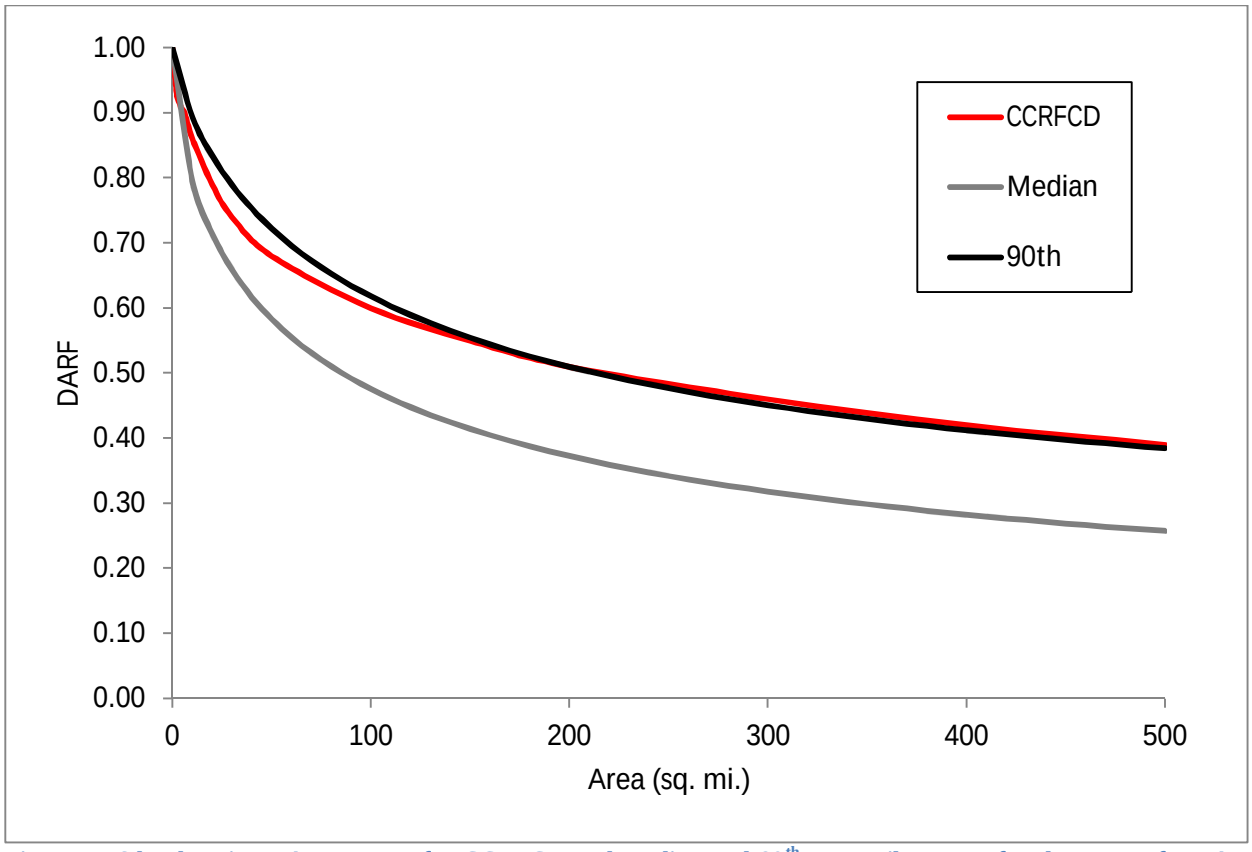

Figure 14 6-hr duration DARF curves for CCRFCD and Median and 90th percentile curves for the mean of HHA 1 through HHA 8

5.1.4. Texas Department of Transportation (TXDOT)

Olivera et al. (2005) present DARF results from a statewide analysis in Texas using NEXRAD radar to assess the DARF relationship for storms for the Texas Department of Transportation (TXDOT). This study is composed of storms from over a two-year period using radar data at 4x4-km resolution in an SC-type analysis framework. Figure 15 presents the TXDOT median results compared with the median DARF results from this study for HHA 1 through HHA 8. The TXDOT results show generally the same shape but with less reduction. This trend of generally higher DARF values (less reduction) could be explained by climatological differences that produce larger storm cells in Texas than Nevada.

5.1.5. Maricopa County

Maricopa County, AZ requires a specific design DARF that is based on a single extreme storm event; the 19 August 1954 Queen Creek storm (USACE, 1974). This storm is the basis for the Maricopa County 6-hr local storm distribution and DARF, which is a GF-type analysis (Sabol and Motamedi, 1999). The comparison shown in Figure 16 presents the Maricopa DARF and both the median and 90th percentile NDOT results for HHA 8. HHA 8 is presented because it is

located at the southern part of Nevada closest to Arizona. There is close agreement up to about 20-sq. mi., after which, the three DARF curves diverge with the Maricopa DARFs providing less reduction. The closest to Maricopa is the 90th percentile DARF relationship.

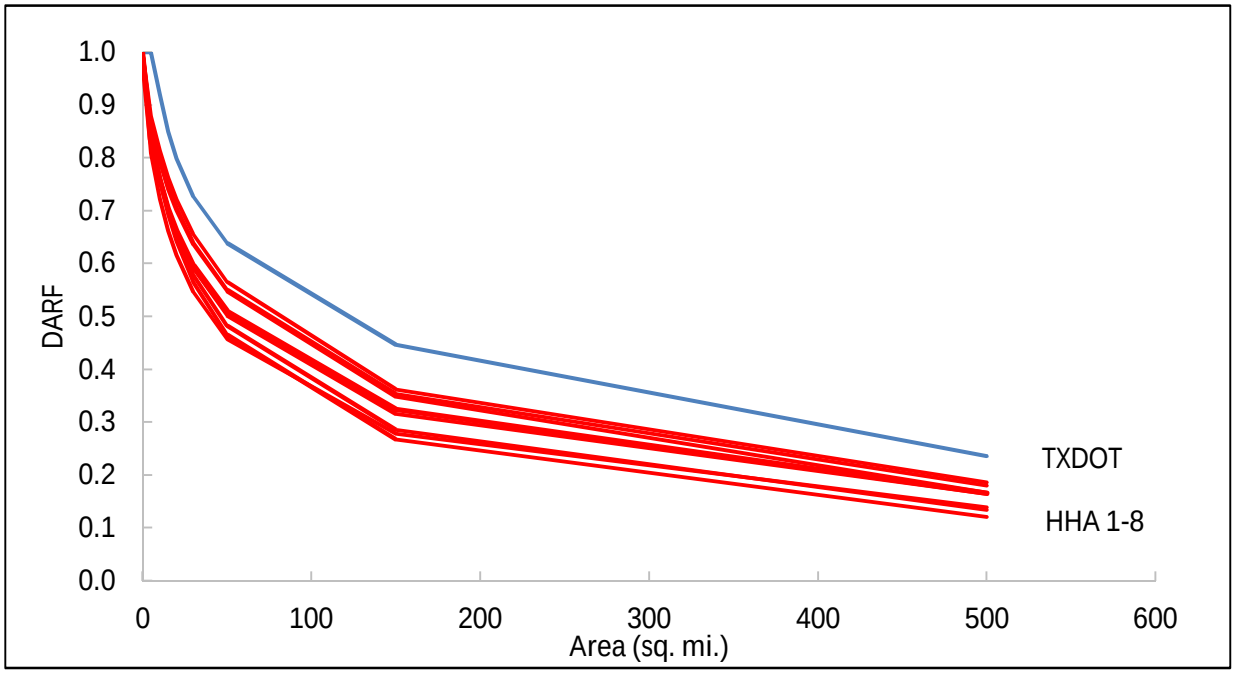

Figure 15 1-hr duration DARF curves for TXDOT (blue) and median DARF curves for HHA 1 through HHA 8 (red)

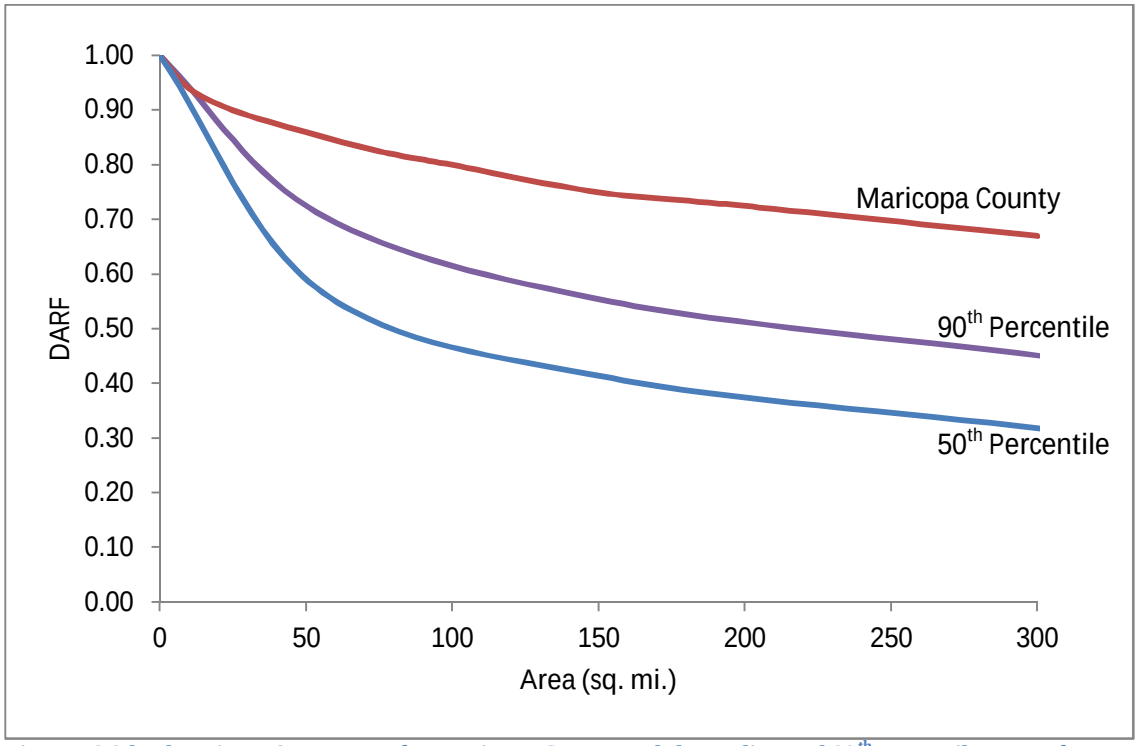

Figure 16 6-hr duration DARF curves for Maricopa County and the median and 90th percentile curves for HHA 8

6. Discussion

The DARF results derived in this study (NDOT) are consistent if not nearly coincident with two studies: 1) Walnut Gulch at the median or 50th percentile; and 2) CCRFCD at the 90th percentile. The NDOT 90th percentile compares closely to the 6-hr Maricopa County DARF, up to about 20 sq. mi., beyond which, there is less reduction seen in the Maricopa results. Compared to other studies, both GF and SC, DARF values are larger (less reduction) than the NDOT results found herein. Only one study, the Utah PMP, presented greater reductions than NDOT. The Utah PMP DARFs indicate an 85% reduction at 50 sq. mi., or a DARF=0.15 (3-hr duration). For all of the HHAs, most of the reduction occurs once the area reaches 50 sq. mi., with 50% reduction at 1-hr duration, and 60% at 6-hr durations.

The DARF values obtained by most other studies are representative of median DARF relationships, which are less conservative than relationships representing percentiles greater than 50%. Median relationships are less conservative since 50% of the events could have less reduction, i.e., the reported DARF would result in applying too much reduction 50% of the time. One reason that other studies only report median DARF relationships likely comes from not considering a large number of storms to reliably estimate larger quantiles, such as the 90th percentile where only 10% would have lesser reduction. In the NDOT results 1,720 events were used, and from the curve fitting, reliable estimates of the 90th percentile were generally found for most durations and HHAs.

However, for some durations, the 90th percentile DARF relationships overlap or cross over each other (Appendix C, Figures C-1 through C-8). This results from having too few storms to reliably estimate the 90th percentile relationships. Notably, HHA 6, includes parts of Death Valley on the south and Yosemite National Park in its northern portion. This HHA has the fewest number of events, with only 34. Eight of these 34 events (24%) fall in cool season months (October-March), the highest proportion among the HHAs. Even for the median DARF relationships, several DARF curves, at different durations, nearly overlap or are not evenly spaced in HHA 6 (Figure 17). This is also somewhat evident in the other HHAs with a low density of storm events (i.e., few events over the HHA area).

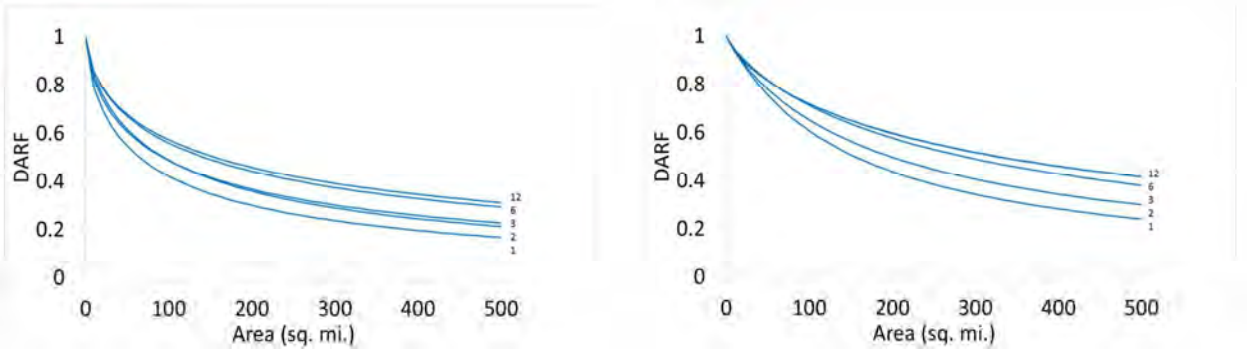

Figure 17 DARF curves for HHA 6 for the median (left) and 90th percentile (right) and each duration (1-, 2-, 3-, 6-, and 12-hour)

A minimum area with no reduction was not specifically evident from the NDOT results. While there appears to be an area between 1 and 5 sq. mi in most HHAs where there is no reduction (DARF=1.0). Since the storm total maps used in this study (e.g., Figure 8) contain multiple cells or clusters that are included in the DARF determination, the result is less reduction and smaller DARFs than would otherwise occur for a single storm cell. Given the scatter evident for small areas having a DARF of 1.0, the minimum area could be assumed to range from 1- to 5-sq. mi. for which no reduction is applied.

Review of the 90th percentile DARF relationship values across the HHAs at short duration, e.g. 1-hr, indicates that almost 50% of the reduction occurs at areas less than 150 sq. mi., beyond which the reduction is much more gradual (Figure 18).This reduction is less dramatic as the duration increases as shown for the 6-hr DARF in Figure 19. The maximum difference between DARF values is between HHAs 6 (Death Valley) and HHA 2 (Northeastern Nevada) and HHA 3 (Lake Tahoe) for the 1-hr duration and between HHA 6 and HHA 3 for the 6-hr duration; which is less than 0.20 for both cases (Figures 18 and 19). There is less of a difference between DARF values among HHAs for smaller areas than larger areas. For areas less than or equal to 100 sq. mi. the difference between HHAs at 1-hr duration is 0.15 or less (DARF ranging from 0.46 to 0.61). As illustrated in Figure 20 showing statewide average relationships, the difference among the DARF values for each duration increases with area.

Of all the areas in Nevada, HHA 2 (Northeastern) and HHA 3 (Lake Tahoe area) have the lowest DARF (most reduction) for 1-hr duration and HHA 3 at 6-hr. HHA 6 (parts of Death Valley and Yosemite) exhibits the least reduction (highest DARF), for areas up to 200 sq. mi. at 1-hr duration, and 300 sq. mi. at 6hr duration. This result could be explained by the highest proportion of wintertime storms (24%) included for HHA 6, compared with the other HHAs. Depending on the duration and HHA, it is reasonable to develop a single relationship across HHAs that exhibit little difference in DARF values. For example, HHAs 4, 5, 7 and 8 could be combined, as seen by their closeness to each other in Figure 18.

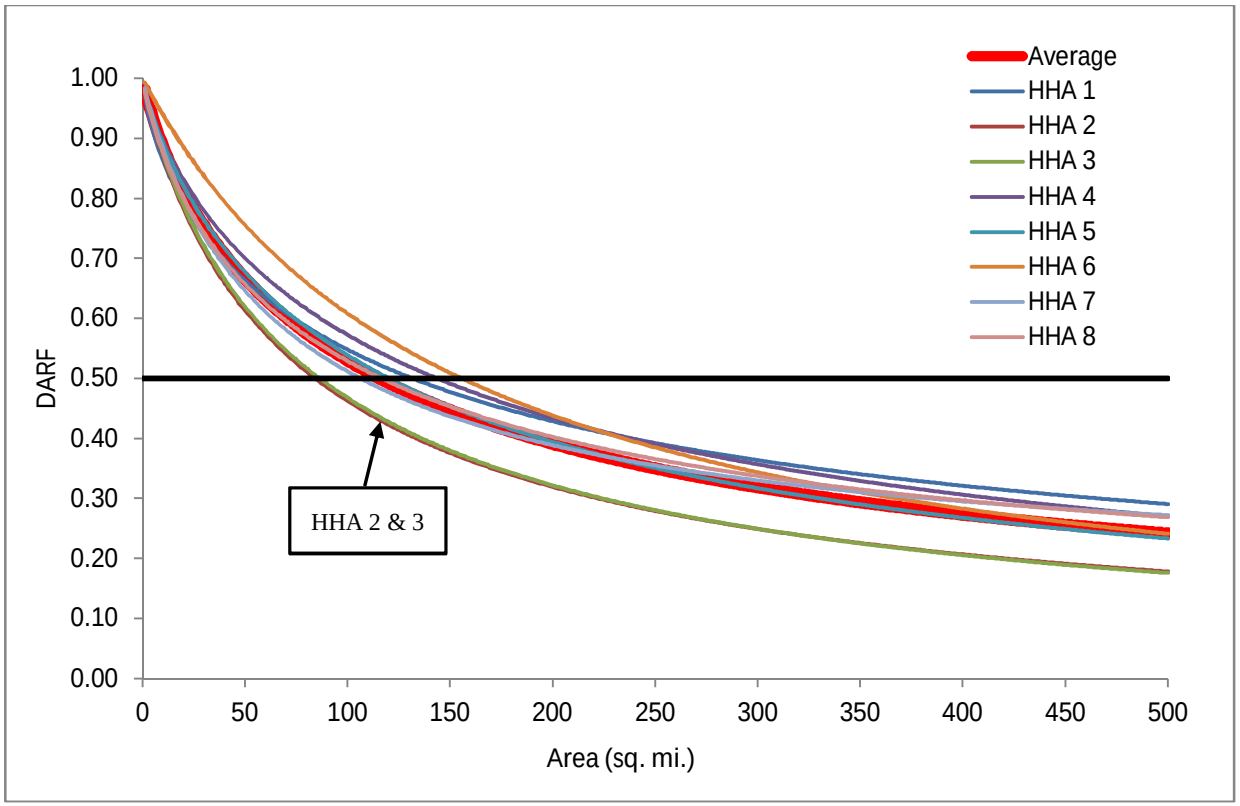

Figure 18 1-hr duration, 90th percentile DARF relationships for HHA 1 through 8

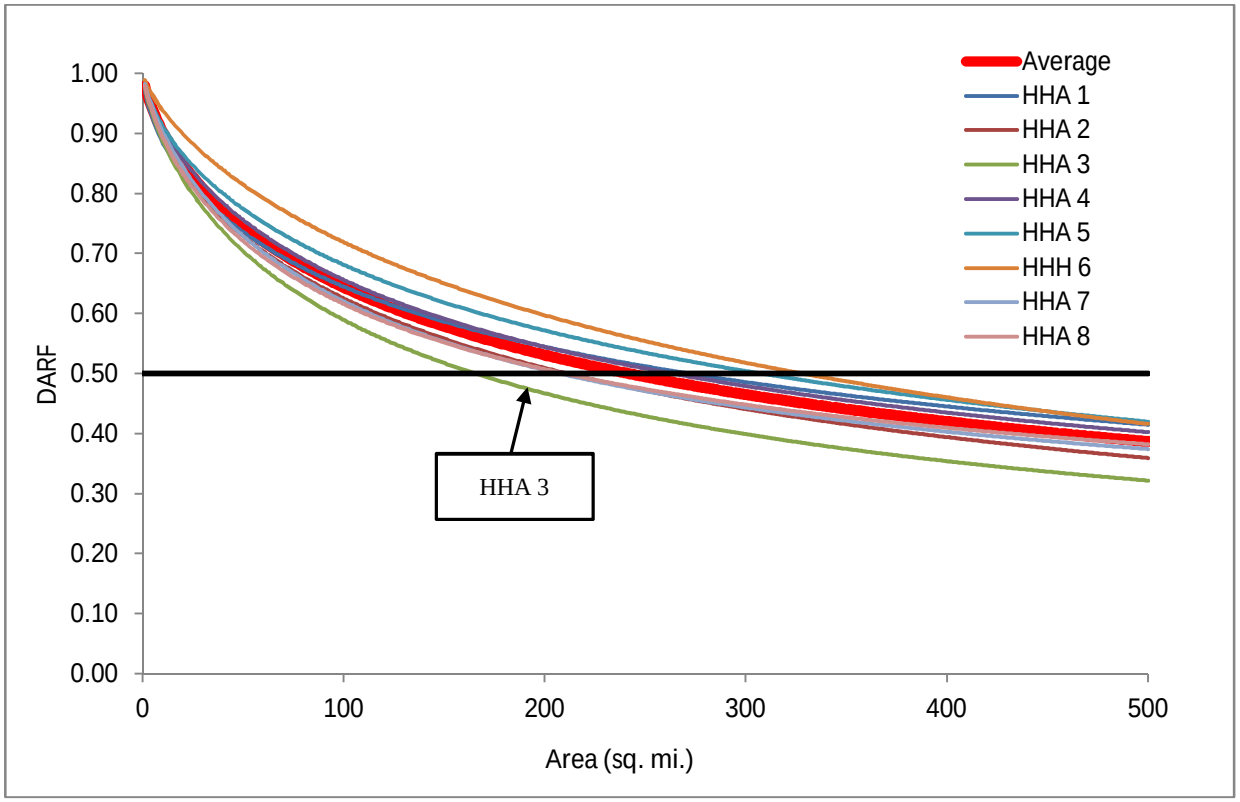

Figure 19 6-hr duration, 90th percentile DARF relationships for HHA 1 through 8

Taking the 90th percentile relationships for durations, 1-, 3-, 6- and 12-hr and averaging across HHAs, a single statewide result can be compared to the average of all the previous studies discussed above (Figure 20). The 2-hr DARF relationship is not shown since it falls closely to the 1-hr relationship. A minimum area was selected for no reduction, i.e. DARF=1.0 for areas < 5.0 sq. mi. Note that there is diminishing difference between durations for a given area with the 6-hr and 12-hr nearly overlapping below 100 sq. mi.

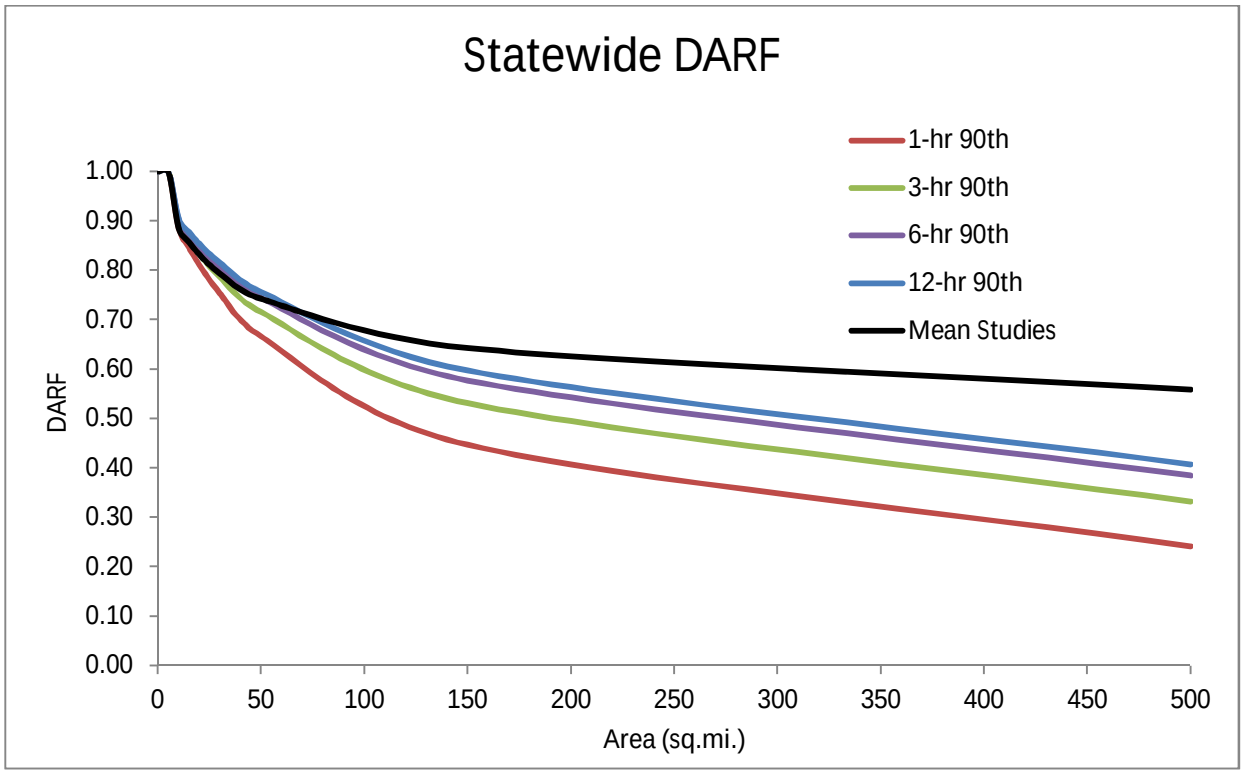

Figure 20 Recommended statewide DARF relationships for 1, 3, 6, and 12-hr duration in comparison with the mean of other studies

7. Summary

The purpose of this TM is to present the analysis results for the development of radar-based DARFs for use in NDOT drainage studies. Analysis of 547 storms from 2005-2014 was performed to determine representative DARFs for Nevada. This period is defined by availability of polygon-based NWS flash flood warnings/flood advisories and reliable radar data. Storms considered were either within a warning/advisory polygon issued by the NWS and/or included in the NCDC database, and therefore are considered extreme or at least with flood-producing rainfall depths and intensities. Of the 547 individual events, there were 1,720 duration-based storm totals developed and used to determine DARF relationships at the median and 90th percentile. These relationships have been identified for each of the HHAs (1-8) covering the state, for 1-, 2-, 3-, 6-, and 12-hour durations, and areas up to 500 sq. mi (Appendices B and C).

Rainfall produced by the events used in this study generally contained one or more peaks (storm

cells), and therefore are considered conservative since less reduction is projected than would occur if only a single storm cell was analyzed. The large number of storms analyzed and the range of reduction factors for a given area illustrates the importance of using a large number of events to determine reliable relationships.

Utilizing the large number of storms resulted in a "cloud" of data points generated for each HHA and duration (e.g., Figure 9 or 10). Had only a few storms been chosen, biased or unreliable results would be likely depending on the individual storm characteristics. The median or 90th percentile relationships presented in this study do not depend on a geometric shape, e.g. elliptical.

Summarizing the average DARF values across the eight HHAs, most of the reduction occurs once the area increases to about 100 sq. mi., and thereafter, declines steadily up to 500 sq. mi. As the duration of the storm progresses, there is less reduction expected due to a larger areal distribution of rainfall. For small areas (<100 sq. mi.) the difference in DARF values between HHAs is 0.15 (or less) for 1-hr duration storms. At this short duration, Lake Tahoe and Northeastern Nevada had the greatest depth reduction with increasing area (most DARF in HHA 2 and 3), whereas, along the western border with California, the least reduction is observed (least DARF in HHA 6) for areas up to 200-300 sq. mi. Because of the small difference in DARF values (areas < 100 sq. mi.) across the State, a single set of DARF relationships for 1-, 3-, 6- and 12-hr durations could be used.

8. Recommendations

The following are recommendations for application of the results found:

- Use of the 90th percentile relationship for each HHA is recommended since it results in more conservative (less reduction) DARF values than the median relationship.
- Design procedures could specify that areas less than 5 sq. mi. should receive no reduction (DARF = 1.0).
- The DARF relationships developed here should only be applied up to 500 sq. mi. and for durations from 1-hr to 12-hr.
- A single set of DARF relationships for 1-, 3-, 6-, and 12-hr durations could be developed by averaging across Nevada since there are small differences among the HHAs for areas below 100 sq. mi.

9. References

Adams, D.K., and A.C. Comrie, 1997. "The North American Monsoon." *Bull. Amer. Meteor. Soc.*, 78, 2197–2213.

Adams, J.L., and D.J. Stensrud, 2007. "Impact of tropical easterly waves on the North American monsoon." *J. Climate*, 20, 1219-1238.

Allen, R. J., and A. T. DeGaetano, 2005. "Areal Reduction Factors for Two Eastern United States Regions with High Rain-Gauge Density." *Journal of Hydrologic Engineering* 10 (4): 327–325.

Asquith, W. H., 1999. "Areal-Reduction Factors for the Precipitation on the 1-Day Design Storm in Texas." Water-Resources Investigations Report: 99–4267.

Asquith, W.H., and J. S. Famiglietti, 2000. "Precipitation Areal-Reduction Factor Estimation Using an Annual-Maxima Centered Approach." *Journal of Hydrology* 230 (1-2): 55–69.

Austin, P. M., and R. A. Houze, 1972. "Analysis of the Structure of Precipitation Pattern in New England." *Journal of Applied Meteorology* 11: 926–35.

Bacchi, B., and R. Ranzi, 1996. "On the Derivation of Areal Reduction Factors of Storms." *Atmospheric Research* 42: 123–35.

Bedient, P. B., W.C. Huber, B.E. Vieux, 2013. *Hydrology and Floodplain Analysis.* Fifth Edition, Prentice-Hall, Inc., One Lake St., Upper Saddle River, NJ 07458. ISBN 0-13-256796-2. p. 801.

Bell, F. C., 1976. "The Areal Reduction Factors in Rainfall Frequency Estimation." NERC Report No. 35.

Brenner, I. S., 1974. "A surge of maritime tropical air—Gulf of California to the southwestern United States." *Mon. Wea. Rev.*, 102, 375–389.

Douglas, M. W., R. A. Maddox, K. Howard, and S. Reyes, 1993. "The Mexican monsoon." *J. Climate*, 6, 1665–1678.

Durrans, S. R., L. T. Julian, and M. Yekta, 2002. "Estimation of Depth Area Relationships Using Radar Data." *Journal of Hydraulic Engineering* 7 (5): 356–67.

Frederick, R. H., V. A. Myers, and E. P. Auciello, 1977. "Storm Depth Area Relations from Digitized Radar Returns." *Water Resources Research* 13 (3): 675–79.

Hales, J. E. 1972. "Surges of maritime tropical air northward over the Gulf of California." *Mon. Wea. Rev.*, 100, 298–306.

Higgins, R. W., Y. Yao, and X. L. Wang, 1997. "Influence of the North American monsoon system on the U.S. summer precipitation regime." *J. Climate,* 10, 2600–2622.

Higgins, R. W., K. C. Mo, and Y. Yao, 1998. "Interannual variability of the U.S. summer precipitation regime with emphasis on the southwestern monsoon." *J. Climate*, 11,2582–2606.

Houghton, J. G, C. M. Sakamoto, and R. O. Gifford, 1975. Nevada's Weather and Climate. Vol. 2. NV Bureau of Mines & Geology.

Jensen, D.T., 1995. Final Report Probable Maximum Precipitation Estimates for Short Duration, Small-Area Storms in Utah. Submitted to the State of Utah, Division of Water Resources

and Division of Water Rights, State Engineer's Office.
Koenker, R., and Hallock, K., 2001. Quantile regression: An introduction. Journal of Economic Perspectives, 15(4), 43-56.
Leclerc, G. and J.C. Schaake, 1972. Derivation of hydrologic frequency curves. Report 142, Mass. Inst. of Technol., Cambridge, 151 pp.
Li, J., R. A. Maddox, X. Gao, S. Sorooshian, K. Hsu. 2003. "A Numerical Investigation of Storm Structure and Evolution during the July 1999 Las Vegas Flash Flood." *Mon. Wea. Rev.*, 131, 2038–2059.
Maddox, R. A., F. Canova, and L. R. Hoxit, 1980. "Meteorological characteristics of flash flood events over the western United States." *Mon. Wea. Rev.*, 108, 1866–1877.
Meyer, A.F., 1928. Elements of Hydrology, 2nd ed. John Wiley, New York.
National Climatic Data Center (NCDC), 2014."Storm Events Database." 2014. Accessed March 14. https://www.ncdc.noaa.gov/stormevents/.
Olivera, F., J. Choi, D. Kim, and M. Li, 2005. *Calculation of Areal Reduction Factors using NEXRAD Precipitation Estimates.* College Station, TX. Texas Transportation Institute. FHWA/TX-07/0-4642-3.
Olivera, F., J. Choi, D. Kim, and M.Li, 2008. "Estimation of Average Rainfall Areal Reduction Factors in Texas Using NEXRAD Data." *Journal of Hydrologic Engineering* 13 (6): 438–48.
Omolayo, A.S., 1993. "On the Transposition of Areal Reduction Factors for Rainfall Frequency Estimation." *Journal of Hydrology* 145 (1): 191–205.
Randerson, D., 1976. "Meteorological analysis for the Las Vegas, Nevada, flood of 3 July 1975." *Mon. Wea. Rev.*, 104, 719–727.
Sabol, G.V., and A.M. Motamedi, 1999. *Design Rainfall Criteria for Maricopa County, Arizona*. Conference Proceedings of the ASCE, Water Resources Planning and Management, WRPMD'99, Tempe AZ, pp. 1-10.
Siriwardena, L., and P. E. Weinmann, 1996. "Development and Testing of Methodology to Derive Areal Reduction Factors for Long Duration Rainfalls." Cooperative Research Centre for Catchment Hydrology.
Srikanthan, R, 1995. "A Review of the Methods for Estimating Areal Reduction Factors for Design Rainfalls." Cooperative Research Center for Catchment Hydrology 3 (3): 1–15.
U.S. Army Corps of Engineers (USACE), 1974. U.S. Army Corps of Engineers, 1974, Gila River Basin, New River and Phoenix City. Streams, Arizona, Design Memorandum No. 2, Hydrology, Part 1: Los Angeles District.
U.S. Army Corps of Engineers (USACE), 1988. Hydrologic Documentation for Feasibility Study - Las Vegas Wash and Tributaries, Clark County, Nevada, U. S. Army Corps of Engineers, Los Angeles District, April, 1988.
U.S. Weather Bureau, 1957. "Rainfall Intensity-Frequency Regime - Part 1: The Ohio Valley", Technical Paper No. 29 (TP-29), Washington, D.C.
U.S. Weather Bureau, 1958a. "Rainfall Intensity-Frequency Regime - Part 2: The Southeastern

United States", Technical Paper No. 29 (TP-29), Washington, D.C.
U.S. Weather Bureau, 1958b. "Rainfall Intensity-Frequency Regime - Part 3: The Middle Atlantic Region", Technical Paper No. 29 (TP-29), Washington, D.C.
U.S. Weather Bureau, 1959. "Rainfall Intensity-Frequency Regime - Part 4: The Northeastern United States", Technical Paper No. 29 (TP-29), Washington, D.C.
U.S. Weather Bureau, 1960. "Rainfall Intensity-Frequency Regime - Part 5: The Great Lakes Region", Technical Paper No. 29 (TP-29), Washington, D.C.
U.S. Weather Bureau, 1964. "Two to Ten Day Precipitation for Return Periods of 2 to 100 years in the Contiguous United States", Technical Paper No. 49 (TP-49), Washington, D.C.
Zehr, R. M., & Myers, V. A., 1984. Depth-area ratios in the semi-arid southwest United States. NOAA Technical Memorandum, NWS HYDRO-40. Silver Spring, MD. August 1984.

10. Appendices

Appendix A – Storm List
Appendix B – Observed Median and 90th Percentile DARF Relationships
Appendix C – Fitted Parameters and DARF Relationships

Appendix A

Table A-1 Event list for each HHA showing radar source

Event	HHA	Date	Radar Source
1	1	6/24/2005	RGX
2	1	7/21/2005	RGX
3	1	7/29/2005	RGX
4	1	7/19/2006	RGX
5	1	7/21/2006	RGX
6	1	6/2/2007	RGX
7	1	6/29/2008	RGX
8	1	7/14/2008	RGX
9	1	7/21/2008	RGX
10	1	6/8/2009	RGX
11	1	7/30/2009	RGX
12	1	7/16/2010	RGX
13	1	8/8/2010	RGX
14	1	10/4/2010	RGX
15	1	10/5/2010	RGX
16	1	12/19/2010	RGX
17	1	6/6/2011	RGX
18	1	7/6/2011	RGX
19	1	7/31/2011	RGX
20	1	9/11/2011	RGX
21	1	8/15/2012	RGX
22	1	12/2/2012	RGX
23	1	6/10/2013	RGX
24	1	7/2/2013	RGX
25	1	7/3/2013	RGX
26	1	7/4/2013	RGX
27	1	7/25/2013	RGX
28	1	8/8/2013	RGX
29	1	8/20/2013	RGX
30	1	7/8/2014	RGX
31	1	7/16/2014	RGX
32	1	7/20/2014	RGX
33	1	7/22/2014	RGX
34	1	7/28/2014	RGX
35	1	7/31/2014	RGX
36	1	8/9/2014	RGX
37	1	8/11/2014	RGX
38	1	8/12/2014	RGX
39	1	8/24/2014	RGX

Event	HHA	Date	Radar Source
40	2	7/25/2007	LRX
41	2	7/26/2007	LRX
42	2	5/31/2009	LRX
43	2	6/5/2009	LRX
44	2	6/11/2009	LRX
45	2	6/15/2009	LRX
46	2	7/3/2009	LRX
47	2	7/25/2009	LRX
48	2	7/29/2010	LRX
49	2	1/17/2011	LRX
50	2	3/16/2011	LRX
51	2	3/31/2011	LRX
52	2	4/17/2011	LRX
53	2	4/20/2011	LRX
54	2	4/21/2011	LRX
55	2	6/2/2011	LRX
56	2	6/6/2011	LRX
57	2	6/7/2011	LRX
58	2	6/13/2011	LRX
59	2	6/15/2011	LRX
60	2	7/5/2011	LRX
61	2	9/11/2011	LRX
62	2	7/15/2012	LRX
63	2	7/22/2012	LRX
64	2	7/24/2012	LRX
65	2	8/13/2012	LRX
66	2	8/15/2012	LRX
67	2	7/3/2013	LRX
68	2	8/20/2013	LRX
69	2	8/28/2013	LRX
70	2	9/2/2013	LRX
71	2	9/3/2013	LRX
72	2	9/4/2013	LRX
73	2	9/7/2013	LRX
74	2	9/12/2013	LRX
75	2	5/20/2014	LRX
76	2	7/20/2014	LRX
77	2	7/29/2014	LRX
78	2	7/30/2014	LRX

Event	HHA	Date	Radar Source
79	2	8/1/2014	LRX
80	2	8/2/2014	LRX
81	2	8/5/2014	LRX
82	2	8/6/2014	LRX
83	2	8/7/2014	LRX
84	2	8/9/2014	LRX
85	2	8/12/2014	LRX
86	2	8/13/2014	LRX
87	2	8/25/2014	LRX
88	3	7/14/2008	RGX
89	3	5/2/2009	RGX
90	3	5/4/2009	RGX
91	3	5/25/2009	RGX
92	3	5/28/2009	RGX
93	3	6/2/2009	RGX
94	3	10/13/2009	RGX
95	3	7/16/2010	RGX
96	3	7/24/2010	RGX
97	3	8/7/2010	RGX
98	3	8/8/2010	RGX
99	3	10/2/2010	RGX
100	3	10/4/2010	RGX
101	3	10/24/2010	RGX
102	3	6/20/2011	RGX
103	3	6/28/2011	RGX
104	3	7/6/2011	RGX
105	3	9/11/2011	RGX
106	3	9/30/2011	RGX
107	3	8/14/2012	RGX
108	3	8/15/2012	RGX
109	3	8/17/2012	RGX
110	3	6/9/2013	RGX
111	3	6/28/2013	RGX
112	3	7/2/2013	RGX
113	3	7/3/2013	RGX
114	3	7/25/2013	RGX
115	3	9/14/2013	RGX
116	3	7/8/2014	RGX
117	3	7/17/2014	RGX
118	3	7/18/2014	RGX

Event	HHA	Date	Radar Source
119	3	7/19/2014	RGX
120	3	7/20/2014	RGX
121	3	7/30/2014	RGX
122	3	8/6/2014	RGX
123	3	8/11/2014	RGX
124	4	1/4/2008	RGX
125	4	1/5/2008	RGX
126	4	5/27/2008	RGX
127	4	7/21/2008	RGX
128	4	5/22/2009	RGX
129	4	5/30/2009	RGX
130	4	5/31/2009	RGX
131	4	7/2/2009	RGX
132	4	7/9/2010	RGX
133	4	7/16/2010	RGX
134	4	7/24/2010	RGX
135	4	10/3/2010	RGX
136	4	7/7/2011	RGX
137	4	7/29/2011	RGX
138	4	7/30/2011	RGX
139	4	7/31/2011	RGX
140	4	7/13/2012	RGX
141	4	7/22/2012	RGX
142	4	7/23/2012	RGX
143	4	8/21/2012	RGX
144	4	6/10/2013	RGX
145	4	7/1/2013	RGX
146	4	7/3/2013	RGX
147	4	7/4/2013	RGX
148	4	7/25/2013	RGX
149	4	7/26/2013	RGX
150	4	7/27/2013	RGX
151	4	7/28/2013	RGX
152	4	8/8/2013	RGX
153	4	9/1/2013	RGX
154	4	9/2/2013	RGX
155	4	5/22/2014	RGX
156	4	7/8/2014	RGX
157	4	7/10/2014	RGX
158	4	7/15/2014	RGX

Event	HHA	Date	Radar Source
159	4	7/17/2014	RGX
160	4	7/18/2014	RGX
161	4	7/20/2014	RGX
162	4	7/28/2014	RGX
163	4	8/2/2014	RGX
164	4	8/6/2014	RGX
165	4	8/11/2014	RGX
166	5	7/25/2007	LRX
167	5	7/11/2008	ICX
168	5	7/15/2008	ICX
169	5	7/20/2008	ICX
170	5	7/21/2008	LRX
171	5	7/27/2008	ICX
172	5	6/5/2009	LRX
173	5	6/14/2009	LRX
174	5	6/15/2009	LRX
175	5	7/2/2009	LRX
176	5	7/24/2009	ICX
177	5	7/24/2009	LRX
178	5	7/25/2009	LRX
179	5	7/26/2009	LRX
180	5	7/29/2009	ICX
181	5	6/5/2010	LRX
182	5	6/7/2010	LRX
183	5	10/4/2010	ICX
184	5	10/22/2010	ICX
185	5	6/15/2011	LRX
186	5	6/17/2011	LRX
187	5	7/6/2011	ICX
188	5	7/6/2011	LRX
189	5	7/26/2011	ICX
190	5	7/29/2011	LRX
191	5	7/30/2011	LRX
192	5	7/31/2011	LRX
193	5	9/15/2011	ICX
194	5	9/16/2011	ICX
195	5	9/16/2011	LRX
196	5	7/13/2012	LRX
197	5	7/14/2012	LRX
198	5	7/15/2012	ICX

Event	HHA	Date	Radar Source
199	5	7/15/2012	LRX
200	5	7/16/2012	ICX
201	5	7/16/2012	LRX
202	5	7/22/2012	LRX
203	5	7/23/2012	LRX
204	5	8/13/2012	LRX
205	5	8/15/2012	LRX
206	5	8/19/2012	LRX
207	5	8/21/2012	LRX
208	5	9/9/2012	LRX
209	5	9/10/2012	LRX
210	5	9/11/2012	LRX
211	5	7/3/2013	LRX
212	5	7/6/2013	LRX
213	5	7/12/2013	ICX
214	5	7/14/2013	LRX
215	5	7/16/2013	LRX
216	5	7/22/2013	ICX
217	5	7/23/2013	LRX
218	5	7/28/2013	ICX
219	5	8/20/2013	LRX
220	5	8/21/2013	LRX
221	5	8/24/2013	ICX
222	5	8/28/2013	LRX
223	5	8/29/2013	LRX
224	5	8/30/2013	ICX
225	5	8/30/2013	LRX
226	5	8/31/2013	ICX
227	5	9/1/2013	LRX
228	5	9/2/2013	ICX
229	5	9/2/2013	LRX
230	5	9/3/2013	LRX
231	5	9/4/2013	ICX
232	5	9/4/2013	LRX
233	5	9/7/2013	LRX
234	5	9/11/2013	ICX
235	5	9/11/2013	LRX
236	5	9/12/2013	ICX
237	5	9/12/2013	LRX
238	5	9/15/2013	LRX

Event	HHA	Date	Radar Source
239	5	2/11/2014	LRX
240	5	7/6/2014	ICX
241	5	7/9/2014	LRX
242	5	7/11/2014	LRX
243	5	7/15/2014	ICX
244	5	7/15/2014	LRX
245	5	7/16/2014	LRX
246	5	7/26/2014	ICX
247	5	7/27/2014	LRX
248	5	7/28/2014	LRX
249	5	7/29/2014	LRX
250	5	7/30/2014	LRX
251	5	7/31/2014	ICX
252	5	7/31/2014	LRX
253	5	8/1/2014	LRX
254	5	8/2/2014	LRX
255	5	8/3/2014	LRX
256	5	8/4/2014	ICX
257	5	8/4/2014	LRX
258	5	8/5/2014	LRX
259	5	8/6/2014	LRX
260	5	8/10/2014	LRX
261	5	8/12/2014a	LRX
262	5	8/12/2014b	LRX
263	5	8/13/2014	LRX
264	5	8/19/2014	ICX
265	5	8/19/2014	LRX
266	5	8/22/2014	ICX
267	5	8/26/2014	ICX
268	5	8/26/2014	LRX
269	6	7/12/2008	ESX
270	6	7/16/2008	ESX
271	6	2/7/2009	ESX
272	6	7/20/2009	ESX
273	6	10/14/2009	RGX
274	6	1/21/2010	ESX
275	6	8/26/2010	ESX
276	6	10/3/2010	ESX
277	6	12/20/2010	ESX
278	6	12/22/2010	ESX

Event	HHA	Date	Radar Source
279	6	5/18/2011	ESX
280	6	6/21/2011	RGX
281	6	7/6/2011	ESX
282	6	7/29/2011	ESX
283	6	7/31/2011	ESX
284	6	7/13/2012	ESX
285	6	7/31/2012	ESX
286	6	8/3/2012	ESX
287	6	8/11/2012	ESX
288	6	8/18/2012	ESX
289	6	8/22/2012	ESX
290	6	9/11/2012	ESX
291	6	10/11/2012	ESX
292	6	3/8/2013	ESX
293	6	7/22/2013	ESX
294	6	7/28/2013	ESX
295	6	8/18/2013	ESX
296	6	8/30/2013	ESX
297	6	8/31/2013	RGX
298	6	8/31/2013	ESX
299	6	9/8/2013	ESX
300	6	7/5/2014	ESX
301	6	7/17/2014	RGX
302	6	7/30/2014	ESX
303	7	7/11/2008	ESX
304	7	7/12/2008	ESX
305	7	7/13/2008	ESX
306	7	7/14/2008	ESX
307	7	7/16/2008	ESX
308	7	7/17/2008	ESX
309	7	7/20/2008	ESX
310	7	7/21/2008	ESX
311	7	7/26/2008	ESX
312	7	7/27/2008	ESX
313	7	8/3/2008	ESX
314	7	8/4/2008	ESX
315	7	8/5/2008	ESX
316	7	8/6/2008	ESX
317	7	8/7/2008	ESX
318	7	8/16/2008	ESX

Event	HHA	Date	Radar Source
319	7	8/25/2008	ESX
320	7	9/8/2008	ESX
321	7	9/17/2008	ESX
322	7	10/4/2008	ESX
323	7	11/26/2008	ESX
324	7	2/7/2009	ESX
325	7	7/3/2009	ESX
326	7	7/20/2009	ESX
327	7	7/25/2009	ESX
328	7	7/26/2009	ESX
329	7	9/4/2009	ESX
330	7	1/19/2010	ESX
331	7	1/21/2010	ESX
332	7	2/6/2010	ESX
333	7	2/7/2010	ESX
334	7	2/9/2010	ESX
335	7	7/16/2010	ESX
336	7	7/30/2010	ESX
337	7	8/7/2010	ESX
338	7	8/8/2010	ESX
339	7	8/17/2010	ESX
340	7	8/18/2010	ESX
341	7	8/25/2010	ESX
342	7	8/26/2010	ESX
343	7	10/2/2010	ESX
344	7	10/3/2010	ESX
345	7	10/4/2010	ESX
346	7	10/20/2010	ESX
347	7	12/20/2010	ESX
348	7	12/22/2010	ESX
349	7	12/23/2010	ESX
350	7	7/3/2011	ESX
351	7	7/5/2011	ESX
352	7	7/6/2011	ESX
353	7	7/7/2011	ESX
354	7	7/8/2011	ESX
355	7	7/9/2011	ESX
356	7	7/10/2011	ESX
357	7	7/29/2011	ESX
358	7	7/31/2011	ESX

Event	HHA	Date	Radar Source
359	7	8/2/2011	ESX
360	7	8/13/2011	ESX
361	7	8/27/2011	ESX
362	7	9/10/2011	ESX
363	7	9/13/2011	ESX
364	7	9/14/2011	ESX
365	7	9/15/2011	ESX
366	7	9/24/2011	ESX
367	7	10/3/2011	ESX
368	7	10/4/2011	ESX
369	7	7/12/2012	ESX
370	7	2012-07-14_01	ESX
371	7	2012-07-14_19	ESX
372	7	7/15/2012	ESX
373	7	7/16/2012	ESX
374	7	7/22/2012	ESX
375	7	7/23/2012	ESX
376	7	7/24/2012	ESX
377	7	7/30/2012	ESX
378	7	7/31/2012	ESX
379	7	8/1/2012	ESX
380	7	8/2/2012	ESX
381	7	8/3/2012	ESX
382	7	8/11/2012	ESX
383	7	8/13/2012	ESX
384	7	8/14/2012	ESX
385	7	8/17/2012	ESX
386	7	8/18/2012	ESX
387	7	8/19/2012	ESX
388	7	8/21/2012	ESX
389	7	8/30/2012	ESX
390	7	8/31/2012	ESX
391	7	9/10/2012	ESX
392	7	9/11/2012	ESX
393	7	10/11/2012	ESX
394	7	7/4/2013	ESX
395	7	7/5/2013	ESX
396	7	7/7/2013	ESX
397	7	7/12/2013	ESX
398	7	7/19/2013	ESX

Event	HHA	Date	Radar Source
399	7	7/20/2013	ESX
400	7	7/22/2013	ESX
401	7	7/23/2013	ESX
402	7	7/25/2013	ESX
403	7	7/26/2013	ESX
404	7	7/27/2013	ESX
405	7	7/28/2013	ESX
406	7	8/18/2013	ESX
407	7	8/19/2013	ESX
408	7	8/20/2013	ESX
409	7	8/22/2013	ESX
410	7	8/24/2013	ESX
411	7	8/25/2013	ESX
412	7	8/28/2013	ESX
413	7	8/29/2013	ESX
414	7	8/30/2013	ESX
415	7	8/31/2013	ESX
416	7	9/1/2013	ESX
417	7	9/2/2013	ESX
418	7	9/3/2013	ESX
419	7	9/4/2013	ESX
420	7	9/6/2013	ESX
421	7	9/8/2013	ESX
422	7	9/9/2013	ESX
423	7	9/11/2013	ESX
424	7	2014-07-04_15	ESX
425	7	2014-07-04_23	ESX
426	7	7/5/2014	ESX
427	7	7/6/2014	ESX
428	7	7/7/2014	ESX
429	7	7/10/2014	ESX
430	7	7/16/2014	ESX
431	7	7/26/2014	ESX
432	7	7/27/2014	ESX
433	7	7/28/2014	ESX
434	7	8/1/2014	ESX
435	7	8/2/2014	ESX
436	7	2014-08-04_00	ESX
437	7	2014-08-04_17	ESX
438	7	8/10/2014	ESX

Event	HHA	Date	Radar Source
439	7	8/11/2014	ESX
440	7	8/12/2014	ESX
441	7	8/13/2014	ESX
442	7	8/18/2014	ESX
443	7	8/19/2014	ESX
444	7	8/21/2014	ESX
445	7	9/7/2014	ESX
446	7	9/8/2014	ESX
447	8	7/10/2008	ESX
448	8	7/12/2008	ESX
449	8	7/14/2008	ESX
450	8	7/17/2008	ESX
451	8	7/20/2008	ESX
452	8	7/26/2008	ESX
453	8	8/3/2008	ESX
454	8	8/4/2008	ESX
455	8	8/5/2008	ESX
456	8	8/6/2008	ESX
457	8	8/7/2008	ESX
458	8	8/8/2008	ESX
459	8	8/15/2008	ESX
460	8	8/25/2008	ESX
461	8	8/30/2008	ESX
462	8	8/31/2008	ESX
463	8	9/8/2008	ESX
464	8	9/17/2008	ESX
465	8	11/26/2008	ESX
466	8	11/27/2008	ESX
467	8	7/2/2009	ESX
468	8	7/3/2009	ESX
469	8	7/20/2009	ESX
470	8	7/23/2009	ESX
471	8	7/24/2009	ESX
472	8	7/26/2009	ESX
473	8	8/23/2009	ESX
474	8	9/4/2009	ESX
475	8	9/5/2009	ESX
476	8	1/19/2010	ESX
477	8	1/21/2010	ESX
478	8	2/6/2010	ESX

Event	HHA	Date	Radar Source
479	8	8/17/2010	ESX
480	8	8/26/2010	ESX
481	8	10/4/2010	ESX
482	8	10/17/2010	ESX
483	8	10/18/2010	ESX
484	8	10/20/2010	ESX
485	8	12/20/2010	ESX
486	8	12/22/2010	ESX
487	8	7/3/2011	ESX
488	8	7/5/2011	ESX
489	8	7/7/2011	ESX
490	8	7/8/2011	ESX
491	8	7/9/2011	ESX
492	8	7/10/2011	ESX
493	8	7/31/2011	ESX
494	8	9/10/2011	ESX
495	8	9/13/2011	ESX
496	8	9/14/2011	ESX
497	8	9/16/2011	ESX
498	8	10/3/2011	ESX
499	8	7/13/2012	ESX
500	8	7/14/2012	ESX
501	8	7/22/2012	ESX
502	8	7/31/2012	ESX
503	8	8/9/2012	ESX
504	8	8/15/2012	ESX
505	8	8/20/2012	ESX
506	8	8/22/2012	ESX
507	8	8/25/2012	ESX
508	8	8/29/2012	ESX
509	8	8/30/2012	ESX
510	8	9/5/2012	ESX
511	8	9/11/2012	ESX
512	8	10/11/2012	ESX
513	8	7/12/2013	ESX
514	8	7/19/2013	ESX
515	8	7/20/2013	ESX
516	8	7/23/2013	ESX
517	8	7/27/2013	ESX
518	8	7/28/2013	ESX

Event	HHA	Date	Radar Source
519	8	8/18/2013	ESX
520	8	8/19/2013	ESX
521	8	8/22/2013	ESX
522	8	8/23/2013	ESX
523	8	8/25/2013	ESX
524	8	8/29/2013	ESX
525	8	8/30/2013	ESX
526	8	8/31/2013	ESX
527	8	2013-09-01_04	ESX
528	8	2013-09-01_18	ESX
529	8	9/2/2013	ESX
530	8	9/6/2013	ESX
531	8	9/9/2013	ESX
532	8	9/11/2013	ESX
533	8	9/14/2013	ESX
534	8	11/21/2013	ESX
535	8	7/5/2014	ESX
536	8	7/6/2014	ESX
537	8	7/7/2014	ESX
538	8	7/8/2014	ESX
539	8	7/10/2014	ESX
540	8	7/27/2014	ESX
541	8	7/28/2014	ESX
542	8	8/1/2014	ESX
543	8	8/3/2014	ESX
544	8	8/12/2014	ESX
545	8	8/14/2014	ESX
546	8	8/20/2014	ESX
547	8	8/21/2014	ESX

Appendix B

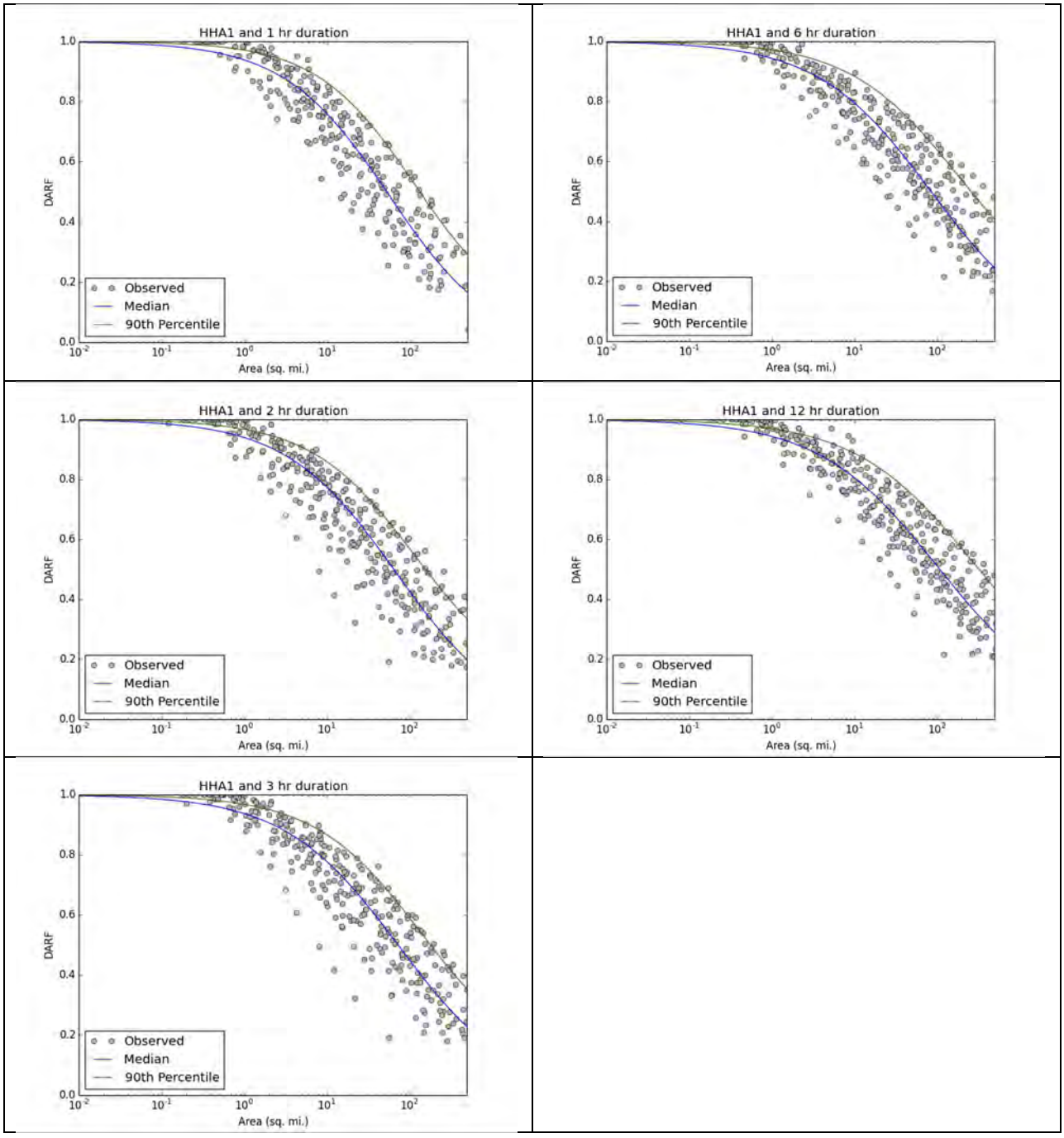

Figure B-1 HHA 1 observed, median, and 90th percentile DARF curves

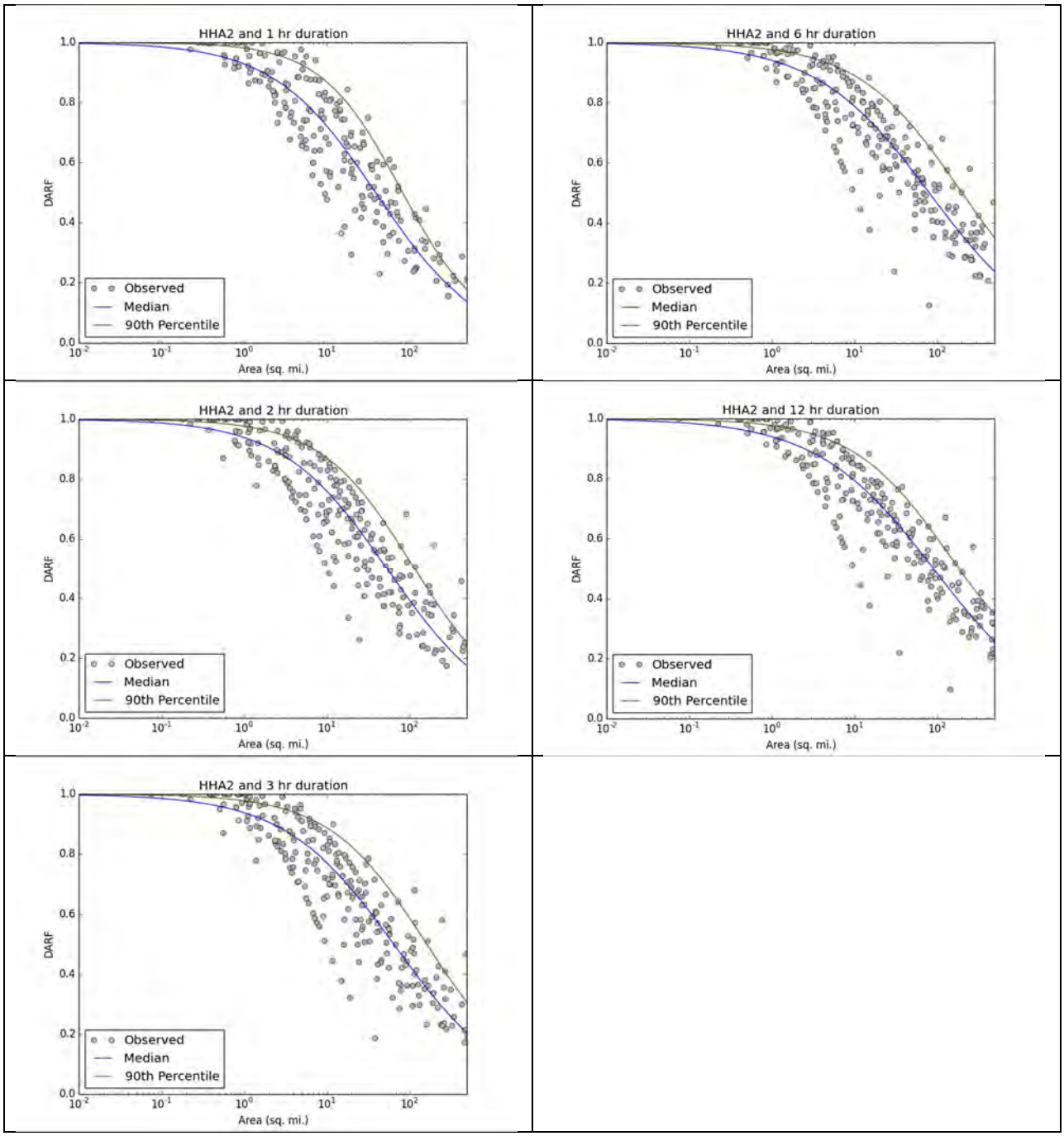

Figure B-2 HHA 2 observed, median, and 90th percentile DARF curves

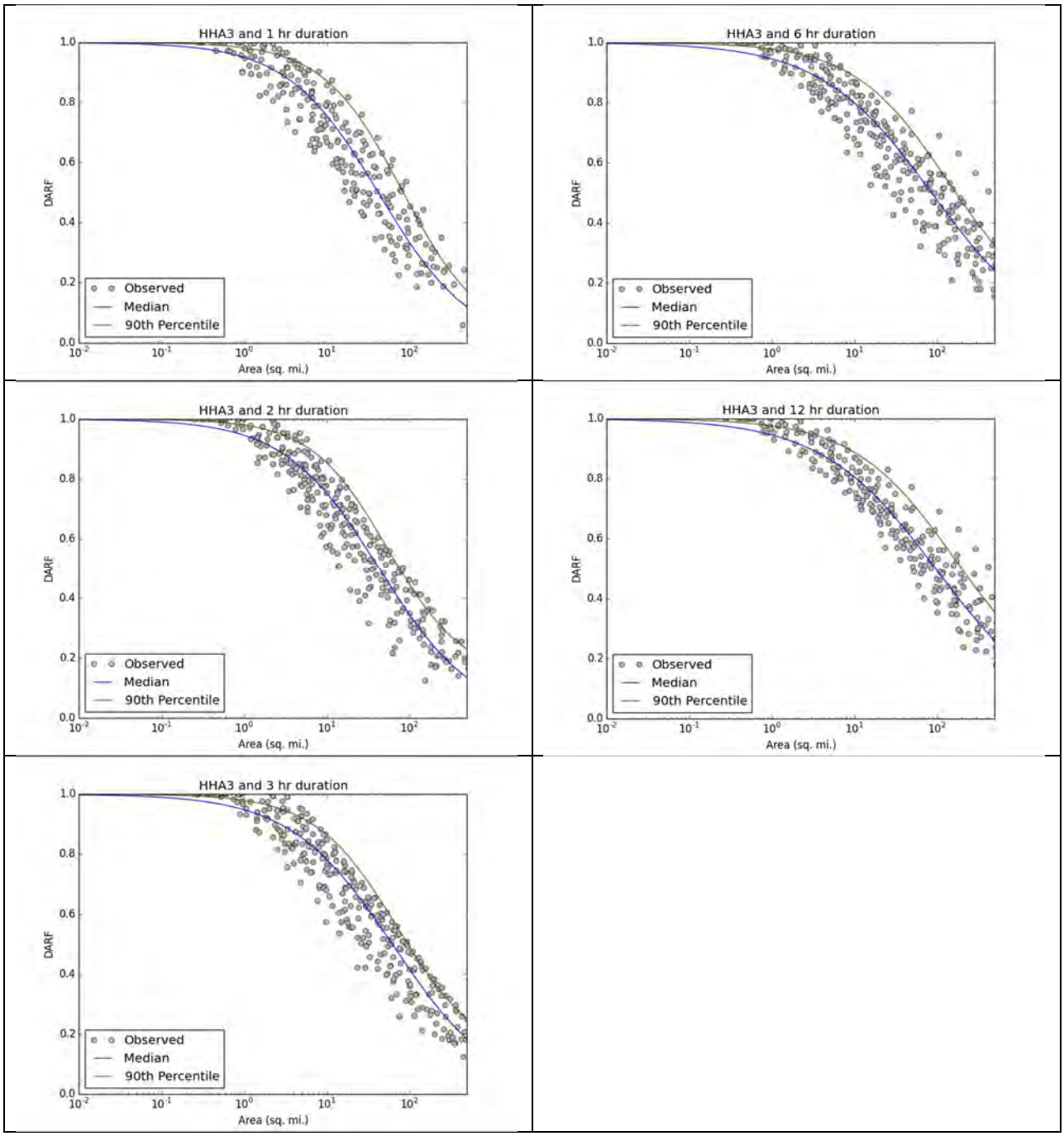

Figure B-3 HHA 3 observed, median, and 90th percentile DARF curves

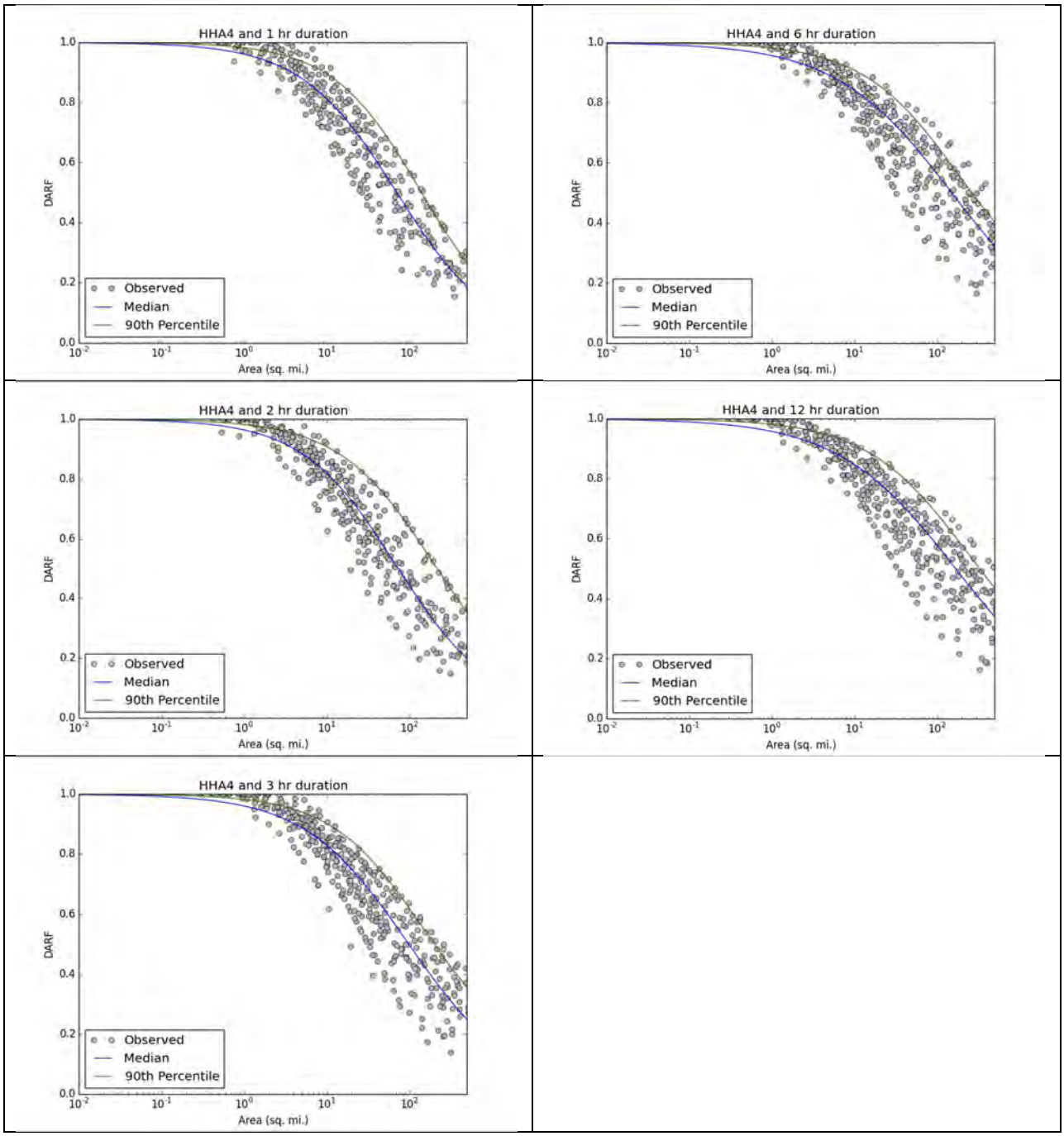

Figure B-4 HHA 4 observed, median, and 90th percentile DARF curves

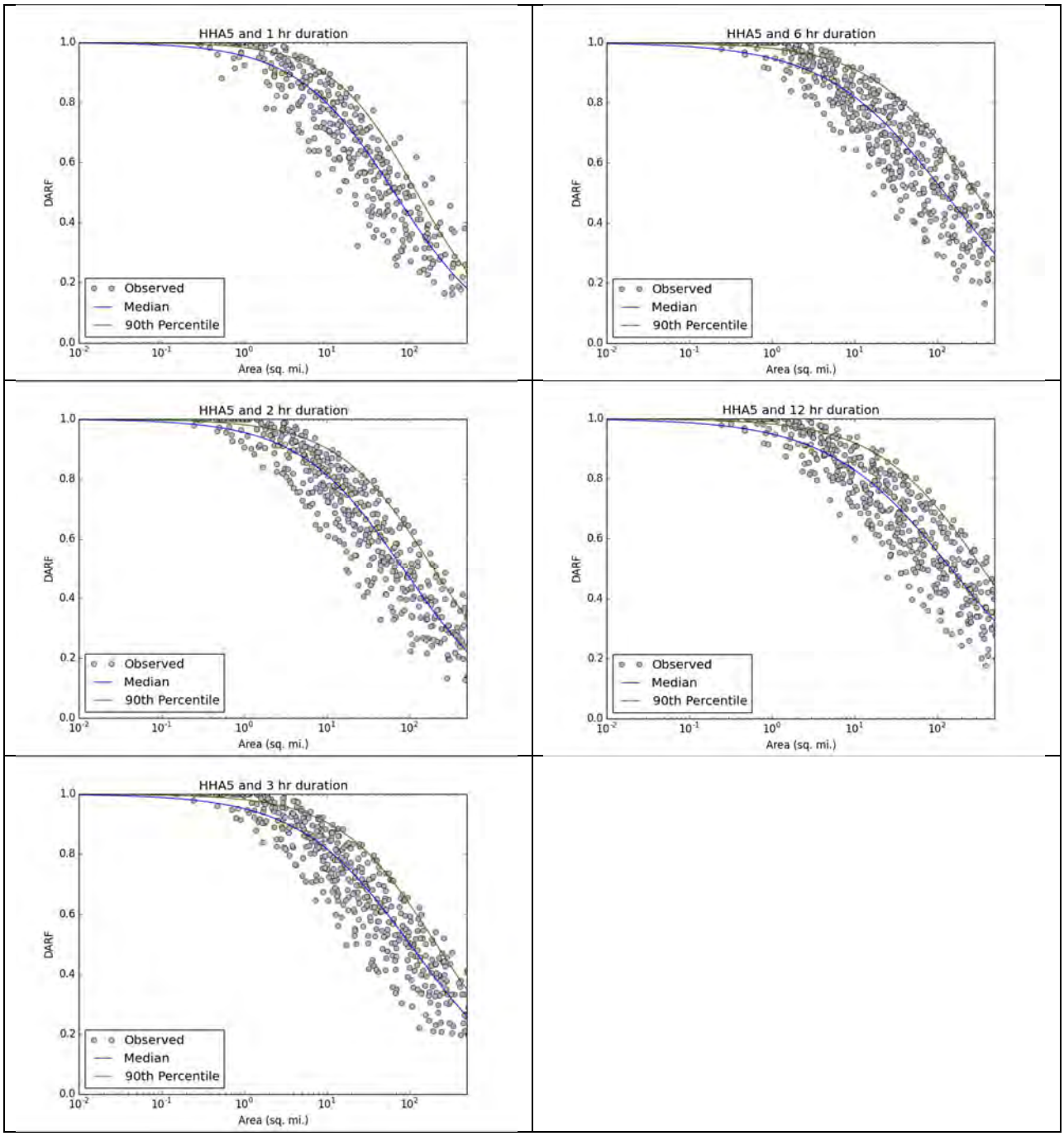

Figure B-5 HHA 5 observed, median, and 90th percentile DARF curves

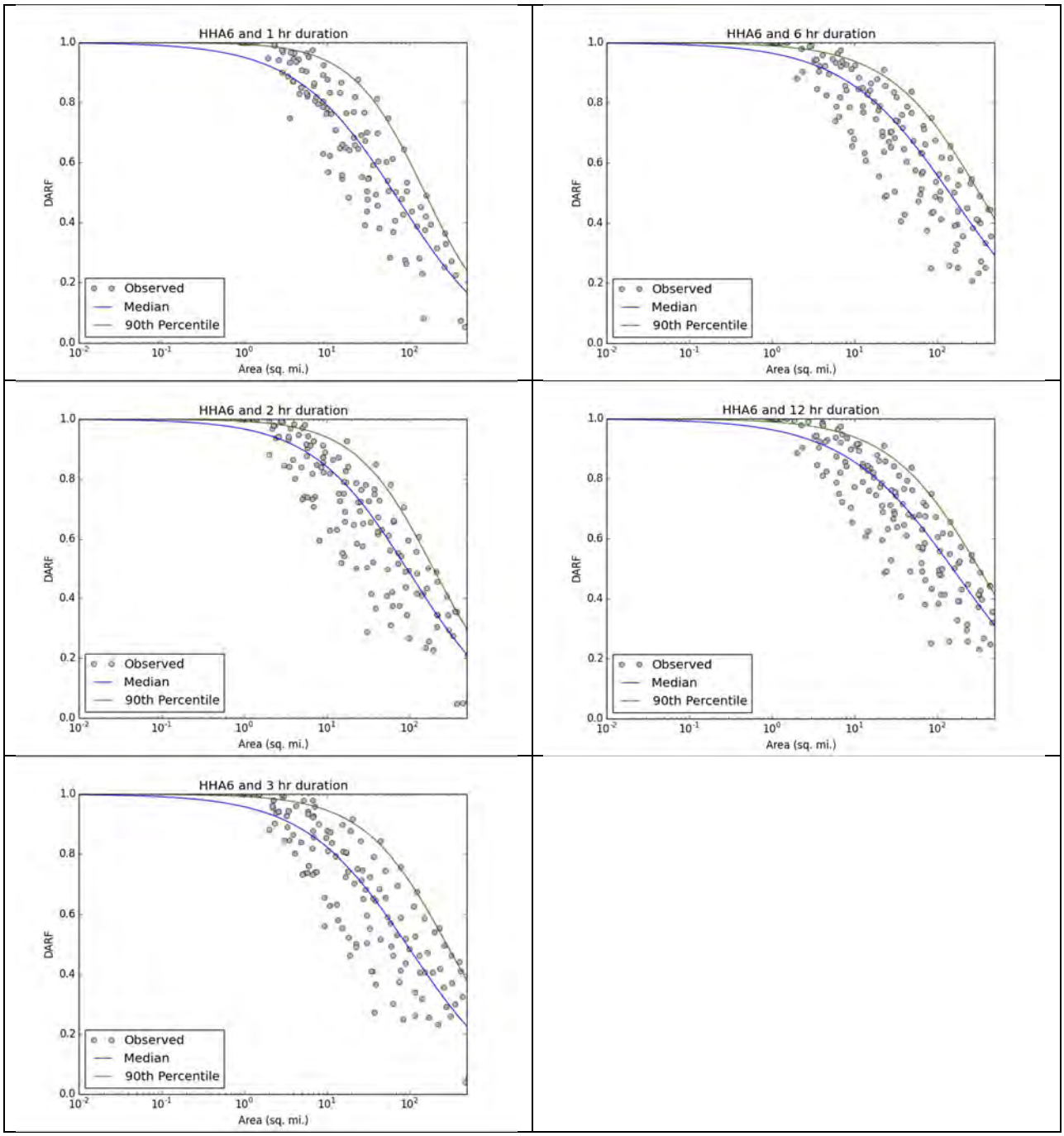

Figure B-6 HHA 6 observed, median, and 90th percentile DARF curves

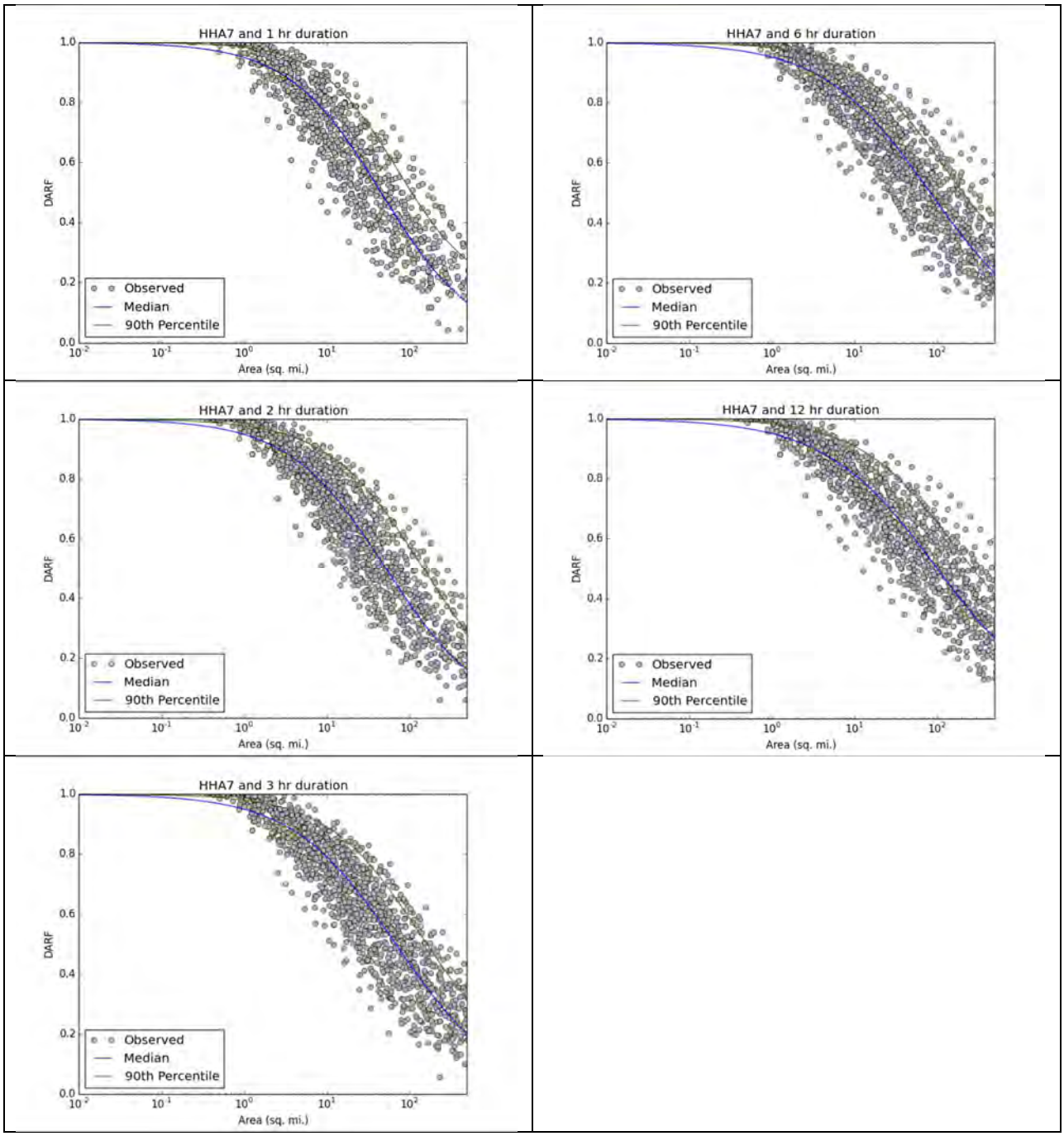

Figure B-7 HHA 7 observed, median, and 90th percentile DARF curves

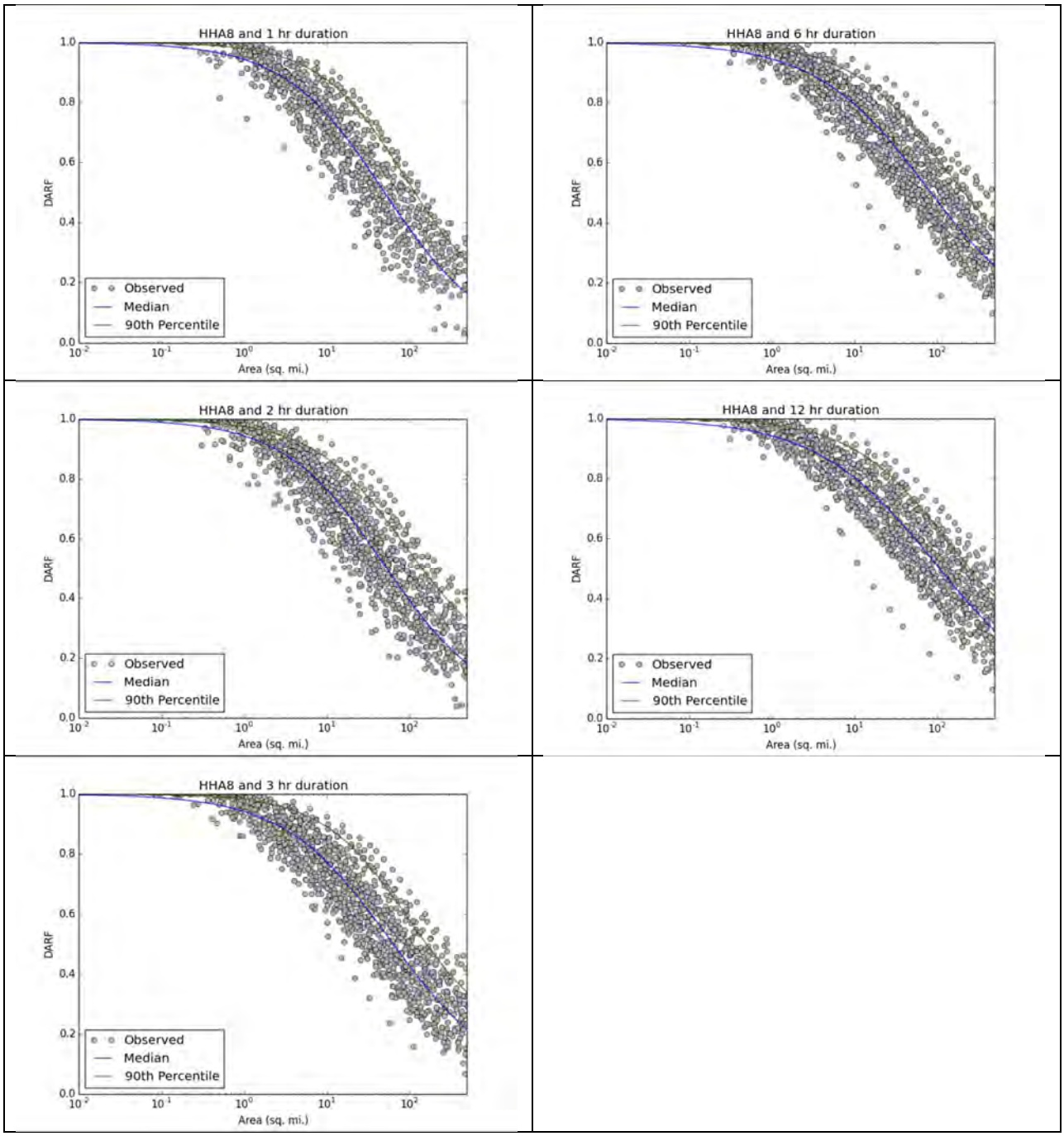

Figure B-8 HHA 8 observed, median, and 90th percentile DARF curves

Appendix C

Table C-1 Fitted parameters by HHA and duration for the 50th Percentile

HHA	1-hr			2-hr			3-hr			6-hr			12-hr		
	a	b	c	a	b	c	a	b	c	a	b	c	a	b	c
1	1.02	15.59	0.68	1.02	15.94	0.65	1.01	15.10	0.63	1.00	16.73	0.63	0.98	16.32	0.60
2	1.01	13.12	0.70	1.01	15.49	0.68	1.02	15.31	0.65	1.01	16.04	0.63	1.01	15.87	0.61
3	1.01	19.22	0.79	1.00	17.53	0.76	1.01	18.31	0.70	1.01	17.58	0.64	1.01	17.62	0.62
4	1.00	24.61	0.75	0.97	26.01	0.77	0.99	23.81	0.69	1.01	22.10	0.61	1.00	22.53	0.61
5	1.01	21.48	0.73	1.01	21.69	0.69	1.02	19.97	0.64	1.02	18.38	0.60	1.02	18.96	0.58
6	1.06	20.34	0.69	1.03	30.17	0.74	1.04	23.53	0.68	1.04	28.34	0.66	1.05	27.21	0.64
7	1.00	19.03	0.77	1.00	18.48	0.74	1.00	18.75	0.69	0.99	19.38	0.67	0.99	18.80	0.64
8	1.00	16.51	0.72	0.97	16.37	0.71	0.97	15.51	0.67	0.96	16.42	0.65	0.97	15.81	0.60

Table C-2 Fitted parameters by HHA and duration for the 90th Percentile

HHA	1-hr			2-hr			3-hr			6-hr			12-hr		
	a	b	c	a	b	c	a	b	c	a	b	c	a	b	c
1	0.95	31.76	0.73	0.91	26.78	0.69	0.92	28.10	0.67	0.90	30.61	0.65	0.96	30.17	0.60
2	0.98	51.87	0.90	0.97	40.10	0.79	0.99	43.16	0.74	0.97	39.89	0.70	0.91	38.73	0.74
3	0.99	54.20	0.90	0.87	42.85	0.94	0.89	41.14	0.87	0.93	41.83	0.76	0.94	37.75	0.71
4	0.99	54.83	0.81	0.99	54.49	0.75	0.89	48.25	0.78	0.88	47.06	0.74	0.90	46.49	0.70
5	0.99	57.43	0.85	1.00	51.93	0.75	0.99	52.19	0.74	0.97	49.01	0.69	1.00	54.70	0.68
6	0.99	152.63	1.00	1.00	129.96	0.92	1.03	126.51	0.85	1.04	93.62	0.77	1.03	93.97	0.77
7	0.85	51.22	0.92	1.00	44.16	0.76	0.92	44.95	0.78	0.83	47.21	0.80	0.83	45.94	0.76
8	0.91	42.58	0.83	0.85	33.05	0.77	0.84	44.12	0.82	0.82	39.32	0.77	0.81	38.55	0.75

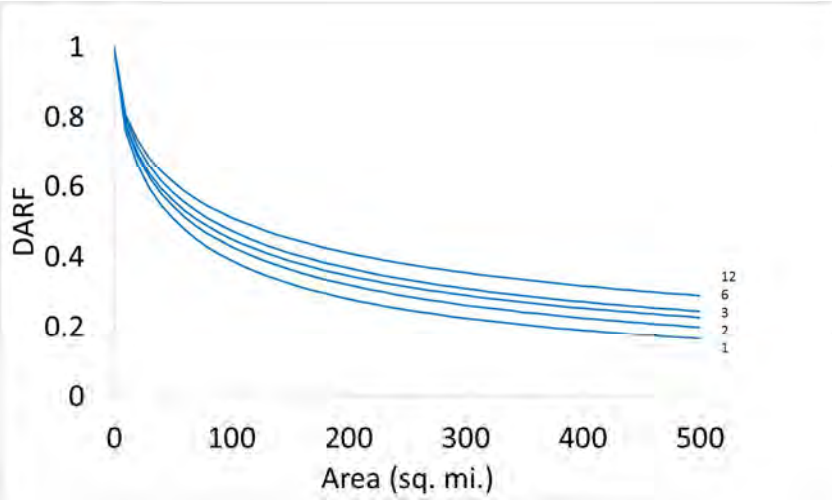

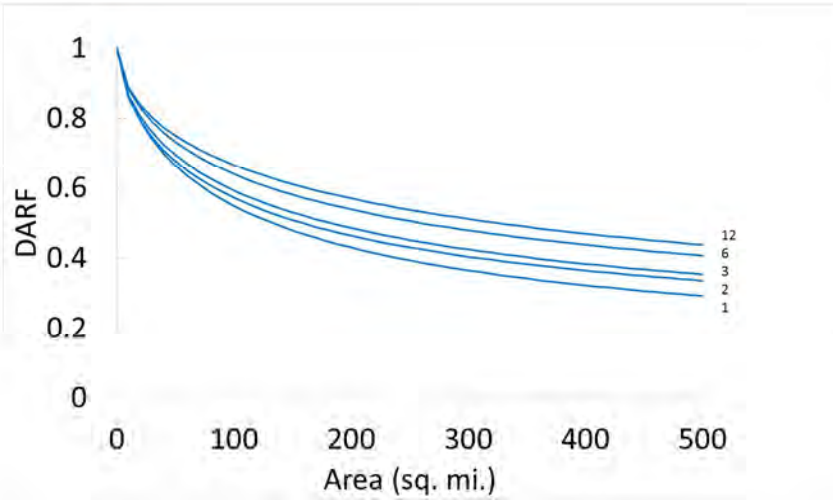

Figure C-1 HHA 1 median (left) and 90th percentile (right)

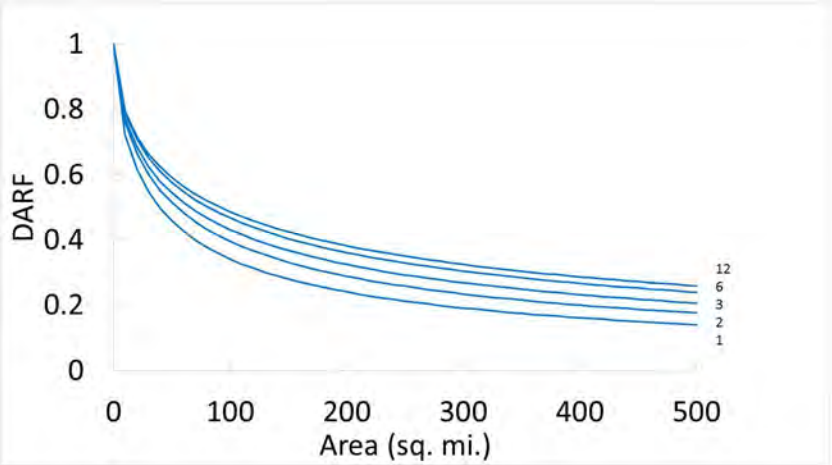

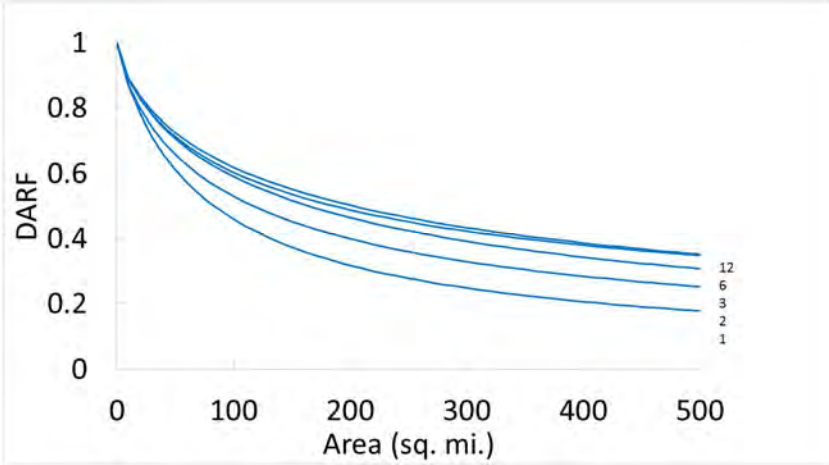

Figure C-2 HHA 2 median (left) and 90th percentile (right)

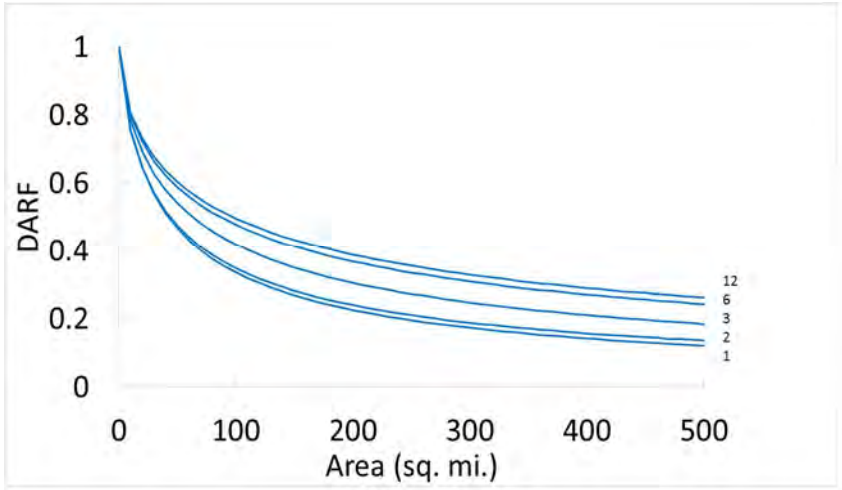

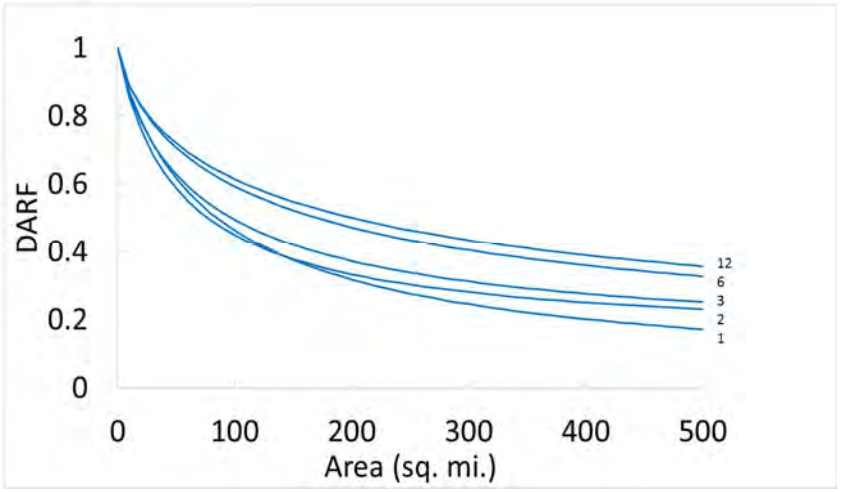

Figure C-3 HHA 3 median (left) and 90th percentile (right)

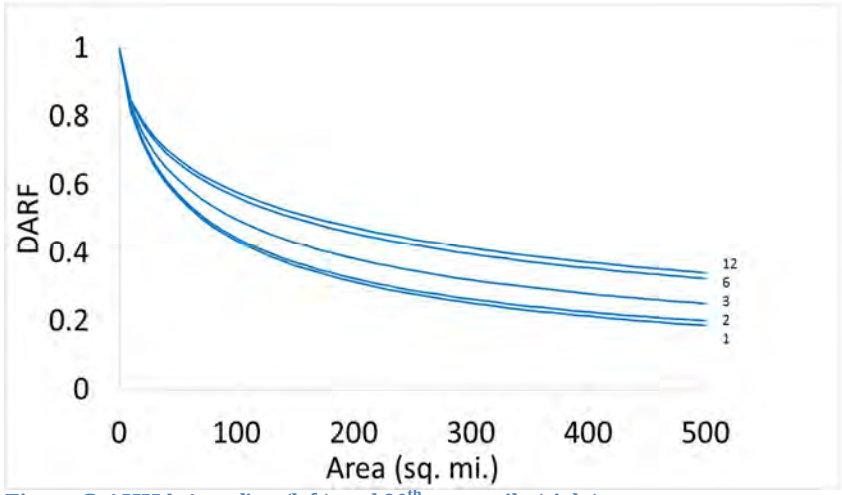

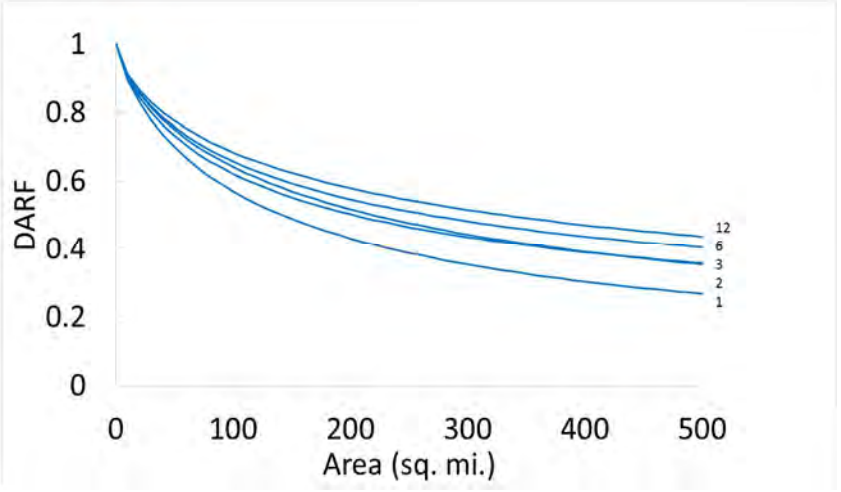

Figure C-4 HHA 4 median (left) and 90th percentile (right)

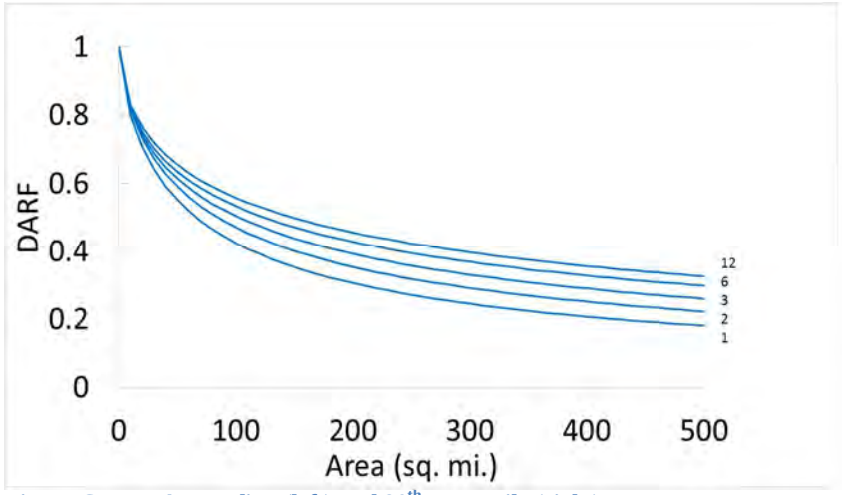

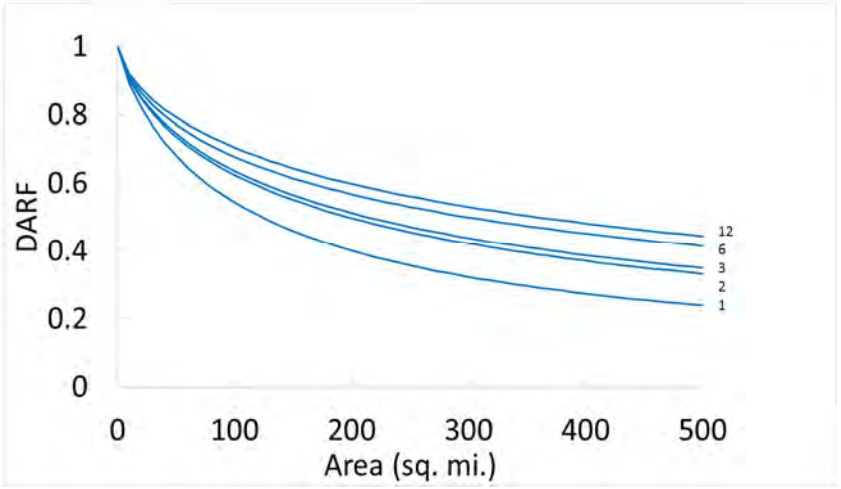

Figure C-5 HHA 5 median (left) and 90th percentile (right)

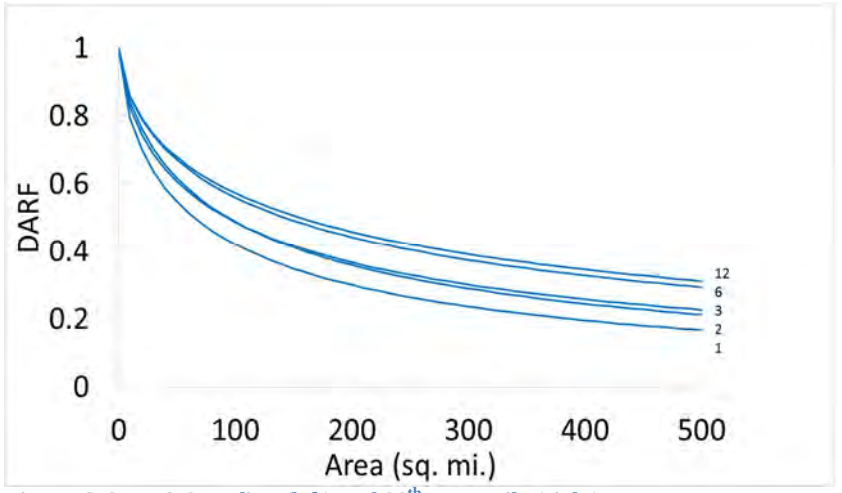

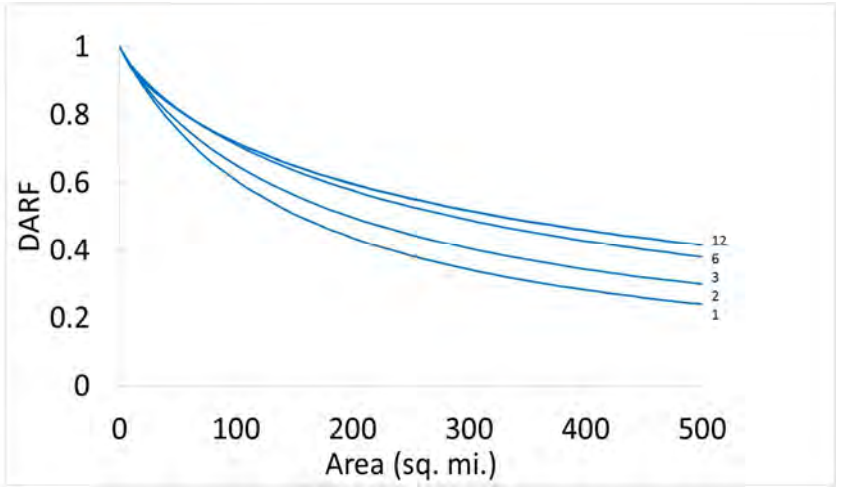

Figure C-6 HHA 6 median (left) and 90th percentile (right)

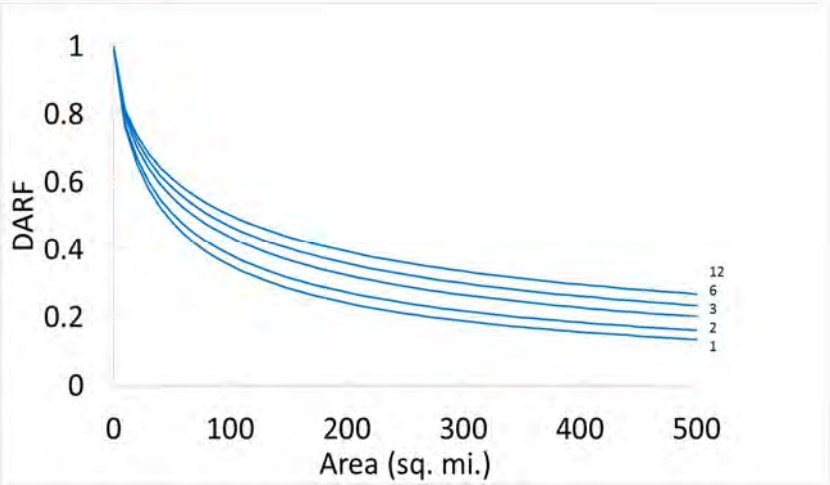

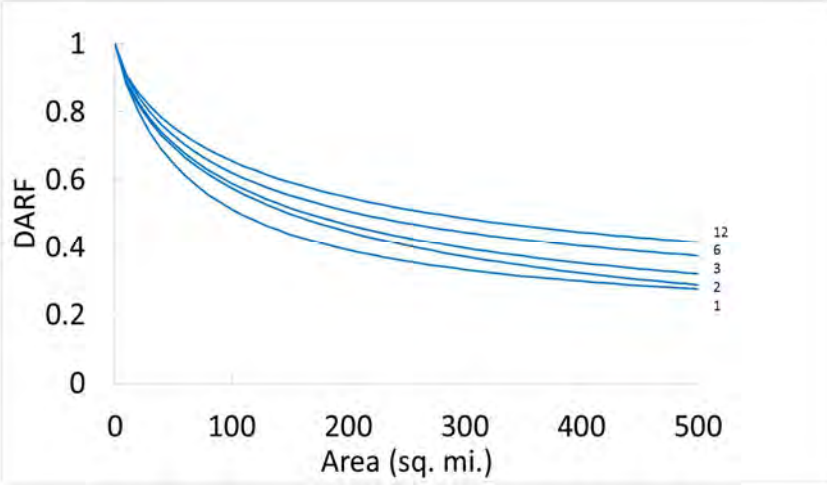

Figure C-7 HHA 7 median (left) and 90th percentile (right)

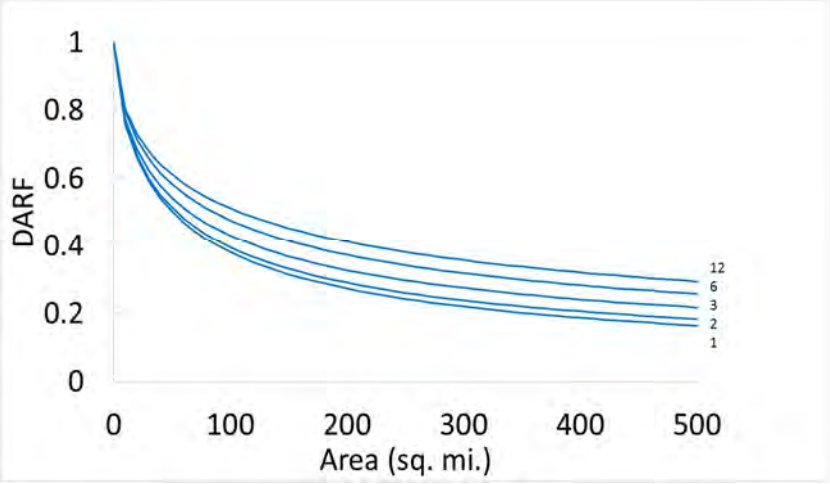

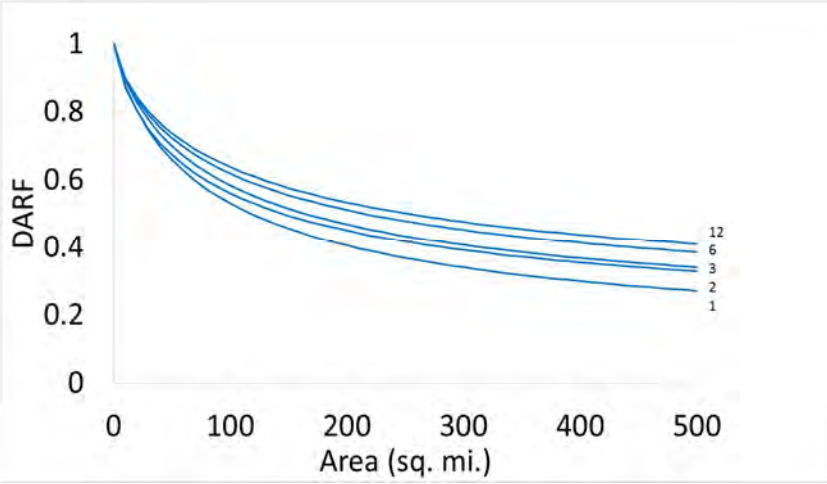

Figure C-8 HHA 8 median (left) and 90th percentile (right)

Kimley»Horn

MEMORANDUM

To:	Nevada Department of Transportation (NDOT) Technical Advisory Panel
From:	Annjanette Dodd, Kimley-Horn and Associates, Inc. Baxter Vieux, Vieux and Associates, Inc.
Date:	June 23, 2015
Subject:	Final Technical Memorandum (TM #5) – Streamlining Hydrologic Prediction Processes (P530-13-803)

INTRODUCTION

The purpose of Technical Memorandum (TM) #5 is to present the results of the evaluation of the Hyetograph and Depth Area Reduction Factors (DARF) development presented in TM's #3 and #4. This TM #5 also serves as the final summary report for this research project.

BACKGROUND

The Nevada Department of Transportation (NDOT) is proposing to use methods and technologies that have shown to significantly improve accuracy and reliability in hydrologic predictions when sizing NDOT infrastructure. The motivation of this research is to improve the accuracy of design storms used as input to hydrologic models for NDOT hydraulic structure design. Principal components of a design storm consist of applying a temporal distribution to point rainfall depth based on duration and return frequency, distributing this depth according to a temporal distribution, and distributing spatially based on a DARF for the drainage area.

Current design storm methods acceptable to NDOT (applicable outside of Clark County, Nevada) are provided in the 2006 NDOT Drainage Manual where:

- The rainfall distribution (temporal distribution) is based on the "Balanced Storm", described in NOAA Atlas 14, Precipitation-Frequency Atlas of the Western United States, and
- DARFs are based on National Weather Service (NWS) Technical Paper No. 29 (TP-29), published by the U.S. Weather Bureau, 1957 through 1960.

The balanced storm is a distribution (hyetograph) where the greatest intensities occur in the middle of the storm duration and provides conservative (high) estimates of precipitation. The DARFs presented in TP-29 were derived from rain gauge networks located in the Midwest and Northeast United States; none were located in the Southwest. No geographical variation in DARF is presented in TP-29, making it less applicable in Nevada.

The purpose of this research is to conduct a detailed analysis of storm events in the State of Nevada for the goal of developing more realistic design storms for use by NDOT throughout the state, excluding Clark County. The design storm approach presented in this research is divided into two main parts: 1) the temporal distribution defined by the hyetograph shape, which was the subject of TM #3; and 2) the spatial distribution defined by representative DARFs, the subject of TM #4. This TM is the fifth, and final, in a series of TM's summarizing the results of this research. The TM's are as follows:

- TM #1 – Review of past methods and recommended approach for design storm development.

- TM #2 – Data plan summarizing available rain gauge and radar data sources for summer and winter periods in Nevada, distributed by Hydrometerological Homogeneous Area (HHA). Eight HHA's were identified in Nevada.
- TM #3 – Methodology and results of the hyetograph development.
- TM #4 – Methodology and results of the DARF development.
- TM #5 – Evaluation of the results of this research and final summary report.

Hyetograph Development

Design storm hyetographs were developed using point rain gauge measurements for the period of record available at each gauge (TM #3). The data sources considered consisted of 371 gauges among four networks within or near Nevada. Of these gauges, 147 had sufficiently reliable records, with data recorded at sub-daily intervals and periods of record long enough to spatially interpolate hyetograph intensities over the state. The range in elevations covered by these gauges is between 480 and 9000 feet. Rain gauge data was processed into 16,771 distinct storm events. A cumulative hyetograph was developed for each storm event, consisting of accumulated rainfall depth versus time for the event duration. These were then made dimensionless by dividing each depth by the total depth and each time step by the total duration. The resulting dimensionless hyetograph represents the percentage depth versus percentage duration.

A key characteristic of the dimensionless hyetograph is the maximum slope (maximum increase in percentage depth versus percentage duration), which corresponds to the maximum rainfall intensity during that event.

For the dimensionless median hyetograph, this maximum intensity is referred to as the median maximum intensity (MMI). The MMI is equivalent to the 50^{th} percentile maximum intensity. The MMI was used to evaluate the variability in duration, depth, seasonality, and geography of the storm distributions. The following were determined:

- The MMI was found to be invariant for storm durations up to 24-hours;
- No strong correlation with rainfall depth was found;
- The MMI associated with summertime convection (July) dominates regardless of location across the state; and
- The MMI varies geographically across the state.

Based on these results, a single hyetograph shape can be developed anywhere in the state based on a specified maximum intensity value. Placement of the MMI within the center of the storm duration is recommended for conservatism even though first quartile storms were predominant. Since the maximum intensity varies geographically, maximum intensity maps were provided, one based on the MMI (50^{th} percentile), and the other based on the 90^{th} percentile maximum intensity. These maps were derived based on advanced, climate-aided interpolation (CAI), where the climatic trend used to interpolate rain-gauge-specific MMI or 90^{th} percentile maximum intensity values is provided by the NOAA Atlas 14, Volume 1 map of 1-hour, 100-year rainfall depths. The CAI interpolation was validated by withholding gauges and applied to the MMI and 90^{th} percentile maximum intensity values (Figure 1 and Figure 2). These maps reflect both terrain and orographic enhancement or rain shadowing effects throughout the state because the NOAA Atlas 14 maps of rainfall depths relied on PRISM (Parameter-elevation Regressions on Independent Slopes Model) in its mapping. The intended use of a maximum intensity map is to identify the hyetograph maximum intensity expected at any given location and use it to determine a location specific hyetograph for a given cumulative rainfall depth. Evaluation of the use of either the MMI or the 90^{th} percentile maximum intensity values is presented below.

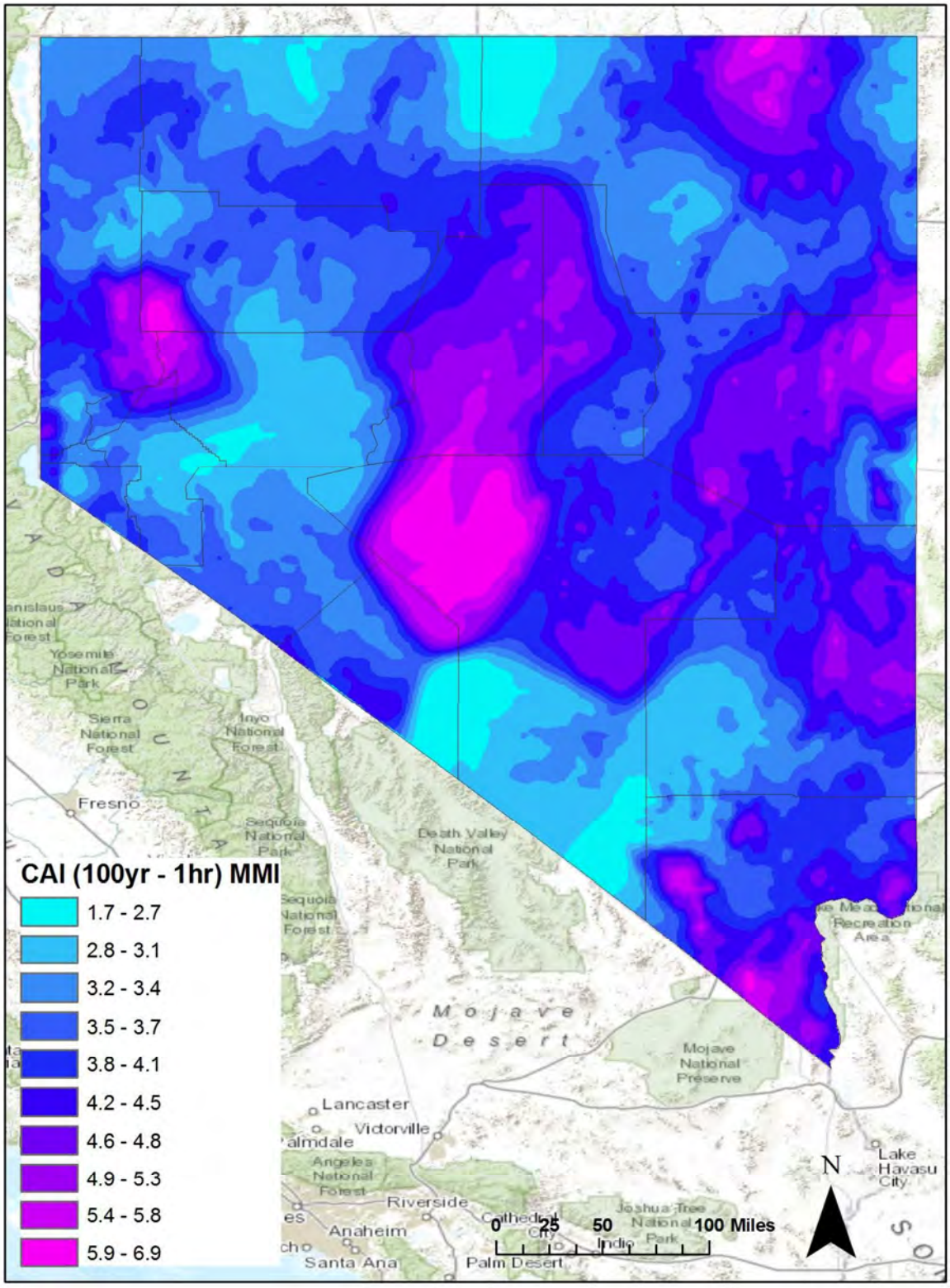

Figure 1: 50th Percentile Median Intensity (MMI) for Nevada.

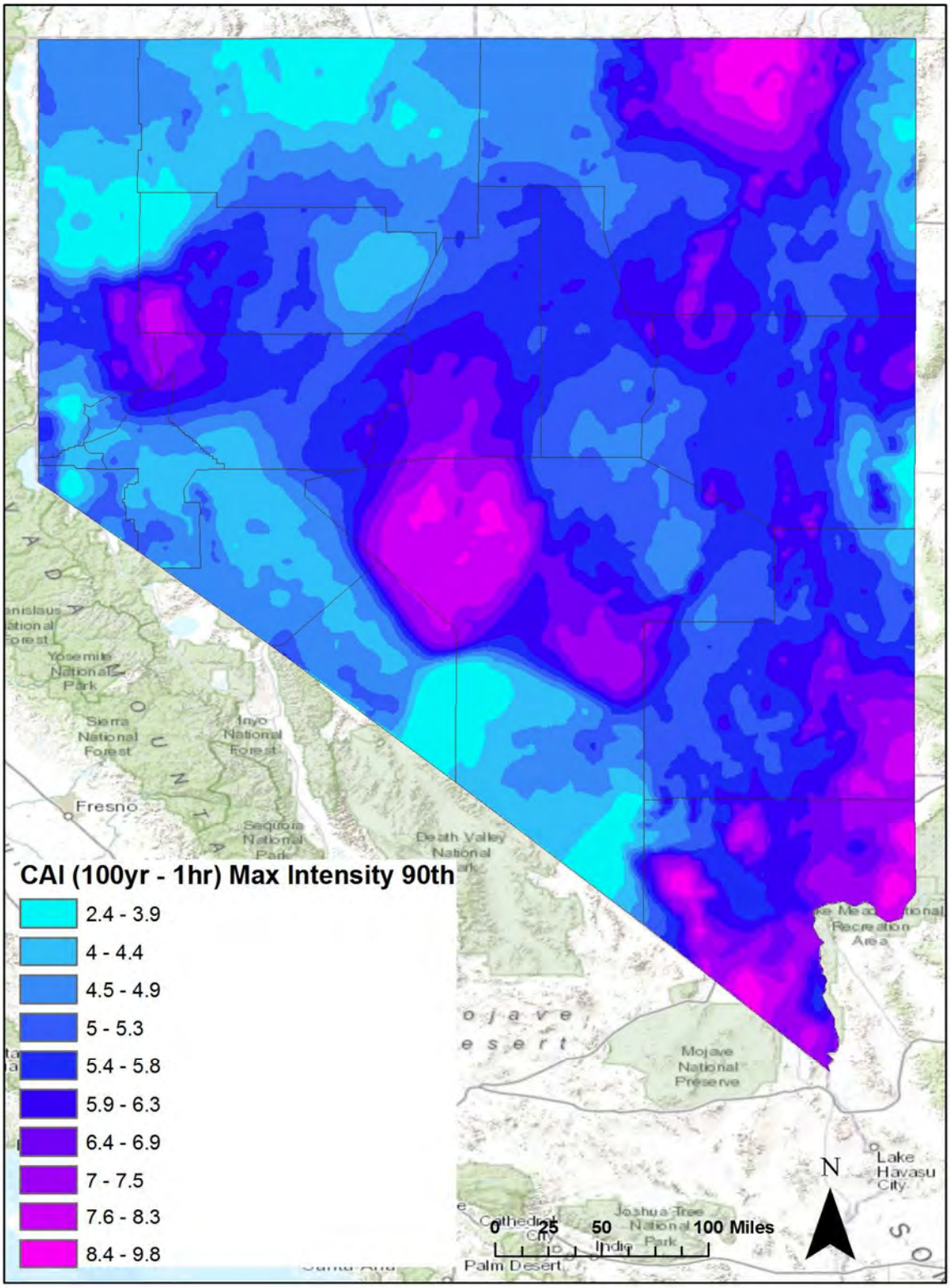

Figure 2: 90th Percentile Maximum Intensity for Nevada

DARF Development

DARFs were developed using precipitation estimates derived from 547 actual storm events, observed by radar, from 2005 through 2014 (TM #4). The events were grouped based on flooding potential and Hydrometeorological Homogeneous Area (HHA) and then aggregated by rainfall duration (HHAs were determined based on the geographic distributions of gauges that are similar in terms of statistical properties regarding precipitation). Storms considered were either within a warning/advisory polygon issued by the NWS and/or included in the National Climate Data Center (NCDC) flash flood database, and are considered extreme or at least with flood-producing rainfall depths and intensities. Of the 547 individual events, there were 1,720 duration-based storm totals developed and used to determine DARF relationships at both the median (50th percentile) and 90th percentile. Relationships were identified for each of the eight HHAs and for the 1-, 2-, 3-, 6-, 12-, and 24-hour durations for areas up to 500 mi^2.

Smoothing the DARF values across the eight HHAs for each duration, it is apparent that most of the reduction occurs once the area increases to about 100 mi^2, and thereafter, declines steadily up to 500 mi^2 (Figure 3 and Figure 4). As the duration of the storm progresses, there is less reduction expected due to a larger areal distribution of rainfall. Because of the small difference in DARF values (areas < 100 mi^2) across the State (TM #4), a single set of DARF relationships for 1-, 3-, 6-, 12-, and 24-hour durations is recommended and presented here for both the median and 90th percentile. The current DARFs used by NDOT (NOAA Atlas), Clark County Regional Flood Control District (CCRFCD), and the Truckee Meadows Regional Drainage Manual (TMRDM) are included in the figures for comparison purposes. Both the NDOT and TMRDM DARFs are based on NOAA Atlas DARFs. The DARFS determined by this research are much less, primarily due to differences in the approach used to obtain depth-area relationships. Evident in Figure 3 and Figure 4, the lesser amount of reduction (higher DARF) stems from the NWS using rain gauge networks, while the DARFs developed herein are derived from the areal extent of rainfall depths measured by radar. Evaluation of the use of the median versus the 90th percentile DARFs determined by this research is presented below.

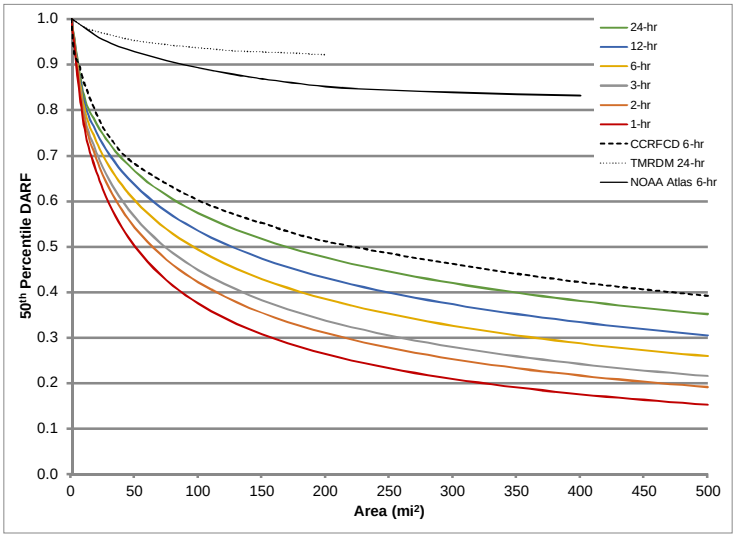

Figure 3: Smoothed 50th percentile depth area reduction factors (DARFs) for storm durations 1- through 24-hours.

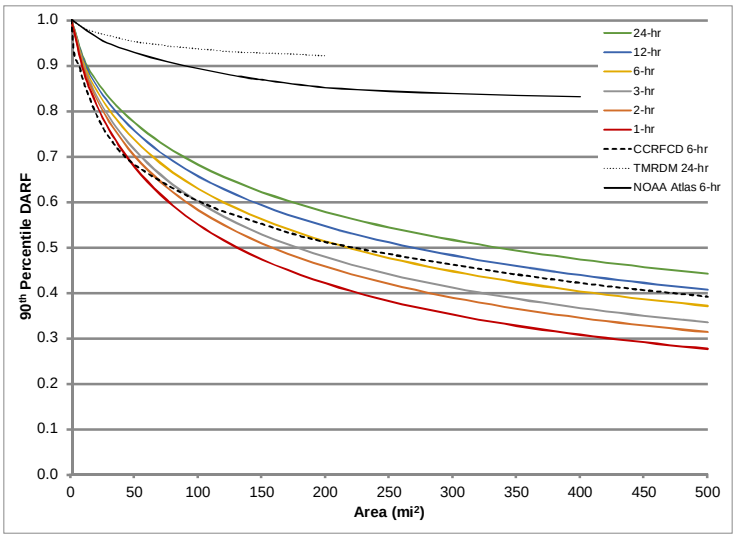

Figure 4: Smoothed 90th percentile depth area reduction factors (DARFs) for storm durations 1- through 24-hours.

EVALUATION OF DESIGN STORM

Components of a design storm include duration, depth, hyetograph shape, DARF, and return frequency. To evaluate the results of this research, hydrologic comparisons are made to design storms determined by the existing NDOT, CCRFCD, and the TMRDM (Washoe County, 2009) Drainage Design Manuals.

Currently, within the jurisdiction of NDOT, either the 6-hour or the 24-hour duration is used, as appropriate. Rainfall depth is obtained from NOAA Atlas 14, Volume 1, the hyetograph shape is determined using a balanced distribution, and DARF values are based on TP-29.

Within the jurisdiction of CCRFCD, the 6-hour duration storm is the preferred design storm. The CCRFCD Drainage Manual provides depth, hyetograph shape and DARFs to be used as part of the storm development.

Within the jurisdiction of Washoe County, the 24-hour duration is the standard design storm duration for hydrologic methods other than the rational method. The TMRDM provides depth, hyetograph shape, and DARFs to be used as part of storm development. Hyetograph shape is based on a balanced storm. The DARFs are based on NOAA Atlas.

For the purpose of the evaluation presented here, a 6-hour, 25-year storm is used for all cases and locations, even though the 24-hour duration is the standard design storm in Washoe County. Three locations are evaluated, Ely, Las Vegas, and Sparks, Nevada, using the design methods presented in the NDOT, CCRFCD, and TMRDM Drainage Design Manuals, respectively. The results are compared to those determined using the results of this research.

Each design storm is routed through a 100 mi^2 watershed, with and without losses, using HEC-HMS, Version 4.0, for peak flow and hydrograph comparisons. Losses are modeled using Green and Ampt infiltration with parameter values representative of soils composed of a mix of loamy sand and sandy loam. These soils allow for moderate infiltration rates for evaluation of the impact on the hydrographs due to infiltration.

Depth

The 6-hour, 25-year storm depths were determined at each location, using the appropriate jurisdiction manual, and are summarized in Table 1.

Table 1. 6-hour, 25-year design storm depths for Ely, Las Vegas, and Sparks, Nevada.

Location	Lat/Long	Depth (in)	Jurisdiction	Source
Ely, NV	39.2482/-114.8880	1.41	NDOT	NOAA Atlas 14, Volume 1
Las Vegas, NV	36.1739/-115.1391	2.05	CCRFCD	CCRFCD Table 505
Sparks, NV	39.5403/-119.7851	1.27	TRMDM	TMRDM, Table 601

Depth-Area Reduction Factors (DARFs)

The 6-hour duration DARFs for each location and area of 100 mi^2 are summarized in Table 2. For both Ely and Sparks, NV, the jurisdictional DARFs were determined from NOAA Atlas 14 and are based on TP-29 since the TMRDM only provides 24-hour DARFs for Sparks, NV.

Table 2. Depth-Area Reduction Factors (DARFs) for Ely, Las Vegas, and Sparks, Nevada using both jurisdictional values and those determined from this research for an area of 100 mi^2.

		6-hour DARF, Area = 100 square miles		
Location	HHA	Jurisdictional	50th Percentile	90th Percentile
Ely, NV	5	0.89[1]	0.49	0.63
Las Vegas, NV	8	0.60[2]	0.49	0.63
Sparks, NV	1	0.89[1]	0.49	0.63

[1]TP-29, [2]CCRFCD Table 502

Hyetograph Development

The results of this research recommend the hyetograph shape be determined as a function of the maximum intensity. Two geographical distributions of maximum intensity are provided, the MMI and the 90th percentile maximum intensity (Figure 1 and Figure 2). As for hyetograph shape, the median cumulative hyetograph shape is similar to a general logistic curve (Figure 5). Given the maximum intensity, a hyetograph at any particular location could be determined using a generalized logistic equation (GLE) applied to the cumulative rainfall depth. The GLE has the form

$$Y(t) = A + \frac{K - A}{(1 + Qe^{-B(t-M)})^{1/\nu}}$$

where

Y(t) = depth fraction at time fraction, t
A = lower asymptote = 0
K = upper asymptote = 1
B = is a parameter that controls the maximum intensity
v = fitting parameter set equal to Q
Q = Fitting parameter affecting slope before max intensity
M = Location of maximum intensity = 0.50

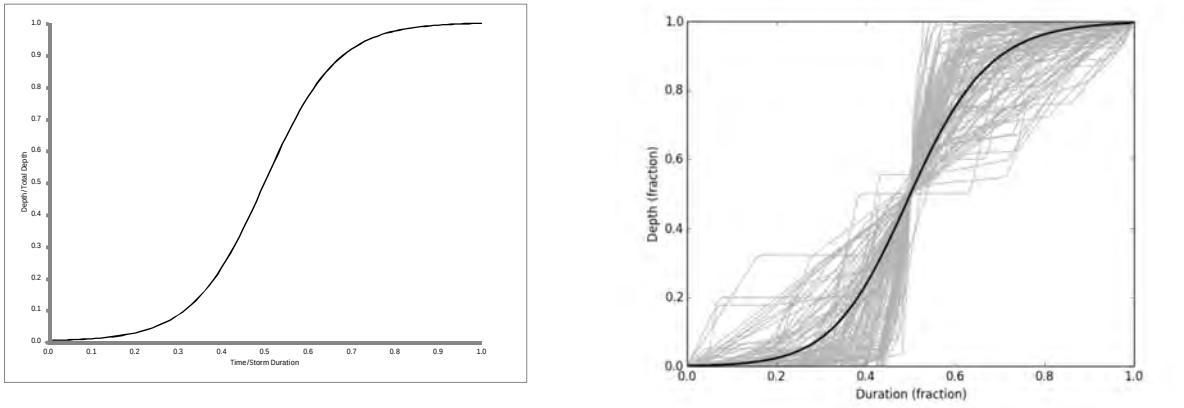

Figure 5: Shape of logistic curve (GLE) (left) and smoothed cumulative hyetograph (right).

The GLE, with its six parameters, can be made to fit most any cumulative rainfall curve produced by a temporary intense burst of rainfall with a given maximum intensity and rainfall depth. The MMI and 90th percentile maximum intensity (Figure 1 and Figure 2) for the three locations, Ely, Las Vegas, and Sparks are summarized in Table 3. The DARFs in Table 2 were applied to the rainfall depths in Table 1 and are summarized in Table 4.

Table 3. Median Maximum Intensity (MMI) and 90th Percentile Maximum Intensity at each location.

Location	Maximum Intensity	
	50th Percentile (MMI)	90th Percentile
Ely, NV	4.49	5.61
Las Vegas, NV	3.61	5.60
Sparks, NV	2.79	3.65

Table 4. Rainfall depths with DARFs applied for 100 mi^2 area.

		Depth (in)		
Location	No DARF	Jurisdictional	50th Percentile	90th Percentile
Ely, NV	1.41	1.25	0.69	0.89
Las Vegas, NV	2.05	1.23	1.00	1.29
Sparks, NV	1.27	1.13	0.62	0.80

A total of nine hyetographs were generated. HEC-HMS was used to estimate hydrographs resulting from each hyetograph considering a watershed with and without losses, where losses were estimated using Green and Ampt infiltration. This was done at each of the three locations. The first hyetograph at each location is based on the existing jurisdictional methodology as provided by NDOT, CCRFCD, and TMRDM for Ely, Las Vegas, and Sparks, respectively and the jurisdictional depth in Table 4; the three hyetographs are summarized in Figure 6. At Ely and Sparks, the jurisdictional hyetographs are based on a balanced storm, determined using HEC-HMS. As expected with a balanced storm, they are much "peakier" than the CCRFCD hyetograph for Las Vegas.

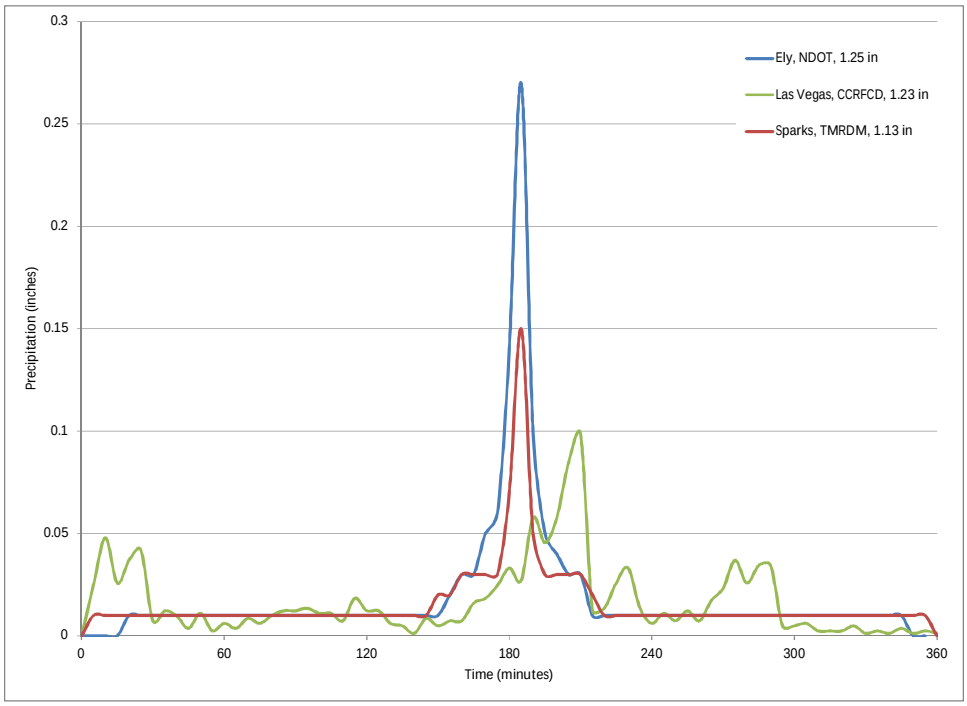

Figure 6: Jurisdictional hyetographs (6-hour, 25-year design storms) for the cities of Ely (NDOT) – balanced storm using depth from NOAA Atlas 14 Volume 1, Las Vegas (CCRFCD) –SDN5 storm distribution from CCRFD Table 503 using depth from CCRFCD Table 505, and Sparks (TMRDM) balanced storm using depth from TMRDM, Table 601.

The remaining eight hyetographs, summarized in Figure 7 through Figure 9, are based on a combination of factors. Four are based on the GLE using the MMI and 90th percentile maximum intensity combined with the 50th and 90th percentile DARFs determined by this research. Two are based on the median hyetograph determined for the HHA in which the City is located; these are different from the GLE. The median hyetograph is a representative hyetograph shape for storms observed in the HHA that Ely, Las Vegas, and Sparks are located in. The purpose of evaluating the median hyetographs is to evaluate the effect on the outflow hydrograph when the tails of the hyetograph are not smooth, as with the GLE hyetographs. The remaining two hyetographs are based on the balanced storm determined within HEC-HMS and the 50th and 90th percentile DARFs determined by this research. The depth-duration factors used to determine the balanced storms were obtained from NOAA Atlas 14, the CCRFCD Drainage Manual Table 505 for the McCarran Airport, and the TMRDM Table 601 for Region 1, for Ely, Las Vegas, and Sparks, respectively.

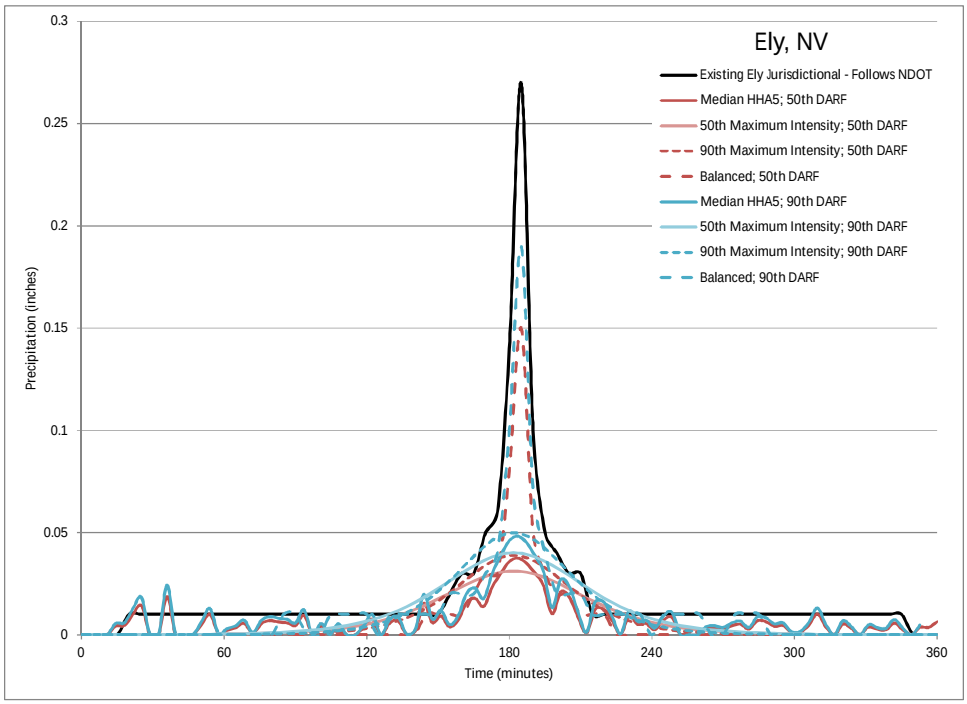

Figure 7: 6-hour, 25-year hyetographs for Ely, Nevada (Median HHA = median of actual hyetographs, 50th Maximum Intensity = GLE hyetograph using median maximum intensity, 90th Maximum Intensity = GLE hyetograph using 90th percentile intensity, Balanced = hyetograph determined using a balanced storm approach).

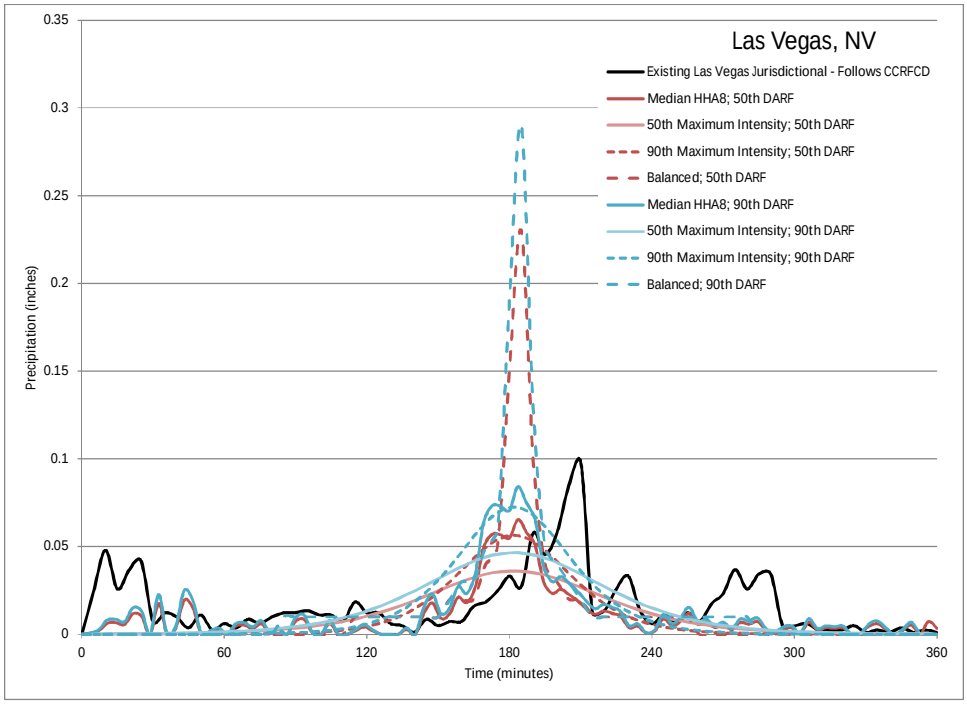

Figure 8: 6-hour, 25-year hyetographs for Las Vegas, Nevada (Median HHA = median of actual hyetographs, 50th Maximum Intensity = GLE hyetograph using median maximum intensity, 90th Maximum Intensity = GLE hyetograph using 90th percentile intensity, Balanced = hyetograph determined using a balanced storm approach).

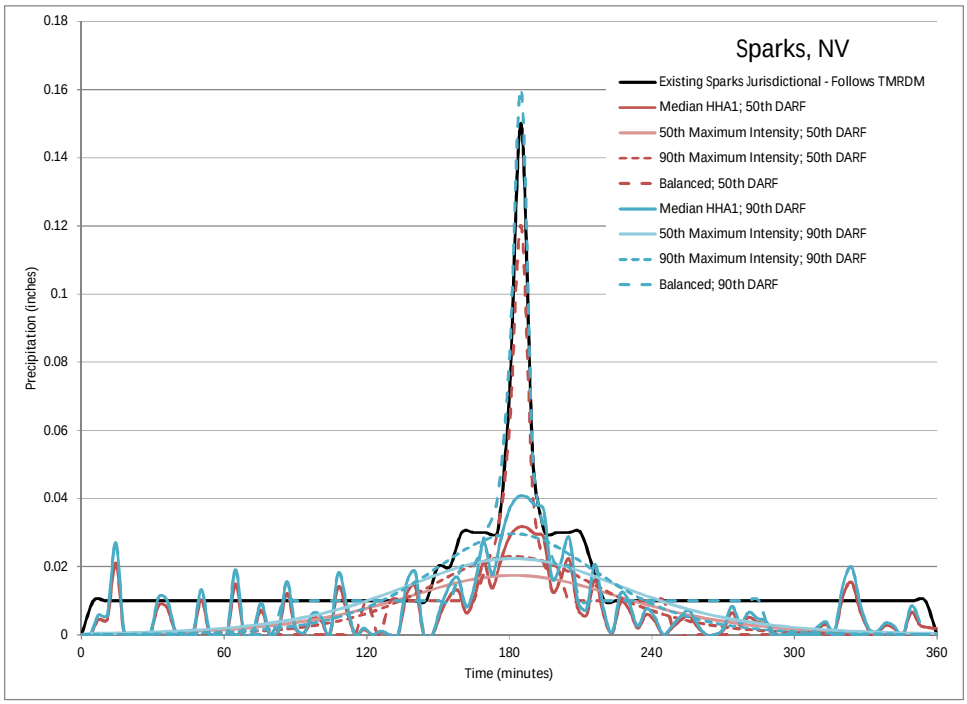

Figure 9: 6-hour, 25-year hyetographs for Sparks, Nevada (Median HHA = median of actual hyetographs, 50th Maximum Intensity = GLE hyetograph using median maximum intensity, 90th Maximum Intensity = GLE hyetograph using 90th percentile intensity, Balanced = hyetograph determined using a balanced storm approach).

Hydrologic Evaluation

Outflow hydrographs were generated using each hyetograph within HEC-HMS for a hypothetical 100 mi^2 watershed. Since the purpose here is to evaluate the design storm results from this research, a single hypothetical watershed is used: 1) without losses and 2) with losses based on Green and Ampt infiltration and parameters, with an *initial content of 0.2*, *saturated content of 0.4*, *suction of 3.5 inches*, *saturated hydraulic conductivity of 0.5 inches/hour* and *impervious of 20% (these parameters are representative of soils composed of a mix of loamy sand and sandy loam and allow for moderate infiltration rates)*. The hydrograph transformation for both cases is based on a Snyder Unit Hydrograph, with a *Lag* of *5.4 hours* and *Peaking Coefficient of 0.5*; which are considered reasonable for a watershed of this size in Nevada.

Ely, Nevada

At Ely, the current NDOT methodology results in a hydrograph with a much higher peak and runoff volume than those determined using the combination of hyetographs and DARFs from this research. When losses are excluded from the hydrology model, there is little difference in the hydrographs resulting from the hyetographs developed using either the Median Hyetograph, those developed based GLE and the MMI or the 90th percentile maximum intensity, or those from the balanced storm (Figure 10). The balanced hyetographs produce the highest peak discharge regardless of whether losses (Green and Ampt) or no losses are considered. The balanced hyetograph results in higher peak flows than the hydrographs that result from the other hyetographs (Figure 11).

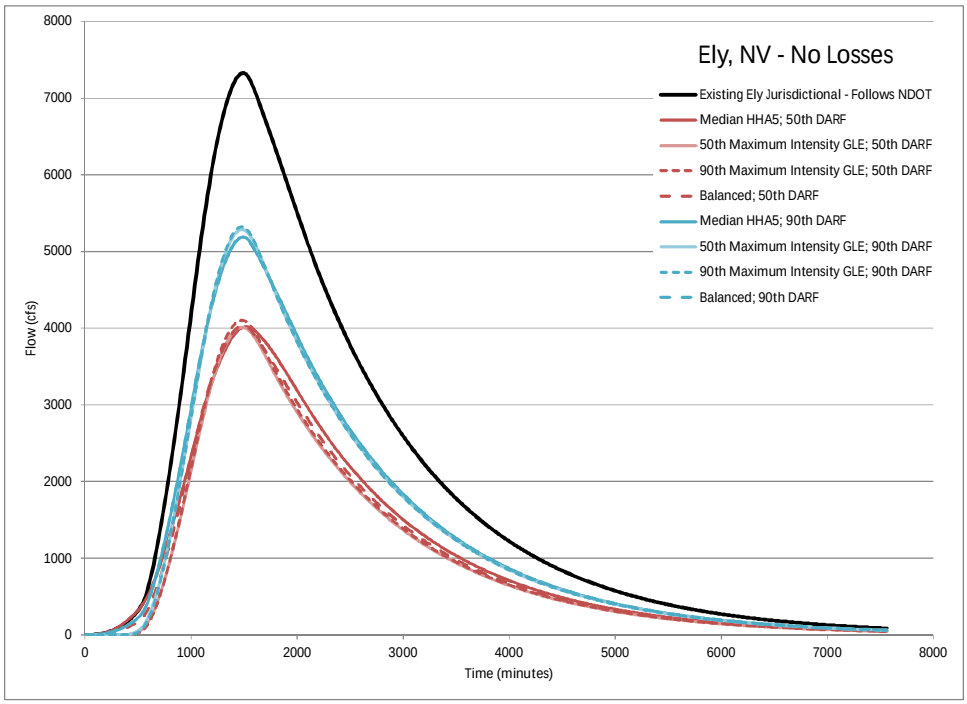

Figure 10: 6-hour, 25-year hydrographs for Ely, Nevada (no losses) for a hypothetical 100mi^2 basin (Median HHA = median of actual hyetographs, 50th Maximum Intensity = GLE hyetograph using median maximum intensity, 90th Maximum Intensity = GLE hyetograph using 90th percentile intensity, Balanced = hyetograph determined using a balanced storm approach).

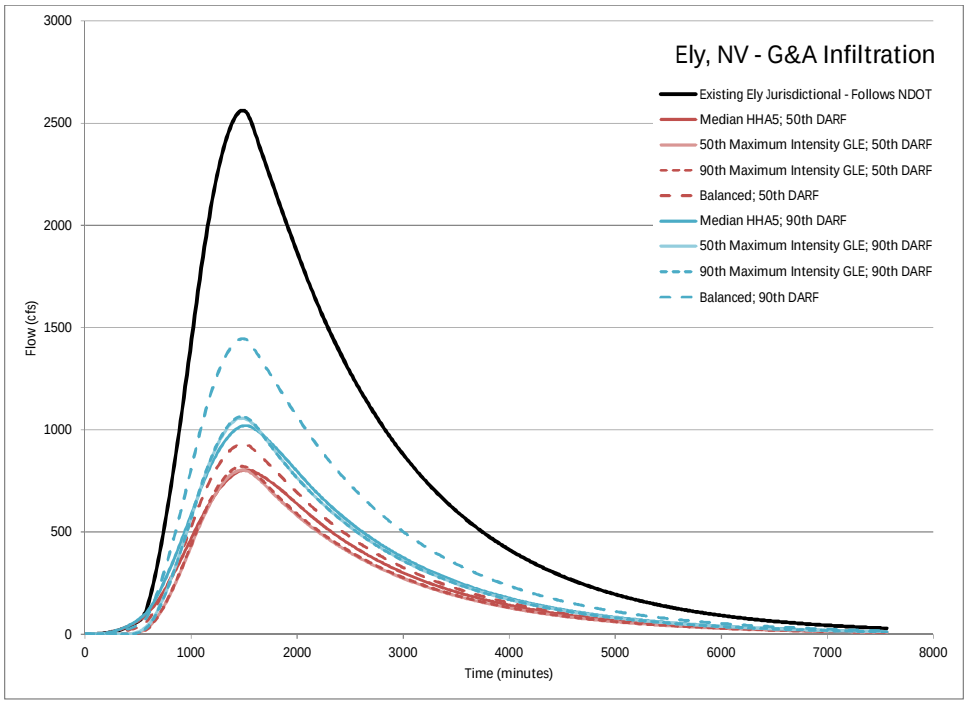

Figure 11: 6-hour, 25-year hydrographs for Ely, Nevada (Green and Ampt Infiltration) for a hypothetical 100mi^2 basin (Median HHA = median of actual hyetographs, 50th Maximum Intensity = GLE hyetograph using median maximum intensity, 90th Maximum Intensity = GLE hyetograph using 90th percentile intensity, Balanced = hyetograph determined using a balanced storm approach).

Las Vegas, Nevada

At Las Vegas, the current CCRFCD methodology results in a hydrograph with a peak flow and runoff volume in the middle of those determined using the combination of hyetographs and DARFs from this research. When losses are excluded from the hydrology model, there is little difference in the hydrographs resulting from the hyetographs developed using either the Median Hyetograph, those developed based on the GLE and the MMI or the 90th percentile maximum intensity, or those from the balanced storm (Figure 12). With Green and Ampt infiltration, the CCRFCD hydrograph and the hydrograph generated using the MMI GLE and 90th DARF are very similar. The balanced hyetographs produce the highest peak discharge regardless of whether losses (Green and Ampt) or no losses are considered (Figure 13).

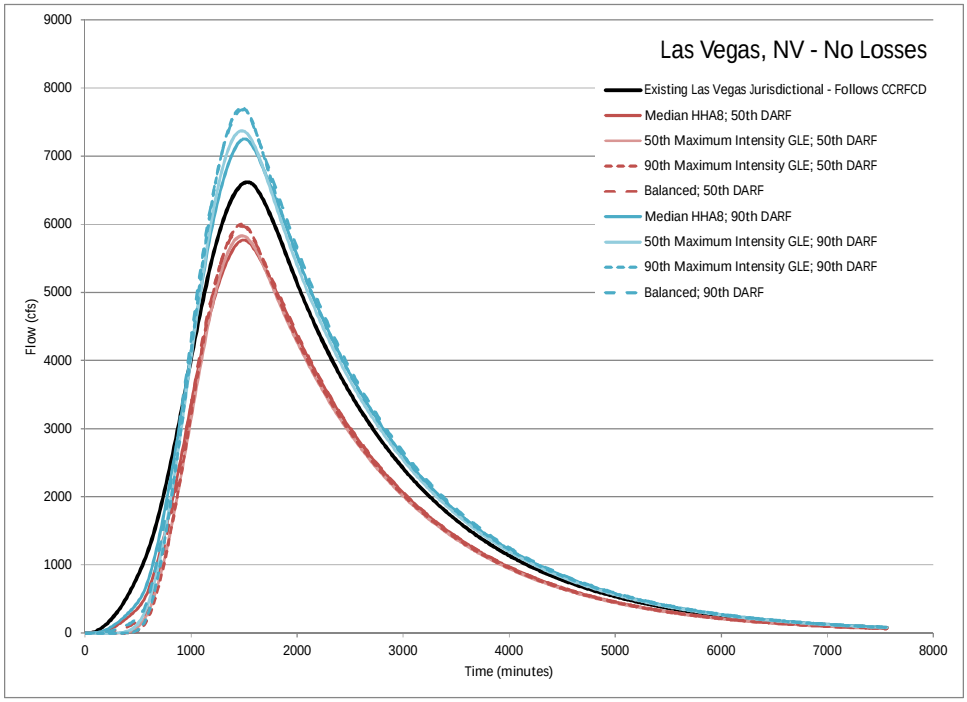

Figure 12: 6-hour, 25-year hydrographs for Las Vegas, Nevada (no losses) for a hypothetical 100mi^2 basin (Median HHA = median of actual hyetographs, 50th Maximum Intensity = GLE hyetograph using median maximum intensity, 90th Maximum Intensity = GLE hyetograph using 90th percentile intensity, Balanced = hyetograph determined using a balanced storm approach).

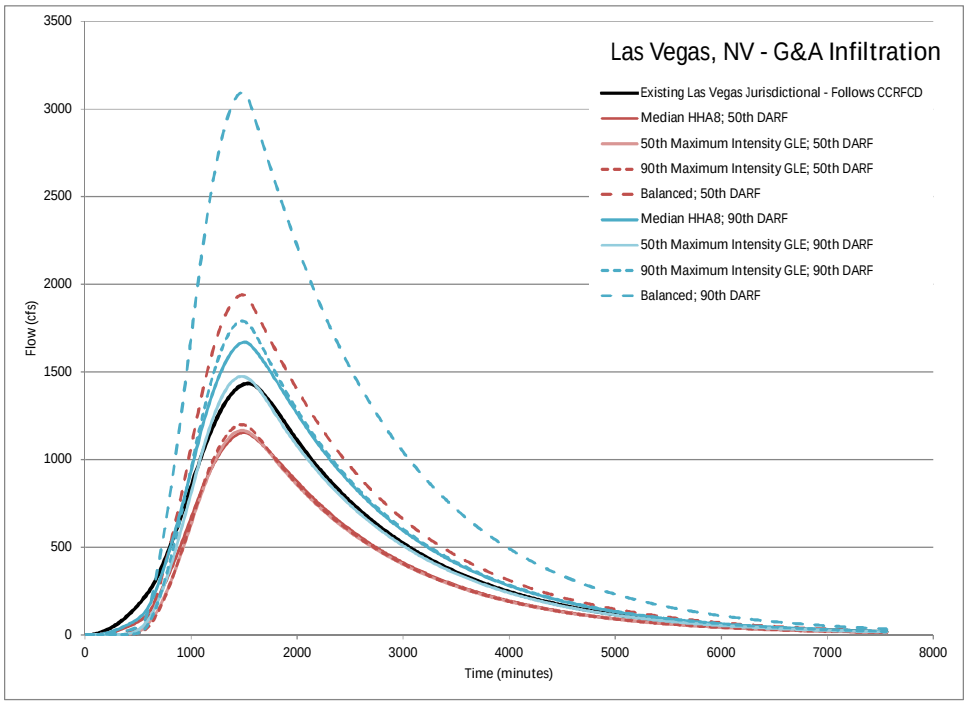

Figure 13: 6-hour, 25-year hydrographs for Las Vegas, Nevada (Green and Ampt Infiltration) for a hypothetical 100mi^2 basin (Median HHA = median of actual hyetographs, 50th Maximum Intensity = GLE hyetograph using median maximum intensity, 90th Maximum Intensity = GLE hyetograph using 90th percentile intensity, Balanced = hyetograph determined using a balanced storm approach).

Sparks, Nevada

Similar to what was observed at Ely, at Sparks the TMRDM methodology results in a hydrograph with a much higher peak and runoff volume than those determined using the combination of hyetographs and DARFs from this research. When losses are excluded from the hydrology model, there is little difference in the hydrographs resulting from the hyetographs developed using either the Median Hyetograph, those developed based GLE and the MMI or the 90th percentile maximum intensity, or those from the balanced storm (Figure 14). With Green and Ampt infiltration, the balanced hyetographs using the 90th percentile DARF, due to its peakier nature, results in more runoff and a higher peak flow than thee other hydrographs. The total precipitation from the 90th percentile DARF, due to its peakier nature (higher rainfall intensity), results in more runoff and peak flows, compared to the other hydrographs when losses (Green and Ampt) are considered (Figure 15).

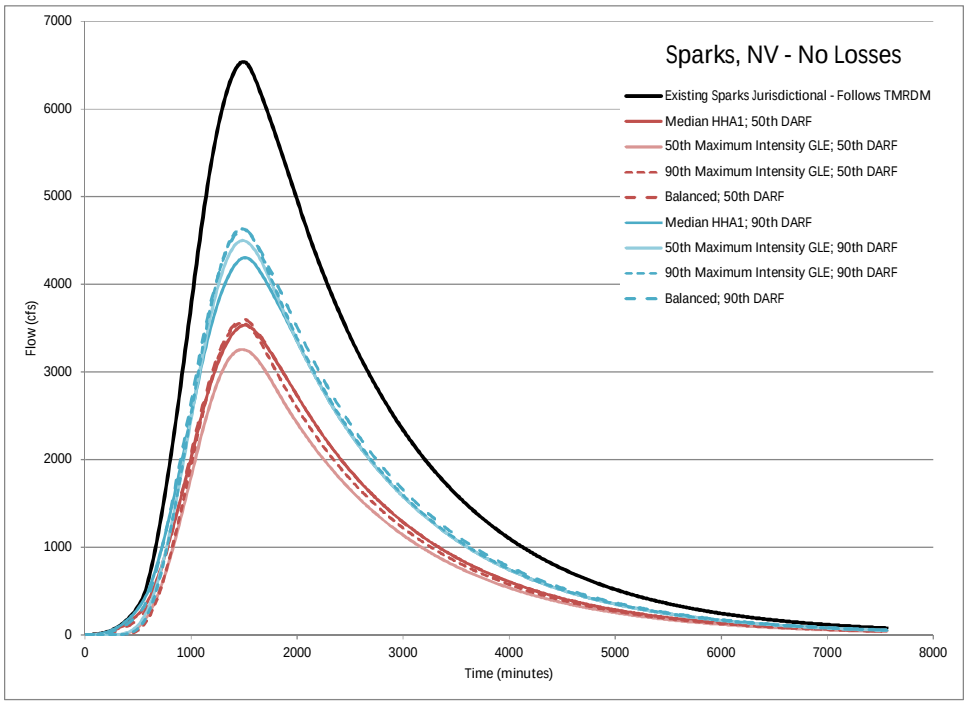

Figure 14: 6-hour, 25-year hydrographs for Sparks, Nevada (no losses) for a hypothetical 100mi^2 basin (Median HHA = median of actual hyetographs, 50th Maximum Intensity = GLE hyetograph using median maximum intensity, 90th Maximum Intensity = GLE hyetograph using 90th percentile intensity, Balanced = hyetograph determined using a balanced storm approach).

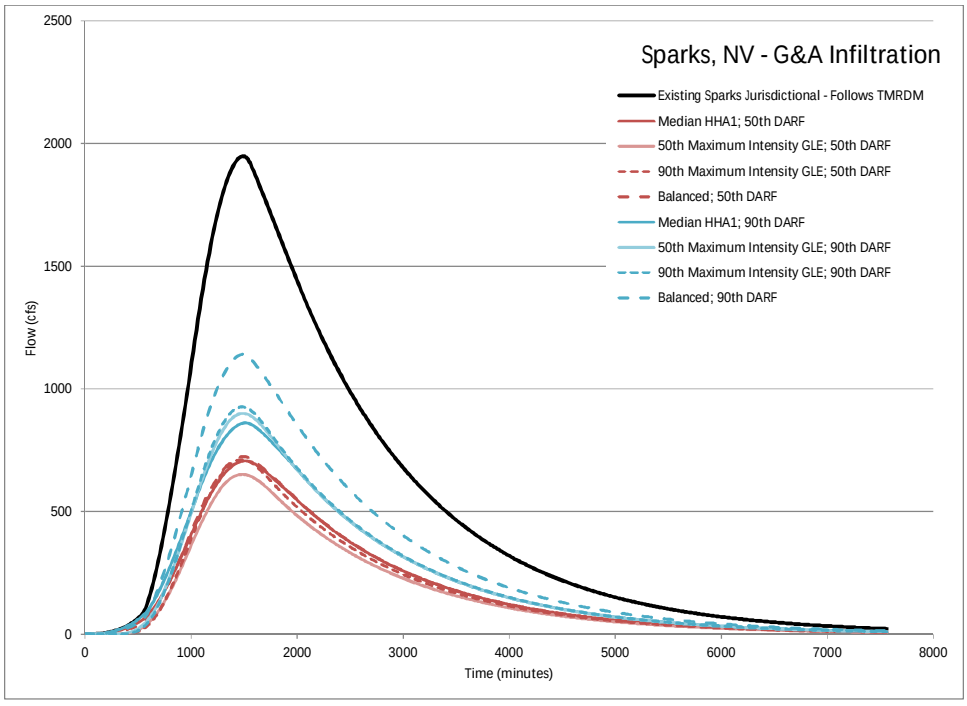

Figure 15: 6-hour, 25-year hydrographs for Sparks, Nevada (Green and Ampt Infiltration) for a hypothetical 100mi^2 basin (Median HHA = median of actual hyetographs, 50th Maximum Intensity = GLE hyetograph using median maximum intensity, 90th Maximum Intensity = GLE hyetograph using 90th percentile intensity, Balanced = hyetograph determined using a balanced storm approach).

SUMMARY

For this research a detailed analysis of storm events was conducted within the State of Nevada to develop design storms for use by NDOT throughout the state, excluding Clark County. The design storm includes a hyetograph shape and DARF relationships for the 1-, 3-, 6-, 12-, and 24-hour storm durations. The recommended hyetograph shape is a general logistic curve (GLE) determined as a function of the maximum intensity and cumulative rainfall depth. Two maps of maximum intensity were provided, one representing the MMI (50th percentile maximum intensity), Figure 1, and the other representing the 90th percentile maximum intensity, Figure 2. One set of curves representing the median (50th percentile) and 90th percentile DARF relationships were provided for the entire state.

A hydrologic analysis was conducted using HEC-HMS to evaluate the differences between the median and 90th percentile maximum intensity, DARF relationships, and three existing jurisdictional methodologies used in three different HHA's throughout the state – Ely (HHA 5), Las Vegas (HHA 8), and Sparks (HHA 1). A summary of the key findings follows:

- The existing jurisdictional methods that are based on a balanced storm and DARFs and NOAA Atlas precipitation depths result in higher peak flows and runoff volumes than those determined from the results of this research, with or without losses.
- Within the CCRFCD jurisdiction (HHA 8), the jurisdictional hydrograph (without losses) falls between the hydrographs from this study. With losses, the jurisdictional hydrograph falls closest to the hydrograph generated by the MMI GLE and 90th percentile DARF hyetograph. The 6-hour, 100 mi^2 DARF from CCRFCD (0.60) is closest to the 90th percentile DARF (0.63) from this research.
- Without losses, there is little difference between the non-jurisdictional hydrographs when the DARF is determined from the same curve. As expected, 90th percentile DARF values result in higher peak flows and runoff volumes. There is little difference in hydrograph peak, whether the MMI or 90th percentile hyetograph is chosen.
- There is little difference between the hydrographs generated by the logistic curve hyetographs or the median hyetographs, indicating that the smoothed tales of the logistic curve hyetographs have little impact.
- Balanced storm hyetographs produce the highest peak flows with or without losses introduced by the Green and Ampt infiltration. Depending on the Green and Ampt parameters, higher intensities will generally result in more runoff.

RECOMMENDATIONS AND PROCEDURE

Recommendations are made for a conservative combination of hyetograph and DARF as follows:

1. Depth-areal reduction factor at the 90th percentile, and
2. Hyetograph at the 90th percentile maximum intensity smoothed by the GLE and centered within the storm duration.

The procedure for applying the DARF and hyetograph consists of determining the design storm duration for the watershed or subwatershed. Then from the statewide 90th percentile DARF curves, select reduction factor for the watershed area. For larger watersheds, no further reduction should be applied than the lowest reduction at 500 mi^2. For watershed areas less than 5 mi^2, no reduction is recommended. The hyetograph should be selected for a watershed or subwatershed from the 90th percentile maximum intensity CAI interpolated map of values (Figure 2). Values can be selected at the centroid of the watershed area. The temporal distribution should be centered with the maximum intensity occurring at the center of the storm duration.

REFERENCES

Bonin, G, Martin, D., Lin, Parzybok, T., Yekta, M., and Riley, D. (Revised 2011), *National Oceanic and Atmospheric Administration's (NOAA) Atlas 14*. Retrieved from the Hydrometeorological Design Studies Center - Precipitation Frequency Data Server located at: http://hdsc.nws.noaa.gov/hdsc/pfds/. NOAA Atlas 14 Volume 1, Version 5.0, Revised 2011.

Clark County Regional Flood Control District. 1999. Hydrologic Criteria and Drainage Design Manual.

NDOT Hydraulics. 2006. Nevada Department of Transportation Drainage Manual, 2nd Edition.

U.S. Weather Bureau, 1961. Rainfall Frequency Atlas of the United States for Durations from 30 Minutes to 24 Hours and Return Periods from 1 to 100 Years. U.S. Weather Bureau Technical Paper No. 40, U.S. Department of Commerce, Washington, DC.

Washoe County. 2009. Washoe County Hydrologic Criteria and Drainage Design Manual.

Nevada Department of Transportation
Rudy Malfabon, P.E. Director
Ken Chambers, Research Division Chief
(775) 888-7220
kchambers@dot.state.nv.us
1263 South Stewart Street
Carson City, Nevada 89712